Relationships Between Severity of Histopathological Lesions of Aleutian Disease in Mink, Measured by Digital Image Analysis, and Antibody Titer and Serum Gamma-Globulin Level

by

Rojman Khomayezi

Submitted in partial fulfilment of the requirements
for the degree of Master of Science

at

Dalhousie University
Halifax, Nova Scotia
August 2018

Table of Contents

List of Tables

List of Figures

Abstract

Aleutian disease (AD), caused by Aleutian mink disease virus (AMDV), is a serious problem for the multi-million-dollar mink industry in Nova Scotia. AD causes infiltration of mononuclear cells in various organs (plasmacytosis), high serum gamma-globulin levels and high anti-AMDV antibody titers, resulting in increased mortality and reduced reproduction rate. Selecting mink that can tolerate the infection is a viable way to control the problem. The first objective of this study was to develop a quantitative method of measuring the severity of histopathological lesions in the kidneys, liver and heart of AMDV-infected mink, using digital image analysis (DIA) software. The second objective was to assess relationships between the severity of AD lesions, assessed by DIA, and anti-AMDV antibody titer and serum gamma-globulin level, which are believed to be indicators of the severity of AD lesions in infected mink. A reproducible and reliable method was developed for the calculation of the percent infiltrated mononuclear cells on H&E stained slides of the kidneys, liver and heart of AMDV-infected mink. Associations between antibody titer and gamma-globulin level and percent infiltrated mononuclear cells measured by DIA software in the kidneys, liver and heart of 299 black mink, inoculated with a local strain of AMDV and monitored for up to 3.5 years, were generally weak, making the serological measures unreliable tools for the identification of tolerant mink, particularly when the time of infection is unknown.

List of Abbreviations and Symbols Used

#	Number of
$	Canadian dollar
%	Percent
°C	Degrees Celsius
µm	Micrometer
μm^2	Square micrometer
AD	Aleutian disease
ADRC	Aleutian disease research center
AMDV	Aleutian mink disease virus
AOI	Area of Interest
CIEP	Counter-immunoelectrophoresis
CO	Carbon Monoxide
CO2	Carbon dioxide
Cy	Cyclophosphamide
DIA	Digital image analysis
dL	Deciliter
dpi	Day post-inoculation
ELISA	Enzyme-linked immunosorbent assay
g	Gram
H&E	Hematoxylin and Eosin
HHV	Human herpesvirus
HSI	Hue-Saturation-Intensity
IAT	Iodine agglutination test
ID_{50}	Lethal dose 50
IHC	Immunohistochemical
INF	Interferon
IPP	Image Pro Plus
kDa	Kilodalton
Kg	Kilogram
Log	Logarithm
mg	Milligram
mL	Milliliter
mm	Milimeter
NS1	Non-structural1
PAS	Periodic Acid-Schiff
PCNA	Proliferating cell nuclear antigen
PCR	Polymerase chain reaction
REML	Restricted maximum likelihood
RGB	Red-Green-Blue
SLEN	Systemic lupus erythematous nephritis
WBC	White blood cell
wpi	Week post-inoculation
γ	Gamma
IgG	Immunoglobulin G
2D	Two dimensional

Acknowledgements

I would like to express my deepest appreciations to my supervisor, Dr. Hossain Farid, for his endless support, guidance and help on this project. The door of his office was open for me whenever I ran into a trouble spot or had a question about my research or writing. I would also like to thank my committee members, Dr. Lori Parsons and Dr. Miriam Gordon, for their passionate participation and contribution to the project.

My special thanks goes to Ms. Flora Riyahi, for her generosity, kindness and thoughtfulness towards me and my wife during the past three years. Heartfelt thanks for all the encouragements and comforts that were sent to me from thousands of miles away by my lovely parents. Last but not least, I would like to dedicate my very profound gratitude to my dear wife, Shiba, for providing me with unfailing support and continuous encouragement. This accomplishment could not have been possible without her patience and limitless love. Thank you from the bottom of my heart.

Chapter 1. Introduction

Mink production is an important agricultural industry in Nova Scotia, the province with the greatest number of mink pelts produced in Canada (Statistics Canada, 2015). Aleutian mink disease virus (AMDV) causes Aleutian disease (AD) that seriously threatens this industry (Farid et al., 2012). The main characteristics of AD are the abundant amount of mononuclear cells, mostly plasma cells, in the blood stream and in different organs of the body (plasmacytosis), viremia, high serum gamma-globulin levels, high anti-AMDV antibody titers, presence of circulating infectious immune complexes and glomerulonephritis (reviewed in Bloom et al., 1994). These pathological problems increase embryonic and adult mortality, reduce reproduction rate (Hansen and Lund, 1988), and diminish pelt quality (Farid and Ferns, 2011), resulting in huge economic losses for the industry. There is no treatment for AD and attempts to produce an effective vaccine against the virus have either failed or were only partially effective (Porter et al., 1972; Aasted et al., 1998; Castelruiz et al., 2005). Additionally, continuous removal of sero-positive animals has not eradicated the virus from ranches in the past three decades (Farid et al., 2012). Unsuccessful removal strategies, along with the observations that some inoculated mink did not develop AD symptoms (Bloom et al., 1994), and that the response of mink to infection is genetically controlled (Aasted and Hauch, 1988; Farid et al., 2018), persuaded some farmers to select their herds for tolerance against the AMDV-infection.

Tolerant animals are defined as those which remain healthy and productive while viral infection persists; whereas resistant animals are those which are capable of preventing viral entry, minimizing viral load or clearing the virus (Råberg et al., 2007). It has been

shown that the tolerant animals have low severe lesions characteristics of AD (Farid and Ferns, 2017). The identification of tolerant animals, particularly at an early age, is important for the establishment of a tolerant herd. Because severity of AD lesions cannot be directly determined in live animals, and there is no proven laboratory test for selecting the truly tolerant animals. Farmers select their animals based on physical health, with or without using the iodine agglutination test (IAT) (Farid 2010), a field test for measuring the level of serum gamma-globulin levels (Henson et al. 1962). However, there is no published information on the relationship between the IAT results and the severity of histopathological lesions (level of health) in AMDV-infected mink. Selection for tolerance based on low anti-AMDV antibody titer is the latest method that ranchers in Canada, USA and Netherlands are using (Farid and Segerval, 2014). Nevertheless, limited published information on relationships between anti-AMDV antibody titer and the severity of histopathological lesions exists (An and Ingram, 1977; Hadlow et al., 1985; Jackson et al., 1996). Finding a serological measurement with a high degree of association with the AD lesions and the level of health can provide ranchers with a tool for identifying tolerant mink.

In addition, measuring the severity of histopathological lesions in AMDV-infected mink is one of the important topics in Aleutian disease studies, especially on the subject of selection for tolerance. The amount of infiltrated mononuclear cells in different organs is the most accurate measure of severity of the lesions in infected mink (Henson et al., 1976). To date, apart from one study by Nieto et al. (1991), all the published reports on histopathological evaluation of AMDV-infected mink were based on subjective methods (Leader et al., 1963; Henson et al., 1966; Jackson et al., 1996; Farid and Ferns, 2011, 2017;

Jensen et al., 2016), in which the tissue slides were manually evaluated under a light microscope and scored based on the visual assessment of the amounts of mononuclear cells infiltration. Results from manual methods are neither comparable among researchers, nor reproducible when performed by the same person (Prasad and Prabhu, 2012). Using digital image analysis systems in human and animal histopathological studies is a fast-developing field that can reduce the defects in the studies using the manual methods, but has not been evaluated in AMDV-infected mink.

The objectives of the current study were (1) to develop a quantitative method of measuring severity of histopathological lesions in the kidneys, liver and heart of AMDV-infected mink, using digital image analysis (DIA) software, Image Pro Plus (IPP) 7.0; and (2) to assess the relationships between the severity of histopathological lesions, measured by IPP 7.0, and two serological measurements, anti-AMDV antibody titers and serum gamma-globulin levels.

Chapter 2. Quantitative measurement of the severity of histopathological lesions in AMDV-infected mink using digital image analysis.

2.1 Literature review

2.1.1 The use of digital image analysis in histopathology

Manual evaluation of histpathological lesions is a subjective measurement and the results are usually not comparable among pathologists (Prasad and Prabhu, 2012). Lack of quantitative results obtained from those manual evaluations is another problem that has led pathology science to a new era of digitization. Digital image analysis (DIA) not only has transformed the way of assessing histopathological lesions from qualitative to quantitative measurements (Prasad and Prabhu, 2012), it has also increased the opportunities to obtain some additional information, such as patterns of lesions, that was invisible to human eye in the past (Laurinavicius et al., 2012). There are many essential factors that have to be considered during the implementation of DIA to attain acceptable reproducibility, reliability, objectivity and speed of histopathological evaluations compared with the conventional manual methods. To achieve optimal results when using a DIA software, it is essential to establish and follow reproducible methods in sampling, tissue preparation and staining, as well as scanning and digital imaging. Although some researchers selected a specific algorithm based on subjective evaluations, i.e. eyeballing the measurements, it would be more reproducible to establish the algorithms based on objective criteria, i.e. comparing the software results with actual values (Riber-Hansen et al., 2012). In other words, the more objective the algorithm, the more reproducible the results.

DIA can be used for a vast variety of purposes, including evaluating morphometry of cells and tissue components, quantification of different types of cells, sub-cellular

molecular studies and automated pattern assessments (Aronson, 2005). Using DIA for grading histopathological lesions by quantifying the expression level of biomarkers is one of the most extensively growing areas in digital pathology. A measurable sign of a disease or a pathological disorder is referred to as a biomarker, which is measured in order to determine the severity of the disease (Aronson, 2005). Biomarkers play a significant role in diagnosis, prognosis and expectation of responses to various treatments (Laurinavicius et al., 2012; Prasad and Prabhu, 2012). Thus, using an automated, reproducible and objective method for measuring biomarkers seems to be more useful than using a manual and subjective method.

2.1.2 Staining techniques

Generally, in any histopathological evaluation, tissue color plays a significant role for obtaining reliable results. Depending on the purpose of the study, histochemical and(or) immunohistochemical stains (IHC) are used by pathologists (Clarke and Treanor, 2017). However, IHC staining methods are the most popular when using DIA, especially when evaluating a biomarker (Prasad and Prabhu, 2012). The reason is that the IHC stains can be designed to stain certain types of cells or cell components differently, making them distinguishable by the DIA software and even by manual evaluation (Noutsias et al., 2012). On the other hand, most histochemical statins, such as hematoxylin and eosin (H&E) and toluidine blue, cannot be cell specified. The H&E is a simple and low-cost staining method, which has been used as a routine staining method in most of the histopathological evaluations during the past decades and many pathologists believe that it will be used for the next 50 years (Gurcan et al., 2009). H&E stains the nuclei of all types of cells blue or

purple and other tissue structures red, pink and/or orange (Clarke and Treanor, 2017), making it difficult to distinguish among some cell components by DIA. A few studies compared H&E with IHC for their merits in DIA. For instance, Went et al. (2006) evaluated bone marrow slides for the amount of infiltrated plasma cells. Slides from 87 human patients with multiple myeloma, monoclonal gammopathy and reactive plasmosytosis, were stained with CD138 antibody (IHC) and H&E. A conventional manual microscopy and a DIA software (KS 300) method were used for both staining methods. They compared the results from the DIA software on CD138 and H&E stained samples with the results from the manual assessment on the same samples and concluded that the image analysis was superior to the manual microscopic assessment in quantification of plasma cells because inter- and intra-observer variability was minimized. It was also concluded that quantification of plasma cells by H&E staining alone cannot be adequate for therapeutic purposes. De Noronha Santos Netto et al. (2012) quantified mast cells in periapical cysts, dentigerous cysts and keratocystic odontogenic tumors in humans, using a DIA software (Image Pro Plus 4.5). They used toluidine blue and IHC staining (Clone G3) methods and found that the mean number of mast cells detected in IHC stained slides (4.1) was significantly higher than those stained by toluidine blue (1.5). Toluidine blue is a histochemical stain which provides a rapid and firm staining of mast cells (Churukian and Schenk, 1981). Soltzberg et al. (2011) used H&E for staining the inflamed murine lung tissues for quantifying infiltrated immune cells (inflammatory cells) by a DIA software (Image Pro Plus 7.0). Two models of *in vivo* inflammation of lung were evaluated in their study; inflammation caused by asthma and cystic fibrosis. It was reported that even though H&E stained both the nuclei of inflammatory cells and the nuclei of interstitial cells the

same, they could successfully consider the interstitial cells as background and eliminate them from being counted by the software. Size and color intensity were the two factors used for defining inflammatory nuclei to the software. They did not, however, explain what size and color intensity were used (the author was contacted by e-mail, but no response has so far been received).

2.1.3 Validation of digital image analysis software

Any test which is used for decision making in various science and applied disciplines, including human and veterinary medicine, must be validated to meet standards of statistical reliability in order to provide a high degree of confidence. According to International Organization for Standardization, (1994), validation defines as "verification, where the specified requirements are adequate for an intended use". The outcomes of any diagnostic test which generates binary results can be classified into four categories, true positives (correctly identified), true negatives (correctly rejected), false positives (incorrectly identified) and false negatives (incorrectly rejected) (Powers, 2011; Eusebi, 2013; Baratloo et al., 2015). The measures of reliability of any test are calculated based on the number of cases in each of the four categories and include measures of accuracy and precision (Sackett, 1992).

Accuracy shows how close a measured value is to the actual (true or reference) value, i.e. the fraction of the total sample that is correctly identified (Doumas, 1997; JCGM200, 2008), and is the most crucial aspect of any analytical method (Araujo, 2009). Different measures of association, such as correlation coefficient, between the actual

(reference) and measured values are often used (Westgard and Hunt, 1973; Altman and Bland, 1983). In case of categorical data, accuracy is calculated as:

(#true positives + #true negatives) / (sample size) =
(#correctly identified + #correctly rejected) / (sample size)

(Powers, 2011; Eusebi, 2013; Baratloo et al., 2015).

The other two measures of diagnostic accuracy are sensitivity and specificity (Sackett, 1992). Sensitivity measures the rate of true positive subjects detected based on the results of a diagnostic test. In another word, sensitivity is the ability of a test to correctly identify subjects who have a given disorder. If the test is highly sensitive and the test result is positive, one can be nearly certain that the subject has the condition. For categorical data, sensitivity is calculated as:

(#true positives) / [(#true positive + #false negative)] =
(#correctly identified) / [(#correctly identified + #incorrectly rejected)]

(Sackett, 1992; Altman and Bland, 1994; Powers, 2011; Eusebi, 2013; Baratloo et al., 2015).

A highly sensitive test is thus desired when identification of the subjects which have the condition is paramount and the condition is present only in rare cases which were erroneously declared as negative.

Specificity measures the rate of true negative subjects, or real negative cases that are correctly predicted negative. In another word, specificity is the ability of a test to correctly identify subjects which do not have the disorder. If the test is highly specific and the test result is negative, one can be nearly certain that the subject actually does not have the condition. It is calculated as:

(#true negatives) / [(#true negative + #false positives)] =

(#correctly rejected) / [#correctly rejected + #incorrectly identified)]
(Sackett, 1992; Altman and Bland, 1994; Powers, 2011; Eusebi, 2013; Baratloo et al., 2015).

A highly specific test is thus desired when accurate identification of the negative subjects is important and the condition is not present only in rare cases which were erroneously declared as positive. Although both these statistical measures are important, it is not possible to have a test with 100% sensitivity and 100% specificity and it is crucial to decide which should be traded off for which. Most tests used in various laboratories produce only a small proportion of false-positive and false-negative results and laboratories are required through accreditation procedures to use the most sensitive and specific tests available. Sensitivity and specificity are not affected by the prevalence of the condition (disease), but diagnostic accuracy increases as the prevalence of the condition increases (Eusebi, 2013).

Precision is another measure of reliability. A precise test is the one in which the amount of random variation is small, and thus produces similar results when the same sample is tested more than once (Doumas, 1997; JCGM200, 2008; Araujo, 2009). The determination of precision is one of the basic steps in the process of achieving repeatability and reproducibility in method validation. Differences between the outcomes of repeated tests are the results of random error, which is calculated by the standard deviation, the variance, or the coefficient of variation (Araujo, 2009). The agreement between any two measurements are calculated by measures of association, such as a correlation coefficient. For categorical data, precision is defined as:

(#true positives) / [(#true positive+ #false positives)] =
(#correctly identified) / [(#correctly identified + #incorrectly identified)]
(Powers, 2011).

Precision is that predicted positive cases are correct real positives (Powers, 2011). Precision is different from sensitivity because precision is the ratio of positive results to the total positive results, including false positives, whereas sensitivity is a measure of the ratio of actual positives to the total of test positives, including positive subjects which were incorrectly identified as negatives. Both accuracy and precision are indicators of closeness of measurements, but accuracy reflects how close a measurement is to a known or reference value, whereas precision reflects how reproducible measurements are, even if they are not the correct value. The measures of accuracy and precision describe sources of variability and reflect a test's basic reliability.

Although different methods of validating the reliability of various tests, such as accuracy, specificity and precision, have been recommended by different regulatory organizations, often incorrect mathematical and statistical measures are used (Araujo, 2009). The methods of computing these parameters vary according to the area of application, but they should be able to confirm that the procedure employed for a specific test is appropriate for its intended use (Araujo, 2009).

Calculation of accuracy and precision is based on the agreement between two measurements. Pearson correlation, which is the measure of linear relationship between two variables, has been widely used as a measure of agreement between two methods, but it has been suggested that it is not an appropriate method (Westgard and Hunt, 1973; Altman and Bland, 1983; Bland and Altman, 1990, 2010). The incorrect use of correlation coefficient for the measuring agreement between two measurements is because of several

reasons, including (i) Pearson correlation measures the strength of a linear relation between two variables but not the agreement between them and it is not accurate when the relationship is not linear, yet the test of linearity has rarely been performed (Araujo, 2009), and (ii) the magnitude of correlation coefficient depends on the range of the measurements, i.e. as the range of values increase, the ,magnitude of correlation coefficient becomes larger (Altman and Bland, 1983; Bland and Altman, 2010).

Spearman's rank correlation is a nonparametric (not dependent on any distribution) measure of the strength of association between the rankings of two variables and is more accurate than Pearson correlation for categorical data and when their relationship is monotonic but not linear (McDonald, 2014). Agreements between two qualitative (categorical) variables can also be computed using the Kappa coefficient, which is a more robust measure than correlation coefficient, because Kappa takes into account the possibility of the agreement occurring by chance (Uebersax, 2010), and is suggested by Sackett (1992) as the measure of precision. Another method of analyzing the agreement between two different assays or between an assay and a set of reference data (standards) is the Bland–Altman plot, which is more appropriate than correlation analysis (Bland and Altman, 1999).

Validation of any DIA software in the field of digital pathology has been performed using the same measurements as explained above, but the calculation procedures have not always been explained in detail. The Pearson correlation or Spearman's rank correlation have often been used to calculate accuracy and precision. For example, Salinas-Navarro et al. (2009) counted retinal ganglion cells, labeled with a fluorescent agent, in adult albino and pigmented mice by using a commercial DIA software (Image Pro Plus 5.1). They

validated their automatic counting method by measuring accuracy, which was calculated as the Pearson correlation between results obtained manually from four different investigators with those from the DIA. In a study which was explained above, Soltzberg et al. (2011), estimated the accuracy of the software by calculating the Pearson correlation coefficient between the automated counting results (software) and manual counting results in the cystic fibrosis model. They also measured the precision of the software based on the coefficient of variation for the number of cells within three different sections of each of the eight lung samples. In another study, the proportion of Ki-67-positive cells in immunohistochemically stained breast cancer samples evaluated using two independent image analysis algorithms and a manual assessment by a pathologist (Laurinavicius et al., 2014). The reference values in that study were prepared using a stereological frame counting method to quantify profiles of structures on 2D sections, which was performed by three independent technicians under the light microscope. The accuracy of the DIA and manual results, relative to the reference values, was estimated using the Pearson correlation.

Rogers et al. (2016) evaluated colitis in mouse colon samples, stained with H&E and CD3 (IHC), using a DIA software (Definiens Tissue Studio). The percentage of the whole area on each slide occupied by infiltrated inflammatory cells was used as a marker representing the intensity of colitis. Validation of the DIA software was performed by comparing the results from each algorithm (two different algorithms designed for H&E and one designed for CD3) to those from a manual semi-quantitative evaluation by a pathologist (0-5 score). Spearman's rank correlation between algorithms and the pathologist's scores was calculated as the measure of accuracy. Goedkoop et al. (2005)

compared the results from a DIA (Leica Qwin) software with a manual method for quantifying infiltrated $CD3^+$ T cells, and with a semi-quantitative method (0-4 scores) for quantifying E-selectin expression (cell adhesion molecule) on IHC stained skin sections from 11 human patients with chronic plaque psoriasis. They compared the results from the DIA software to those from the conventional manual quantification and semi-quantitative analyses using the Pearson correlation and Spearman's rank correlation, respectively. They did not mention whether those two measurements considered the accuracy of the DIA software or any other measure of reliability.

Rizzardi et al. (2012) used tissue microarrays of ovarian serous carcinomas in human patients stained with an antibody directed against S100A1 (IHC) to determine the capability of commercially available DIA software (Genie Histology Pattern Recognition software) by comparing its results to those obtained from visual analysis by a pathologist. The comparison of manual and DIA results was performed for two different subjects, (1) the segmentation of the images into carcinoma containing areas versus non-carcinoma containing areas, and (2) quantification of stain intensity within areas of carcinoma. Spearman's correlation was used to compare the pathologist's manual scoring versus the software results for the stain intensity measuring study. Bland-Altman plots were used to compare segmentations results from the software with manual segmentation. They did not, however, mention whether the Spearman's correlation and the results from Bland-Altman plots considered accuracy or another measure of reliability. In another study, the Bland-Altman plots were used to compare manual and two DIA software (Image Pro Plus 5.1 and Image SXM) results to quantify the binding ability of *Plasmodium Falciparum*-infected red blood cells to host receptors *in vitro* (Paton et al., 2011). The results of the Bland-

Altman plots considered the accuracy of the DIA software. The above examples show the widespread use of correlation coefficient and Bland-Altman plots in computing precision. There was no mention of the test of linearity in any of the papers where Pearson correlations were calculated, and there was no mention of sensitivity or specificity.

In addition to the measures of association, the results of DIA were compared with actual (reference) values using analysis of variance. For example, Wang et al. (2009) measured the expression of Survivin (a cancer biomarker) in rectal adeno carcinoma samples from 98 human patients. The samples were stained by an IHC (anti-Survivin monoclonal antibody) and evaluated using Image Pro Plus 5.0. The measured parameters included density mean, area sum and mean integrated optical density. A visual evaluation was also performed by two investigators. They graded each sample according to the staining intensity of Survivin as negative, equivocal, weak and strong. The non-parametric Kruskal-Wallis test (one-way ANOVA on ranks) was perform to calculate the significance of differences between the DIA results and those from the two investigators in order to validate the DIA results. They did not, however, mention whether the calculated difference between DIA results and the reference values were considered as accuracy or other measures of validation. Comparing the means of two methods using t-test or analysis of variance is an incorrect method of estimating agreement (Westgard and Hunt, 1973; Altman and Bland, 1983; Bland and Altman, 1990), because the result shows the presence or absence of statistically significant difference between the means.

There are a few papers where sensitivity and specificity of DIA software have been reported. Kratz et al. (2005) evaluated a digital image analysis system (CellaVision DM96) for automated digital counting of different white blood cells on blood smears. Image

analysis results were compared with direct microscopic evaluations as the reference. Clinical sensitivity and specificity of the system were calculated based on positive and negative results from image analysis compared with direct microscopy as the reference. Methods of calculating sensitivity and specificity were not explained nor was a reference cited. Correlation coefficients between the number of each cell type obtained from image analysis and direct microscopy were also calculated, but it was not referred to any of the measures of reliability. There was no mention of testing of the linearity of the variables. No comparison was made between correlation coefficients, sensitivity or specificity.

Accuracy alone cannot be an efficient and reliable measurement to validate a DIA software in digital pathology where the results are binary, such as counting certain cells or nuclei. This is because of the fact that in such studies false positive (incorrectly counted cells or nuclei) and false negative (uncounted cells or nuclei) results are inevitable and will affect the reliability of the test. Thus, sensitivity (true positive rate) and precision (positive predictive value) are the two measurements which are recommended to be used to validate DIA results (Janowczyk and Madabhushi, 2016). These measurements can be used separately or combined, called F-score, which generates a more accurate measure of reliability and is calculated as follows (Janowczyk and Madabhushi, 2016):

F-score= (2*True positives) / (2*true positives + false positives+ false negatives)

The F-score is actually the harmonic mean of sensitivity and precision (Powers 2011).

It can be concluded that the use of associations methods, such as correlation coefficient, Spearman's rank correlation, the Kappa coefficient, or mean comparison methods, such as t-test or ANOVA, are not valid methods of calculating agreements for

categorical data. Measures of diagnostic validation, i.e., accuracy, sensitivity, specificity and precision, suggested for categorical data are more appropriate.

2.1.4 Algorithms developed for Image Pro Plus

It is important to develop an algorithm for any DIA software in order to follow an accurate and consistent evaluation. In order to obtain reproducible and objective results, the same algorithm should be followed in every image that is analyzed in a study. Such algorithms depend on the objectives of the study, as well as the method of staining used for the tissue samples. The designed algorithm in any DIA software can be recorded and saved in a specific format called "Macro". Then the saved macro can be recalled for other images, which would be a great asset for reducing the evaluation time.

One of the popular commercial DIA software used in pathology is Image Pro Plus (IPP), in which different algorithms for various purposes have been developed. Steps which were followed in developing algorithms for the IPP have been explained in detail in some studies. For example, Marcos-Graces et al. (2017) stained human skin slides with H&E, Masson's trichrome and Picrosirius red, and compared results of measuring collagen bundle orientation by the Fourier analysis and semiquantitative evaluation methods. Fourier analysis is a mathematical algorithm, available in some of the commercial image analysis software, which basically converts data into periodicities and frequencies. Thus, frequencies that occurred in an image will be presented in a frequency spectrum, called power plot of that image (Rintoul et al., 1998). They (Marcos-Graces et al., 2017) used IPP 7.0 software for the Fourier analysis and designed a macro for that purpose. The steps that they followed for creating the macro were: (1) using the Best-Fit tool to maximize contrast

between collagen bundles and background; (2) conversion of original color images to grayscale images; (3) the fast Fourier transform was applied for obtaining the 2D power plot of the images; (4) in order to choose the central frequencies, the obtained 2D power plots were segmented with automatic threshold values; and (5) to obtain the collagen orientation index of the images, the maximum dimensions (length and width) of the segmented structures were automatically calculated. They performed the semiquantitative assessment of collagen orientation based on a five-scale, ranging from 1 for extremely parallel orientations to 5 for extremely random.

A computerized method was developed for analyzing infiltration areas of leukocytes (TCR+ and ED-2+ cells) on IHC stained rat brain tumor slides using IPP 3.0 (Johansson et al., 2001). The staining procedure, the digital imaging method and the image analysis method were optimized to obtain the most reproducible method. One image was taken from the whole section of the tumor with X12.5 magnification and six to 20 images were taken with X100 magnification, depending on the size of the tumor. The X100 images were then merged to create a single image using Adobe Photoshop (version 5.0; Adobe Systems, Mountain View, CA). Images were transferred to IPP software. The Contrast-Enhancement tool (which is called Best-Fit tool in the newer versions of IPP) and then the Flatten Background filter was used to reduce illumination variations. An irregular Area of Interest (AOI) was used to select the tumor area. The RGB (red-green-blue) images (original color) were then converted to HSI (hue-saturation-intensity). The color intensity (threshold) was manually chosen using the Select Measurements option in the Measure menu. Then the percentage of the stained area out of the unselected area by the AOI was calculated by using the Count command. The performance of the software on both the

X12.5 and X100 magnifications was compared. No significant differences between the two magnifications was found, which indicates a high correlation coefficient between them. It was thus concluded that even using images with low magnification can be sufficiently efficient and reproducible in evaluating large tissue sections.

Despite the importance of developing such algorithms, there are several reports where there is no mention of the steps followed in developing an algorithm when using IPP. Castro Souza Junior Neto et al. (2017) used IPP to quantify mast cells as a biomarker indicating degree of inflammation in cutaneous wounds of 60 male rats treated with *Ximenia americana* extract. Tissues were stained with H&E and toluidine blue. They neither explained, nor validated the method they followed in the DIA software. Sheethal et al. (2014) performed a study on quantification of mast cells in inflammatory periapical and gingival lesions stained with toluidine blue, using Image Pro Express software, which is produced by the same company as IPP. They did not explain or validate their method either. Version 4.5 of IPP was used for an automatic quantification of cell nuclei labeled with proliferating cell nuclear antigen (PCNA) immunohistochemistry by Francisco et al. (2004). The PCNA is a 36 kDa nuclear protein with high expression levels in the late G1 and S cell-cycle phases. Thus, evaluation of PCNA is used as an alternative to cellular proliferative analysis (Somanathan et al., 2001). They (Francisco et al., 2004) prepared eleven sections of reticular oral lichen planus (an inflammatory condition that affects mucous membranes inside the mouth) from human patients stained by PCNA immunohistochemistry. A total of 154 digital images were taken from those sections. The labeled nuclei were made distinguishable by defining parameters such as mean density (grayscale value), red density, green density, blue density, area, minor axis, perimeter rate

and roundness. The digital analysis results were compared with visual counts of manually identified labeled nuclei on printed images from the slides. Comparison of the results from the two methods showed a significant correlation (0.964), and a high level of correctly counted labeled nuclei by the software was achieved. However, the main parameters that were adjusted for achieving the high correlation between digital and manual results were mean density (grayscale value) and area threshold. In other words, mean density and area threshold were the most useful elements to be used in defining PCNA labeled nuclei when using the software. They concluded that the IPP 4.5 software, using an algorithm with automatic definition of those two parameters, was a reliable alternative for manual quantification of PCNA labeled nuclei.

2.1.5 The use of DIA to measure the severity of Aleutian disease lesions

Visual evaluation of histopathological lesions of AD have often been used to qualitatively estimate severity of the disease (Leader et al., 1963; Henson et al., 1966; Farid and Ferns, 2011; Jensen et al., 2016; Farid and Ferns, 2017). There is only one report in which the severity of kidney lesions in AMDV-infected mink was estimated quantitatively (Jackson et al., 1996). Jackson et al. (1996) visually measured the percentage of renal cortical tubules and interstitium replaces by plasma cells and lymphocytes on H&E stained samples. Although evaluating histopathological lesions by DIA is a fast-growing area in various fields of human and animal pathology, there is only one published article where the severity of AD lesions was measured by DIA (Nieto et al., 1991). Nieto et al. (1991), evaluated the severity of histopathological lesions of kidney samples from 154 AMDV-infected mink using DIA software (VIDSM II automatic image analyzer loaded with

General Area software). They performed a morphological and differential morphometrical evaluation of glomerular parameters on H&E, periodic Acid-Schiff (PAS) and silver-methenamine stained kidney samples. The objective of their study was to analyze various types of glomerulonephritis in result of AMDV-infection and to classify them according to the standards suggested by the World Health Organization classification for systemic lupus erythematous nephritis (SLEN). The glomerular lesions in AD have been described and proposed as a comparative study model for the SLEN (Muller-Peddinhaus and Trautwein, 1983). They measured (1) total glomerular area; (2) surface of the mesangial area; (3) number of epithelial cells/glomerulus; (4) number of endothelial cells/glomerulus; (5) number of mesangial cells/glomerulus; (6) total number of cells per glomerulus; (7) number of mesangial cells per 1000 μm^2; and (8) number of glomerular cells/100 μm^2 of glomerulus area. The existence of five main forms of glomerulonephritis in kidneys of AMDV-infected mink was reported based on those eight measurements (explained in Section 3.1.3).

2.2 Materials and methods

2.2.1 Image preparation and counting the infiltrated cells

A Leica DM500-Microscope (Leica Microsystems, 2018), which was equipped with a high-quality camera was used to capture an original color image (RGB), with the dimension of 2048 X 1536 pixels, from each of five kidney, liver, heart and lung tissue slides with 10X magnification. These images were saved as digital files (.tif format) and transferred to the Image Pro. Plus (IPP) version 7.0 (http://www.mediacy.com/imageproplus). The purpose of using this software was to

automatically count the number of infiltrated mononuclear cells (plasma cells, lymphocytes and macrophages) on each image, which is based on detecting infiltrated cells according to the color intensity of their constituted pixels. The automatic counting of infiltrated mononuclear cells on the five images of each of the four organs was found to be inaccurate because H&E stained all nuclei the same, and the software was unable to distinguish between the nuclei of infiltrated mononuclear cells and the nuclei of normal cells. Thus, using the manual feature of the software for counting the infiltrated cells seemed to be more logical. In this method, clicking on each of the infiltrated cells added the cells to a list of counted objects and the total number of infiltrated cells was recorded (Appendix 1). For making sure that the true mononuclear cells were counted, several images from each organ were discussed with a veterinary pathologist at the Pathology Laboratory, Nova Scotia Department of Agriculture.

2.2.2 Software setup for counting total number of cells

The automatic-counting feature of the IPP 7.0 was used for quantification of the total number of cells, which was needed for calculating the proportion of infiltrated cells. The total number of cells included the infiltrated mononuclear cells and normal cells. The software recognizes and counts the nuclei of the cells, which appear darker than cell cytoplasm contents. Because cell nuclei have different color intensities, it was necessary to find a range of color intensity (threshold) by which the software most accurately counted the number of nuclei present on an image. For this purpose, total number of cells was manually counted on one randomly chosen area on each of the five kidney RGB images. The areas with the dimension of 510 X 380 pixels were identified by the “Rectangle AOI”

tool of the software, that were covering 6.17% of the entire image (2046 X 1534 pixels). The AOI information was saved in order to be reused in the next steps.

Each RGB image is a mixture of three color channels, red, green and blue. Color intensities of constituted pixels in an image can range from 0 to 255. The ability of DIA software in distinguishing pixels is based on their color intensities in each color channel, and helps the operator in detecting and counting certain objects (i.e. cells) on any image. Thus, by setting a threshold, the software counts all the objects that have color intensities within the selected threshold. Attempts were made to find a specific threshold by which the software counts nuclei on the RGB images. Since it was not possible to simultaneously count the number of nuclei with a single threshold for three color channels, each of the channels was evaluated separately to determine which color channel and which threshold counts the nuclei of cells more accurately.

Each RGB image was converted to three black-and-white images (grayscale) based on the three color channels by choosing “RGB color model” in the “color channel” option, under the “Process” menu (Appendix 1). The size threshold was determined based on the size of the nuclei of normal and infiltrated cells on a sample of cells measured by the “Manual Measurement” command of the software. The size threshold of 10–10,000 pixels was selected in the “Select Measurement” section of the “Count/Size” menu. In cases where cells were joint together (cell clusters) the “Watershed Split” tool in the “Count/Size” menu, under the “Edit” option was used to separate them. This tool separates the clusters based on the size threshold defined for the intended objects. The saved AOI in the manual counting stage was recalled and used on the same areas of the three grayscale images and the automatic counting was performed with different ranges of grayscale

(grayscale threshold). For this purpose, the "Count/Size" option under the "Measure" menu was selected. In the window of the "Count/Size" and by the "Selected Ranges" option, different ranges of grayscale were set and the automatic counting was performed with each of them (Appendix 1). For the images in the red channel, the automatic counting was started from the threshold 0-60, continued with ten unit increments up to the 0-120, and then with five unit increments up to the 0-175 (total of 17 ranges). For the blue channel, the automatic counting was started from the threshold 0-100, increased by ten units to the 0-145 and then increased by five units to the 0-195 (total of 14 ranges). For the green channel, the automatic counting was started at the threshold 0-20, increased by ten units to the 0-40 and then increased by five units up to the 0-95 (total of 14). The starting thresholds were the points where the software started to count and the ending thresholds were the points where the number of incorrect counts rapidly increased. To simplify the presentation of the grayscale thresholds, each threshold was given a score from 1-36 (Table 2.2.1), and the term "range score" was used instead of "grayscale threshold" in this document.

The results of automatic counting in each range score were compared with manual counting results and were classified into correctly counted (IPP correctly identified the cell nuclei), incorrectly counted (there was no cell nuclei but was counted by IPP) and uncounted (cell nuclei was not recognized by IPP) cells. Sensitivity and precision of the software in performing the counting process with each of the range scores within the three color channels were calculated according to the following equations (Sackett, 1992; Altman and Bland, 1994; Powers, 2011; Eusebi, 2013; Baratloo et al., 2015), and the F-score was calculated using equation suggested by Janowczyk and Madabhushi (2016).

Specificity was not calculable since it was not possible to define a value as a true negative (cells that did not exist and were not counted by IPP).

Sensitivity = true positive or correctly counted / (true positive or correctly counted + false negative or uncounted)

Precision = true positive or correctly counted / (true positive or correctly counted + false positive or incorrectly counted)

F-Score = 2*true positive or correctly counted / (2*true positive or correctly counted + false positive or incorrectly counted + false negative or uncounted)

Table 2.2.1 Scores given to each grayscale threshold

Grayscale threshold	Score	Grayscale threshold	Score	Grayscale threshold	Score	Grayscale threshold	Score
0-20	1	0-65	10	0-110	19	0-155	28
0-25	2	0-70	11	0-115	20	0-160	29
0-30	3	0-75	12	0-120	21	0-165	30
0-35	4	0-80	13	0-125	22	0-170	31
0-40	5	0-85	14	0-130	23	0-175	32
0-45	6	0-90	15	0-135	24	0-180	33
0-50	7	0-95	16	0-140	25	0-185	34
0-55	8	0-100	17	0-145	26	0-190	35
0-60	9	0-105	18	0-150	27	0-195	36

2.2.3 Using the Best-Fit tool to minimize variations among slides

Although attempts were made to follow the same procedure in taking images from slides, there were still some differences among images in terms of brightness and contrast. This could be related to the procedures followed for preparing and staining the tissue slides in the laboratory. The number of uncounted and incorrectly counted cells, and consequently the estimated values of sensitivity, precision and F-score in each color channel, showed some variability among images, which could have been partly the result of the differences

in brightness and contrast of the images. For reducing such variabilities, the "Best-Fit" tool was used on the same areas of the five kidney images which were previously used. The "Best-Fit" tool stretches the histogram of pixel values by assigning the bottom 3% of the values to the shadow point (0), the top 3% of the values to the highlight point (255) and distributing the rest of the values across the scale. Consequently, different pixel value histograms of images were converted to approximately the same coordinate and height, meaning that the variability in contrast and brightness of images was reduced. As a result of using the Best-Fit tool the software started to count the nuclei of the cells from the threshold 0-5 in all of the color channels, in contrast to the results before using the Best-Fit tool where the starting thresholds differed among the color channels. Nevertheless, a very few cells were counted by the software at the thresholds less than 0-20. Thus, the 0-20 threshold was set as the starting point, and increased by five units to 0-130 (total of 23 range scores), where the number of incorrectly counted cells increased. Then the total cells were automatically counted with each of the 23 thresholds in the red channel which was the best color channel to use for counting the total number of cells (explained in the Results Section). Sensitivity, precision and F-score were calculated to compare changes in these parameters as a result of using the Best-Fit tool.

In order to determine the best range scores for counting the total number of cells in other organs (liver, heart and lung), the same procedure as explained above was followed using the Best-Fit tool in the red channel on three areas on each of three new kidney, liver, heart and lung slide images. The best range scores for counting the total number of cells in each organ was determined based on the estimated sensitivity, precision and F-score values in each range score.

2.2.4 Degree of similarity among different areas of a slide

The degree of similarity among different areas of a slide was measured by comparing similarities in pixel intensities (pixel values) of those areas on the same image. Each pixel has a color intensity value, which ranges from zero (the darkest) to 255 (the lightest) and is called pixel value. The software calculates the mean, standard deviation, minimum, maximum and the sum of pixel values in each pre-determined area using the option "Histogram" of the "Measure" tool. Three areas on each of the previously used five kidney slide images were selected for analysis: top-left, top-right and bottom right. The dimension of each area was 510 x 380 pixels (a total of 193,800 pixels/area).

2.2.5 Statistical analysis

Four analyses were performed to identify the best software set up for counting the total number of cells using SAS 9.4 for Windows (SAS Institute Inc., Cary, NC). First, sensitivity, precision and F-score for each of the range scores of each color channel (17 range scores for the red, and 14 for blue and green) were calculated on each of the five kidney images. The maximum values of sensitivity, precision and F-score were determined and differences among the three color channels for the maximum values were tested using the ANOVA procedure. Multiple comparison of means was performed using the Tukey test. Standard deviation and coefficient of variation of the maximum values for each color channel were calculated by the PROC MEANS. In order to find the range score where both sensitivity and precision were high, the difference between sensitivity and precision at various range scores were calculated for each color channel, and the number of individuals

for which the difference fell within 0-0.05, 0-0.10 and 0-0.15 were counted. Second, the residual sums of squares of Loess procedure with the smoothing parameters of 0.1, 0.3, 0.6 and 0.9 were used to find the effect of using the Best-Fit tool on reducing the variations among slides in the red channel. Third, in order to find the range score with the highest value of sensitivity, precision and F-Score in the red channel with the Best-Fit option for measuring the total number of cells in each of the four organs (kidney, liver, heart and lung), means of sensitivity, precision and F-Score of the nine slides of each organ at each of the 23 range scores were calculated. To find the range score with the lowest difference between sensitivity and precision, the means of absolute differences between sensitivity and precision at each range score were calculated. The Loess procedure with the smoothing parameters of 0.1, 0.3, 0.6, and 0.9 was also used to confirm the findings explained above. Fourth, to determine the degree of similarity among different parts of each slide Spearman's rank correlation coefficients were calculated for the mean pixel values on all pairs of measurements on each slide.

2.3 Results

2.3.1 Finding the best color channel

The total number of normal and infiltrated cells which were manually counted on each of the five kidney images were 296, 302, 318, 322 and 342. The means of maximum sensitivities across the range scores were not statistically different among the three color channels (P=0.29), although the red channel had the largest value (Table 2.3.1). Differences among the three color channels were significant for the mean of maximum precision (P<0.01) and maximum F-score (P=0.014). The mean of maximum precision in the blue

channel was significantly lower than that in the red channel, but was comparable with the mean of maximum precision in the green channel. The mean of maximum F-score was significantly higher in the red channel compared with those in the blue and green channels, which were not statistically different. Variations among the five slides for the maximum sensitivity, precision and F-scores in the red channel were between 6- and 23-fold smaller than those in the blue channel and between 6.5- and 11-fold smaller than those in the green channel, as indicated by their standard deviations and coefficients of variation (Table 2.3.2).

Table 2.3.1 Means of maximum sensitivity, precision and F-score of the three color channels¥

Color channel	Max. Sensitivity	Max. Precision	Max. F-score
Blue	0.812a	0.916 a	0.793a
Green	0.797a	0.960ab	0.797a
Red	0.953a	0.994b	0.962b
Root Error Mean Square	0.165	0.028	0.086

¥Means followed by different letters are different at P<0.05

Table 2.3.2 Standard deviation (SD) and coefficient of variation (CV) for maximum sensitivity, precision and F-score in the three color channels.

Color channel	Max. sensitivity		Max. precision		Max. F-score	
	SD	CV	SD	CV	SD	CV
Blue	0.199	24.62	0.043	4.65	0.106	13.31
Green	0.202	25.37	0.021	2.24	0.105	13.26
Red	0.031	3.29	0.002	0.20	0.013	1.35

The number of individuals for which the difference between sensitivity and precision at each range score fell within 0-0.05, 0-0.10 and 0-0.15 are shown in Table 2.3.3. For the red channel, differences between sensitivity and precision were lower than 0.15 in all five slide images in the range scores 28 to 32, except for the range score 31 with four

images. The differences in four of the five images were less than 0.10 in the red channel corresponding to range scores 29 to 32. There was no range score where difference between sensitivity and precision for all the five images were lower than 0.15 for the green and blue channels. In the blue channel, the estimates of the differences were lower than 0.15 in three of the five images in range scores 33, 35 and 36. The differences were lower than 0.15 in three images in the green channel (range score 14). Overlaid distributions of sensitivities and precisions of a typical slide for each of the three color channels are shown in Fig. 2.3.1a for the blue, Fig. 2.3.1b for the red and Fig. 2.3.1c for the green channels.

Table 2.3.3 Number of observations according to the magnitude of difference between sensitivity and precision at different range scores

Red channel				Green channel				Blue channel			
Range score	0 to 0.05	0 to 0.10	0 to 0.15	Range score	0 to 0.05	0 to 0.10	0 to 0.15	Range score	0 to 0.05	0 to 0.10	0 to 0.15
27	1	2	4	13	0	1	2	33	1	1	3
28	2	3	5	14	1	2	3	34	0	1	2
29	1	4	5	15	1	2	2	35	0	1	3
30	2	4	5	16	0	1	2	36	1	2	3
31	2	4	4								
32	3	4	5								

2.3.2 The effects of using the Best-Fit tool

Of the four smoothing parameters (0.1, 0.3, 0.6, 0.9) which were tested by the Loess plots of sensitivity, precision and F-score of the red channel against the range scores, the 0.1 parameter generated the lowest residual sums of squares for both before and after the Best-Fit tool. Using the Best-Fit tool reduced the residual sums of squares of the Loess plots for sensitivity, precision and F-score against the range scores by 5.95-, 7.21- and 6.78-fold, respectively (Table 2.3.4). The reduced variations are also evident on the Loess plots

with the smoothing parameter of 0.1 before and after using the Best-Fit tool for estimated sensitivity (Fig. 2.3.2a vs Fig. 2.3.2b), precision (Fig. 2.3.2c vs Fig. 2.3.2d) and F-score (Fig. 2.3.2e vs 2.3.2f).

Table 2.3.4 Residual sums of squares of sensitivity, precision and F-score of the red channel before and after using the Best-Fit tool obtained from the Loess plot analysis with the smoothing parameter of 0.1.

Measurement	Sensitivity	Precision	F-score
After using the Best-Fit tool	0.59	0.29	0.47
Before using the Best-fit tool	3.51	2.09	3.19
Fold changed	5.95	7.21	6.78

2.3.3 Finding the best range score for different organs

The total number of normal and infiltrated cells which were manually counted on the nine images in the red channel after using the Best-Fit tool was 2946, 1875, 936 and 2977 on the kidney, liver, heart and lung slides, respectively. Estimates of sensitivity, precision and F-score over the range scores for the heart, kidney, liver and lung are shown in Fig. 2.3.3a, 2.3.3b, 2.3.3c and 2.3.3d, and the corresponding absolute differences between sensitivity and precision are shown in Fig. 2.3.4a, 2.3.4b, 2.3.4c and 2.3.4d. For all organs, sensitivity estimates increased as range score increased, reached a peak and then declined, whereas estimates of precision were 100% at low range scores, then declined at the high range scores. The opposite direction of changes in sensitivity and precision as a result of increments of the range scores necessitates finding a range score where both measurements were large, and at the same time difference between sensitivity and precision was low. For the heart, both sensitivity and precision were greater than 0.90 at range scores 14 and 15, where F-score was also greater than 0.90 (Fig.2.3.3a) and absolute differences between sensitivity and precision were less than 0.15 (Fig. 2.3.4a, Table 2.3.5). The range

score (grayscale threshold) 15 (0-90) was selected for this organ. For the kidney, both sensitivity and precision were greater than 0.85 at range scores 14 to 20, and F-score estimate was greater than 0.85 at the range scores 11 to 20, with the highest estimates for all measurements at range scores 14 and 15 (Fig. 2.3.3b). The absolute differences between sensitivity and precision were less than 0.10 at the range scores 14 to 21 (Fig.2.3.4b, Table 2.3.5), and range score 15 (0-90) was selected as the best for this organ. For the liver, both sensitivity and precision were greater than 0.85 at the range scores 11 to 13, and F-score estimates were greater than 0.85 at the range scores 10 to 16 (Fig. 2.3.3c).

The absolute differences between sensitivity and precision in the liver were less than 0.10 at the range scores 11 and 12 (Fig. 2.3.4c, Table 2.3.5), and range score 11 (0-70) was selected as the best for this organ. The greatest estimates of sensitivity and F-score for the lung were lower than those in other organs. Both sensitivity and precision were greater than 0.75 at range scores 4 to 18, and F-score estimates were greater than 0.75 at the range scores 4 to 17 (Fig. 2.3.3d). The absolute differences between sensitivity and precision were less than 0.10 at the range scores 13 to 17 (Fig. 2.3.4d, Table 2.3.5). The best range score selected for the lung was 13 (0-80), although estimates of sensitivity, precision and F-scores were smaller than those in the other organs. The Loess plots (Fig. 2.3.5a, 2.3.5b, 2.3.5c and 2.3.5d) show the scatter plots and the local regression of sensitivity, precision and F-scores for each organ, and confirm the findings explained above.

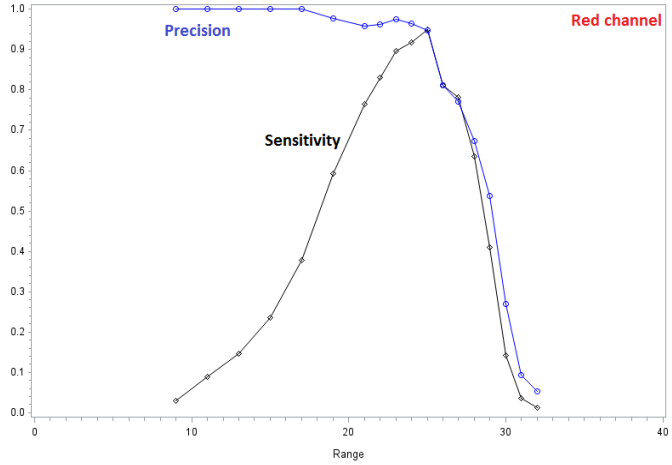

(a)

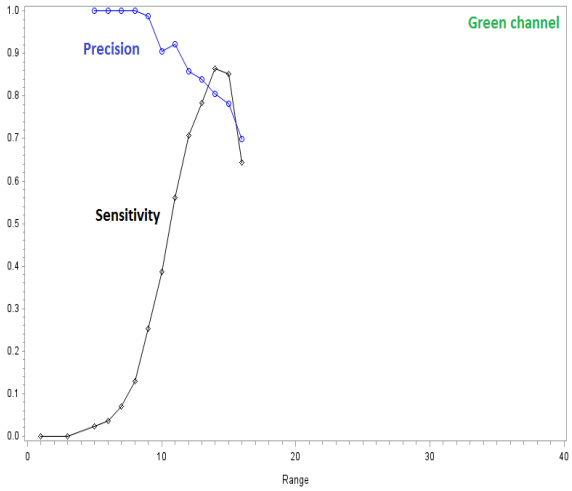

(b)

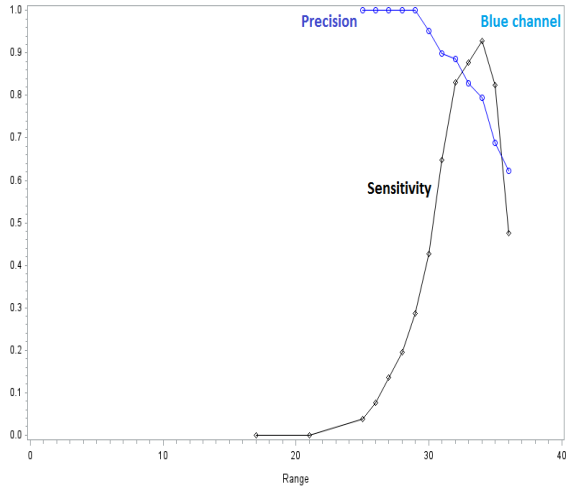

(c)

Figure 2.3.1 Sensitivities and precisions of typical images in the red (a), green (b) and blue (c) channels.

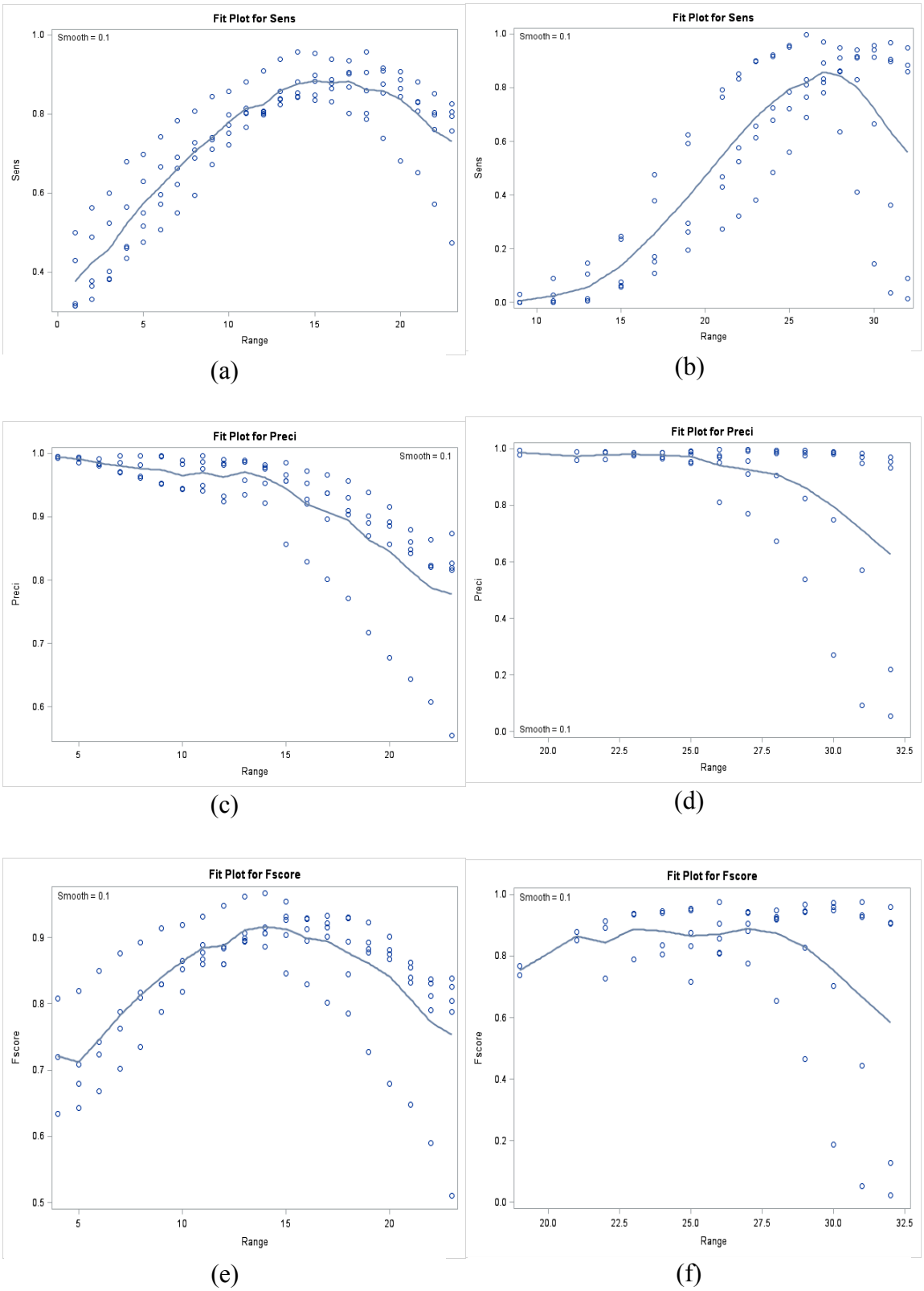

Figure 2.3.2 Sensitivities (a and b), precisions (c and d) and F-scores (e and f) before (b, d and f) and after (a, c and e) using Best-Fit tool, smoothing parameter 0.1.

Table 2.3.5 Range scores where sensitivity, precision and F-score estimates were high for each of the four organs, and range scores where absolute differences between sensitivity and precision were smaller than 0.10 and 0.15.

Organ	High estimates	Range score of high sensitivity and precision	Range scores of high F-score	Absolute difference less than 0.10	Absolute difference less than 0.15
Heart	>0.90	14-15	13-17	13	12-21
Kidney	>0.85	14-20	11-20	14-21	12-23
Liver	>0.85	11-13	10-16	11-12	10-16
Lung	>0.75	4-18	4-17	13-17	11-23

2.3.4 Degree of similarity among different areas of a slide

Pixel values on the three areas on each of the five kidney slide images ranged between 0 and 255 on every measurement, with means ranging from 128.05 to 172.08 and sum of pixel values ranged between 25,200,000 and 33,800,000. Means of the three measurements of mean pixel values estimated by the software varied within a narrow range of 138.34 and 161.58 among slides, with comparable estimates of standard deviations (9.16 to 15.89), which resulted in small and comparable coefficients of variation (Table 2.3.6). Means of pixel values of the three areas on each slide also varied within narrow ranges, but coefficients of variations were greater than those among slides (Table 2.3.6). Spearman's rank correlation coefficient between top-left and top-right, top-left and bottom-right, top-right and bottom-right were 0.90 (p=0.037), 0.70 (p=0.188), and 0.90 (P=0.037), respectively.

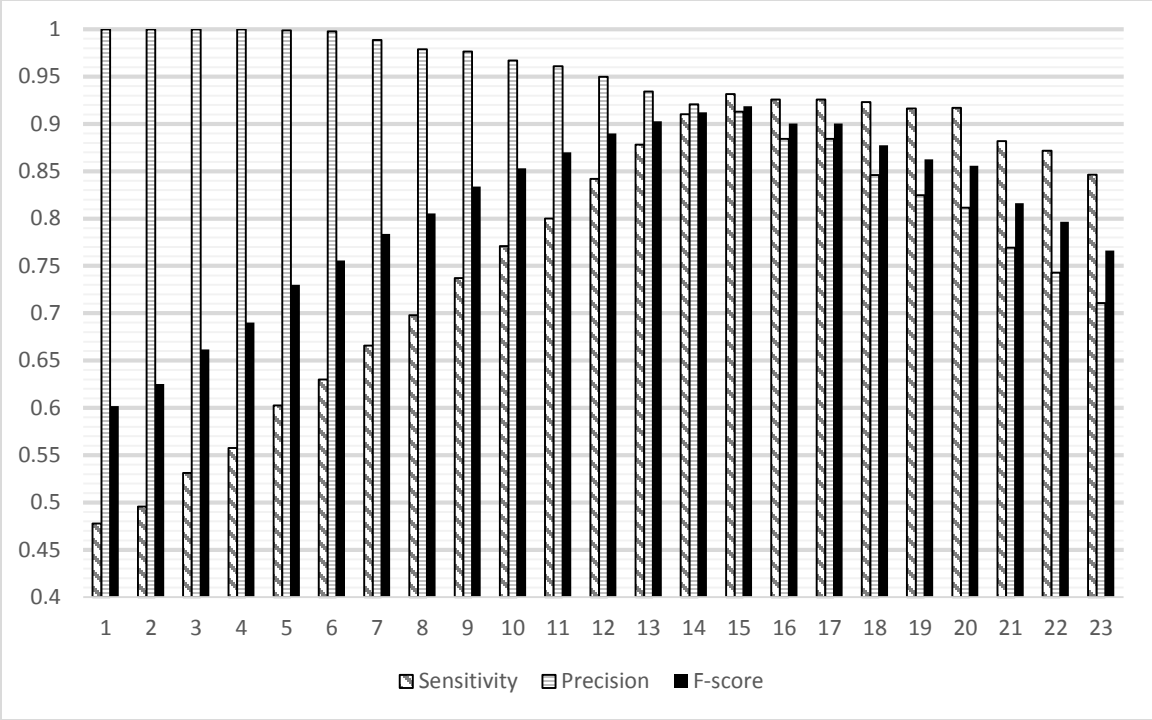

Figure 2.3.3a Means of sensitivity, precision and F-score of nine areas over the 23 range scores in the heart.

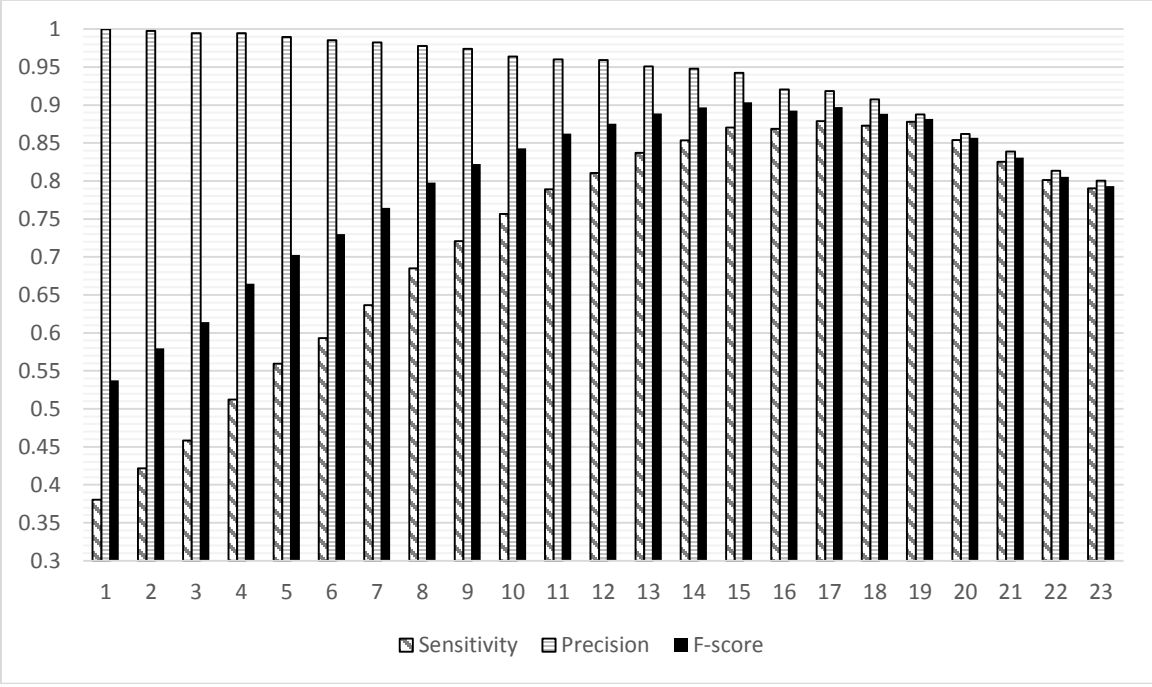

Figure 2.3.3b Means of sensitivity, precision and F-score of nine areas over the 23 range scores in the kidney.

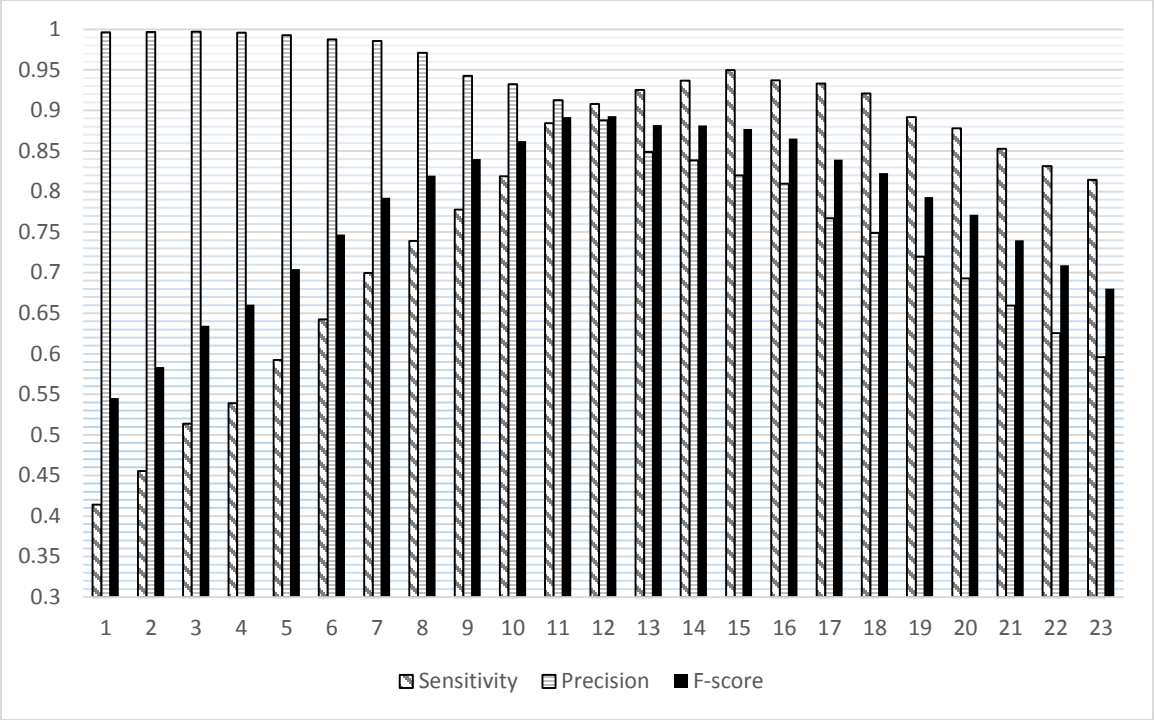

Figure 2.3.3c Means of sensitivity, precision and F-score of nine areas over the 23 range scores in the liver.

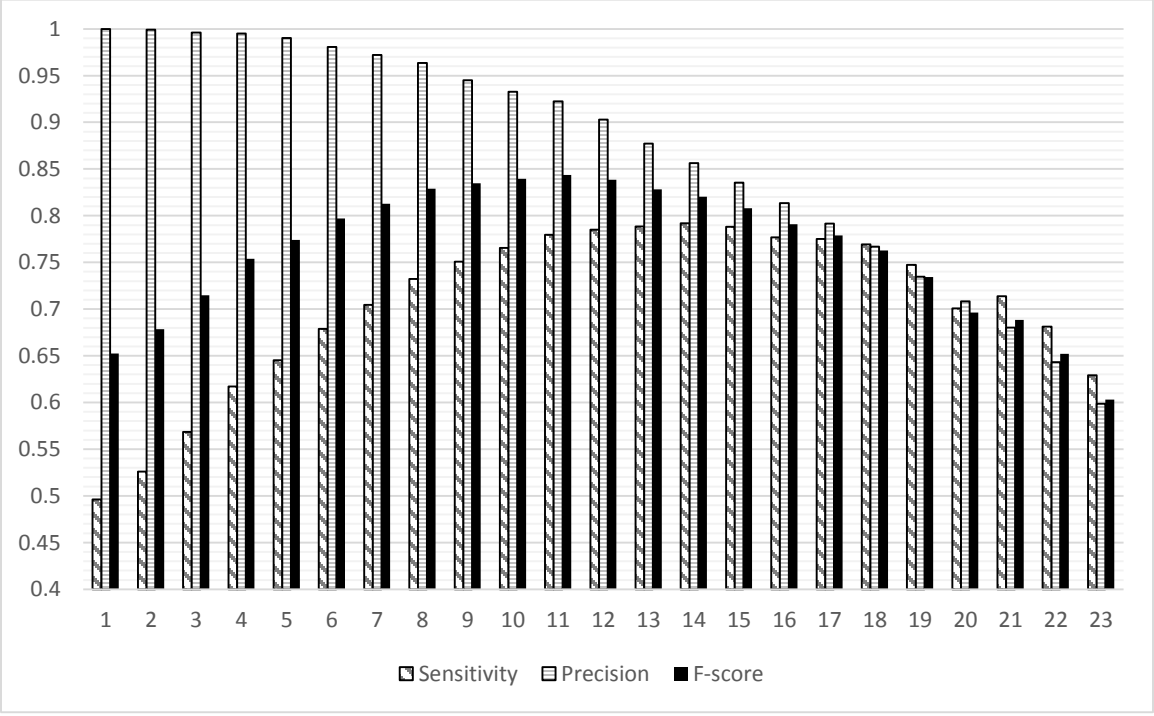

Figure 2.3.3d Means of sensitivity, precision and F-score of nine areas over the 23 range scores in the lung.

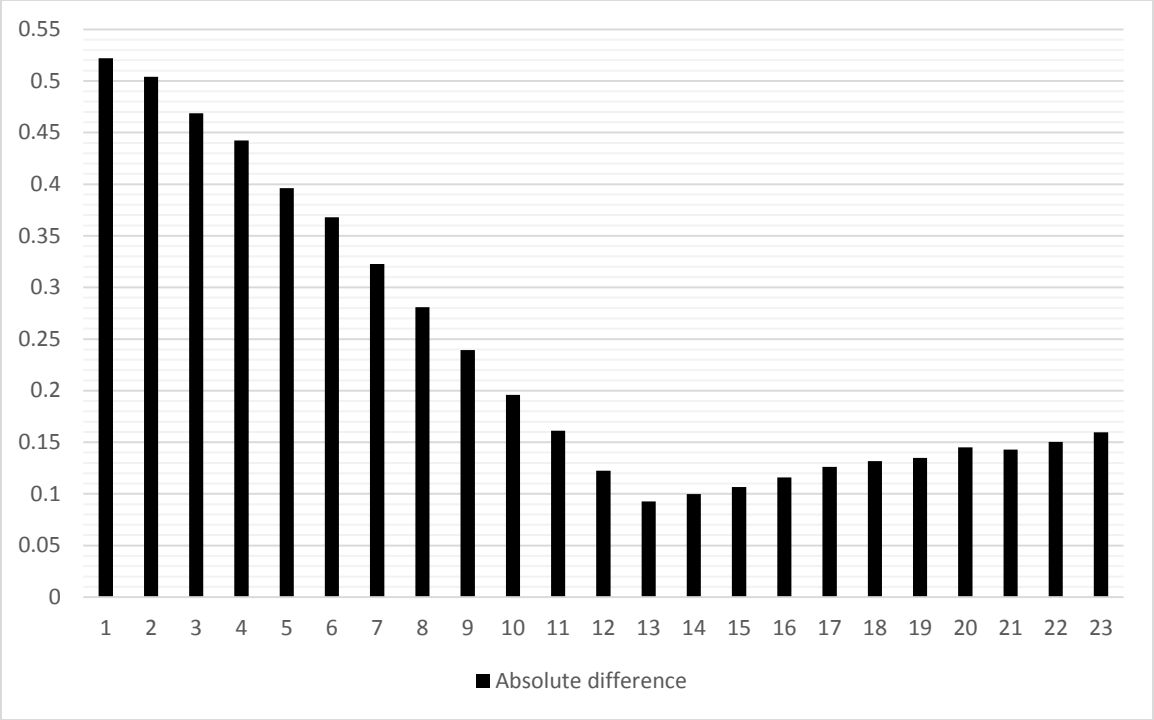

Figure 2.3.4a Means of absolute differences between sensitivity and precision within 23 range scores for nine areas on the heart slides.

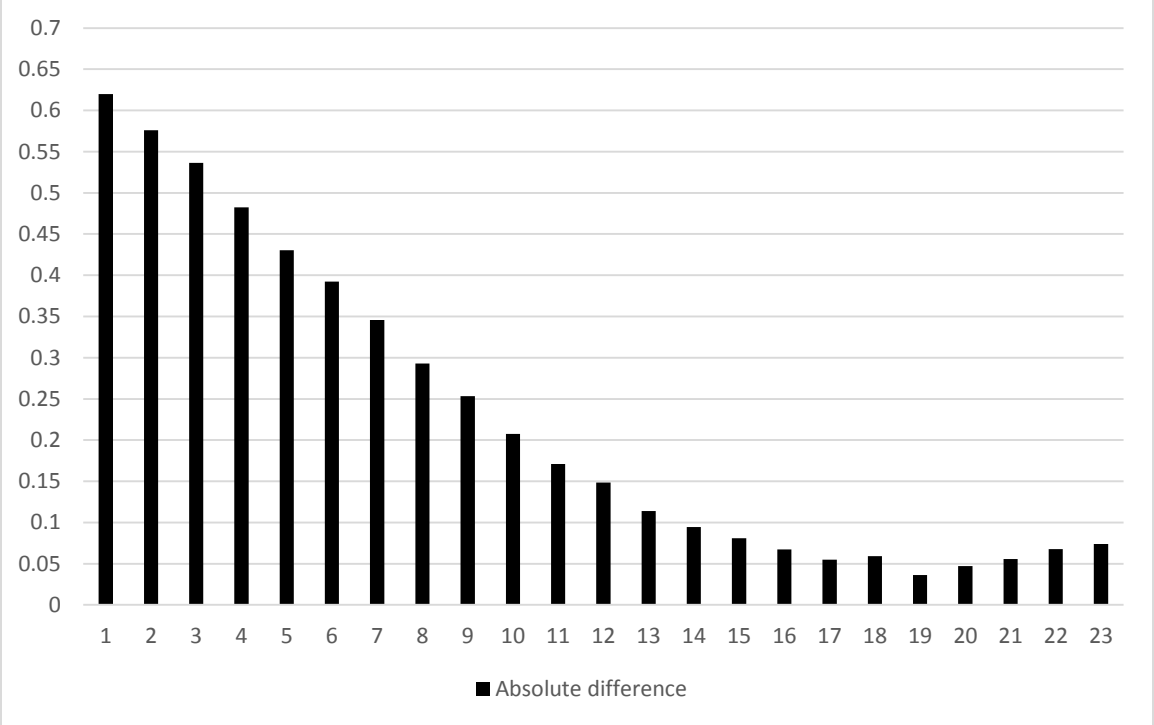

Figure 2.3.4b Means of absolute differences between sensitivity and precision within 23 range scores for nine areas on the kidney slides.

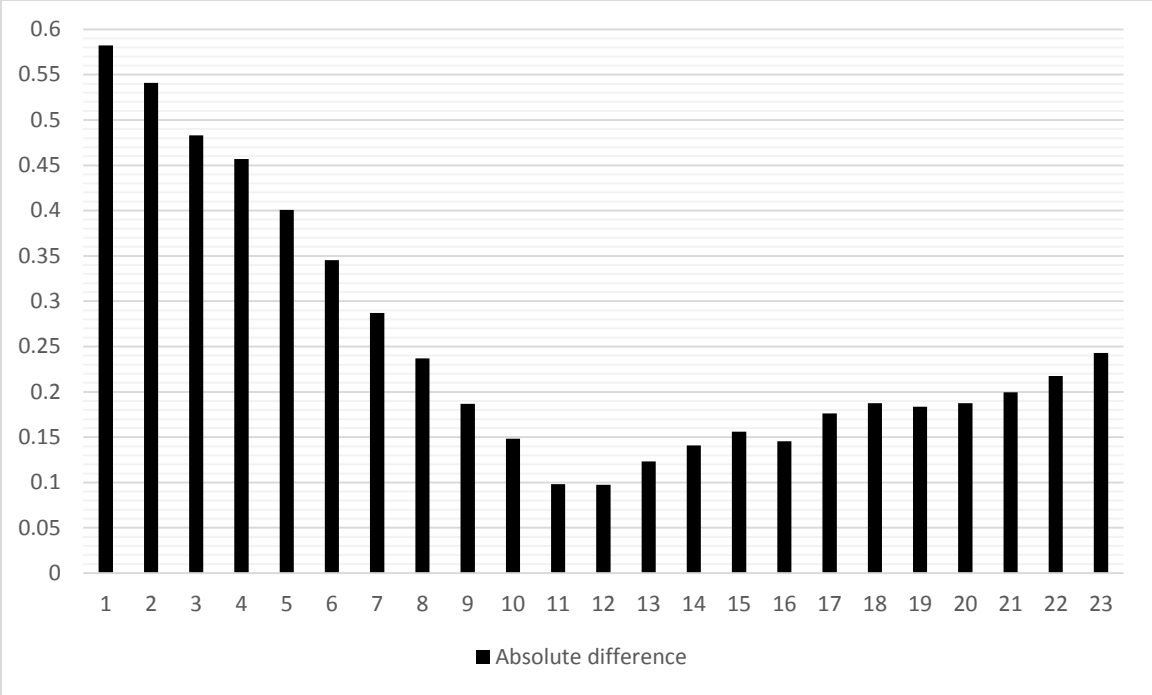

Figure 2.3.4c Means of absolute differences between sensitivity and precision within 23 range scores for nine areas on the liver slides.

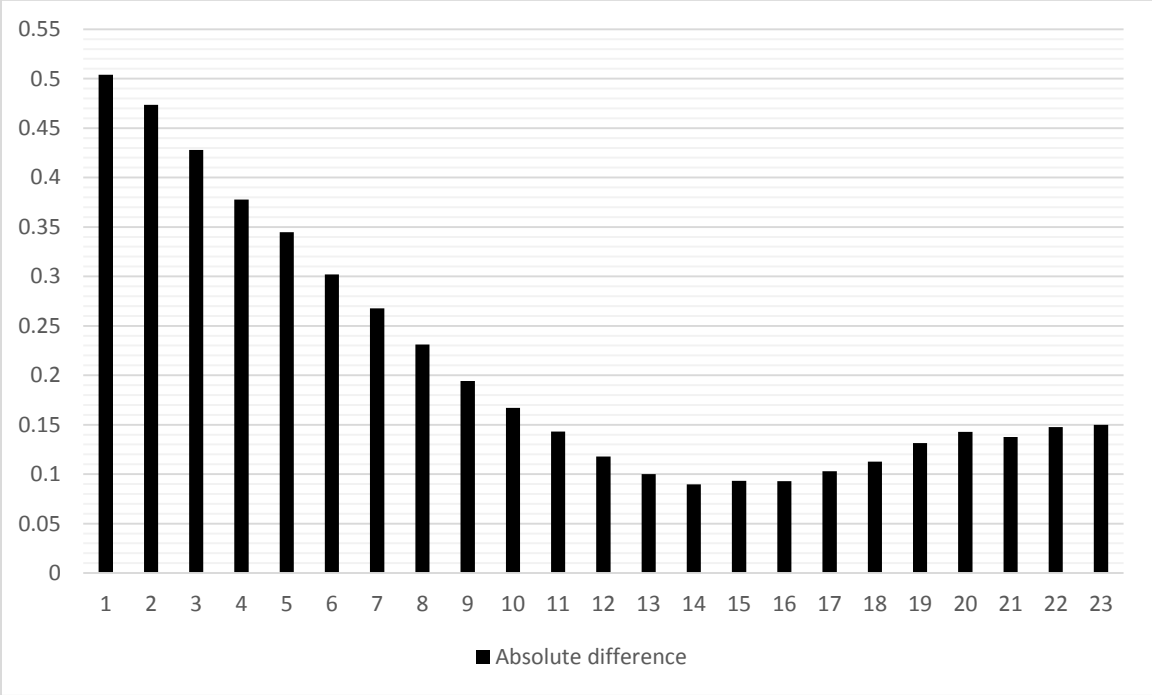

Figure 2.3.4d Means of absolute differences between sensitivity and precision within 23 range scores for nine areas on the lung slides.

Table 2.3.6 Descriptive statistics of pixel values of the five kidney slides and the three areas with each slide.

Slide number	Within slides			Within area	
	Mean	SD	CV	Range of means	Range of CV
1	147.88	15.76	10.6	131.92 – 163.44	30.7-46.8
2	138.34	9.16	6.6	128.05 – 145.60	29.6-33.1
3	158.65	11.38	7.2	145.53 – 165.90	29.4-34.2
4	161.58	11.52	7.1	149.25 – 172.08	30.1-32.3
5	155.14	15.89	10.2	137.05 – 166.88	32.0-38.9

SD: Standard deviation
CV: Coefficient of variation

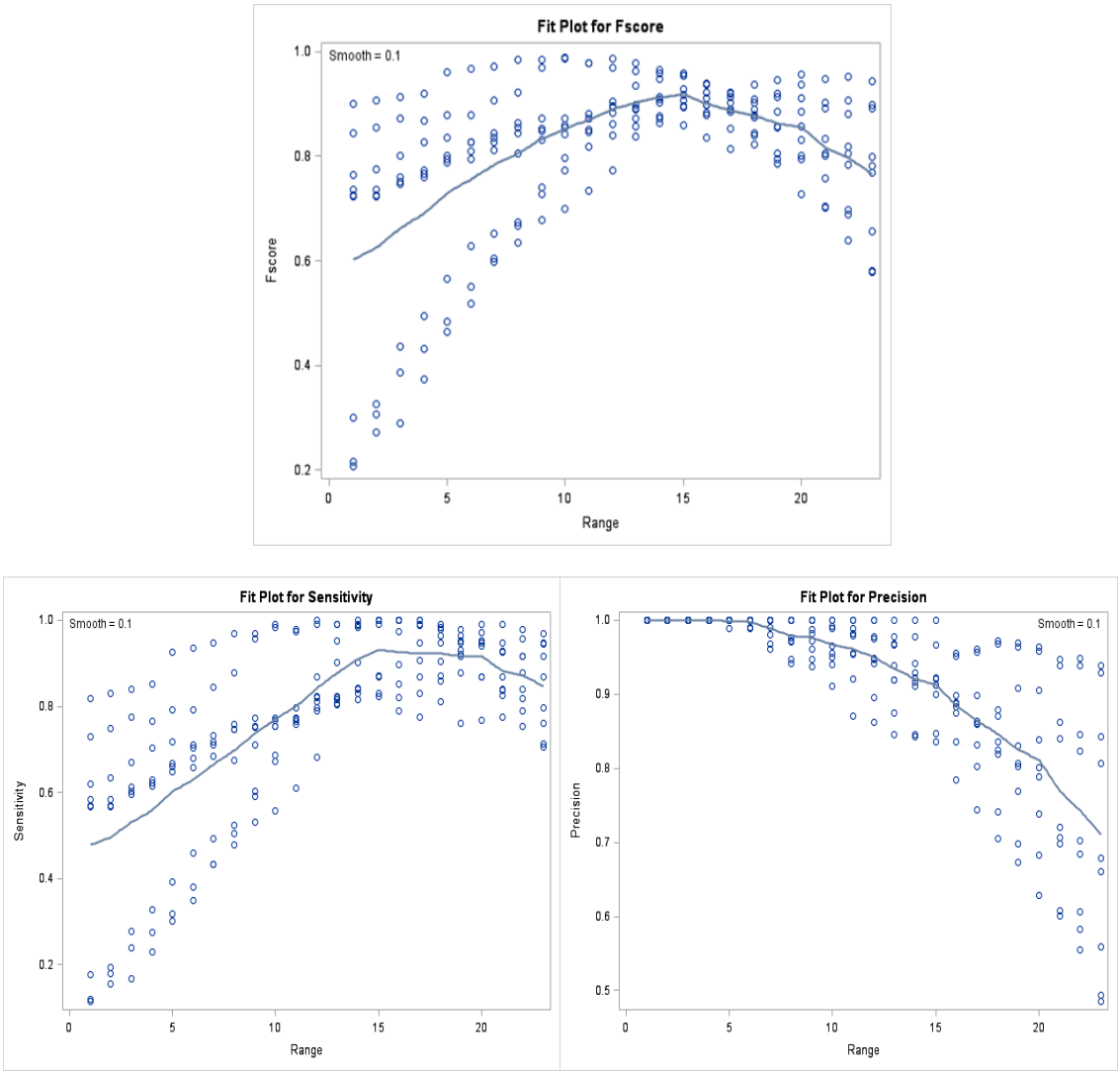

Figure 2.3.5a Sensitivity, precision and F-score at different range scores for nine areas on heart slide images in the red channel.

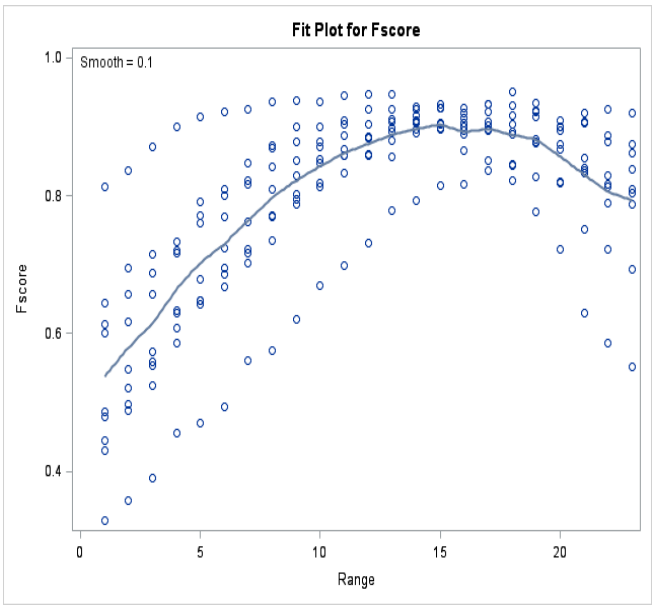

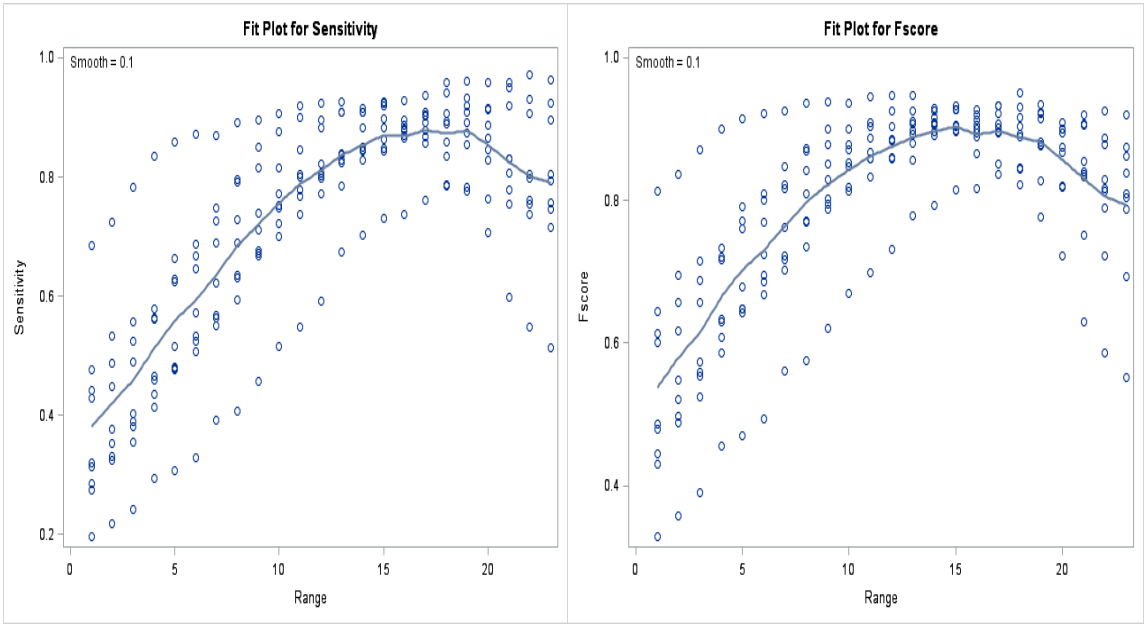

Figure 2.3.5b Sensitivity, precision and F-score at different range scores for nine areas on kidney slide images in the red channel.

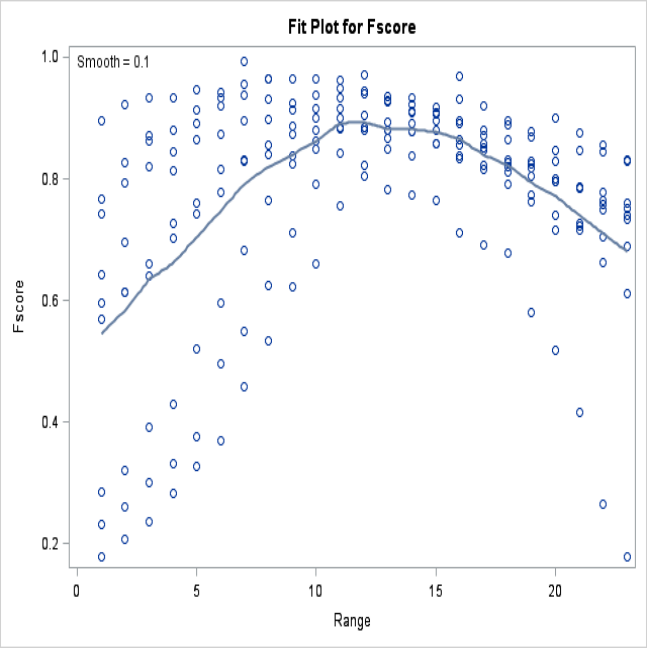

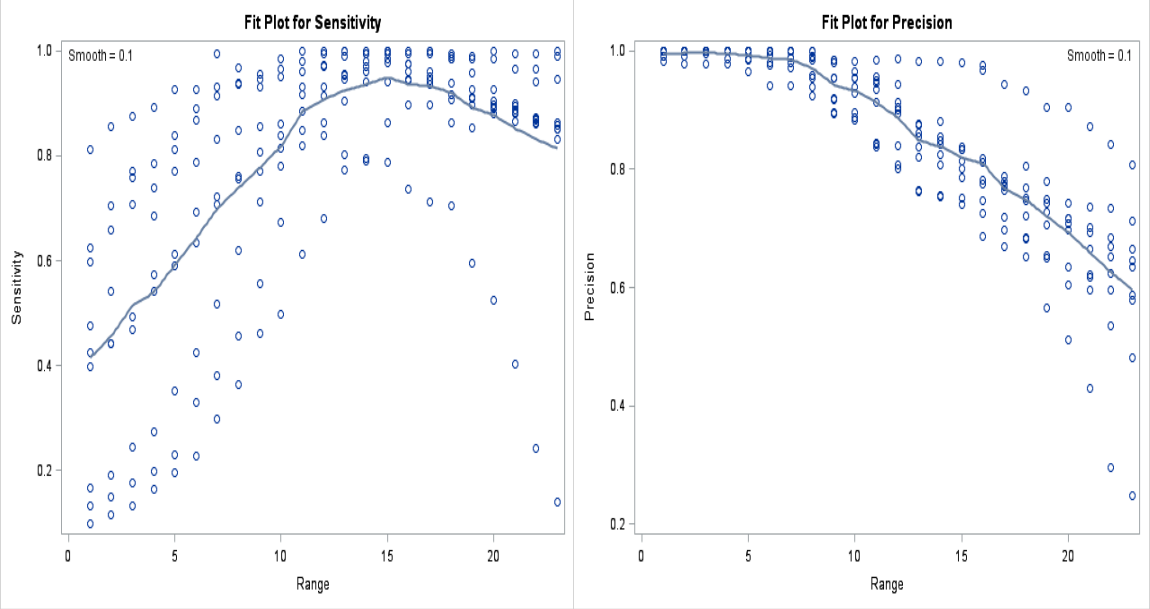

Figure 2.3.5c Sensitivity, precision and F-score at different range scores for nine areas on liver slide images in the red channel.

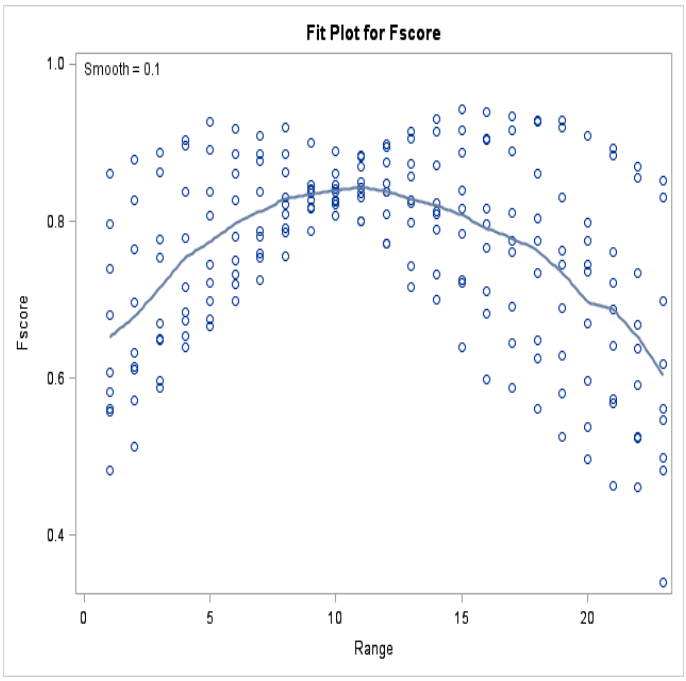

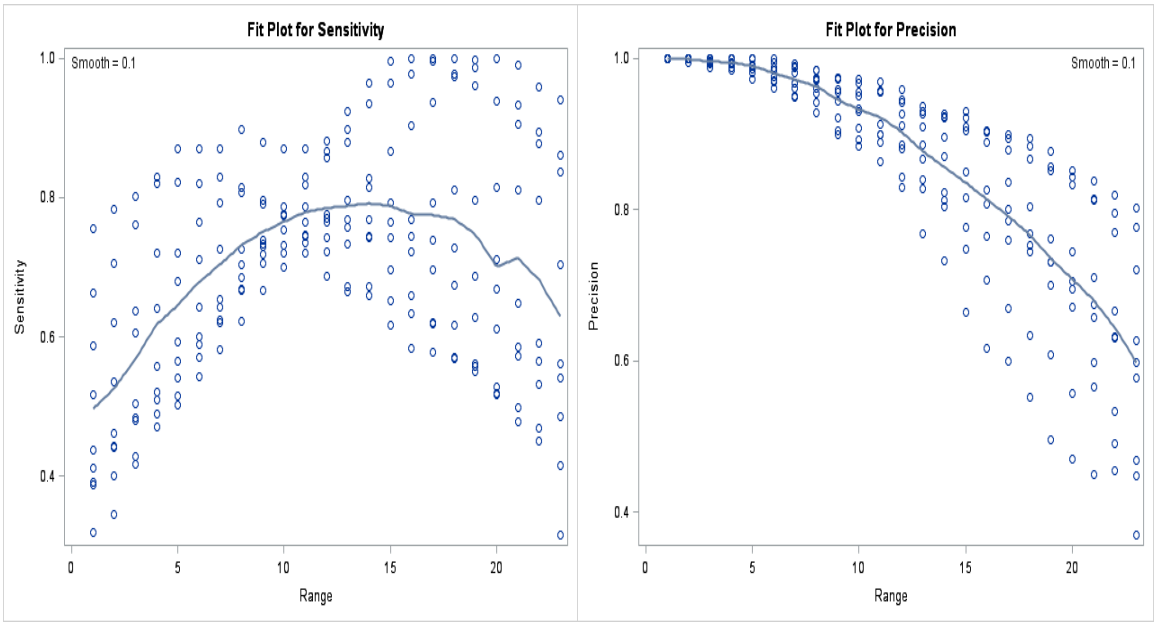

Figure 2.3.5d Sensitivity, precision and F-score at different range scores for nine areas on lung slide images in the red channel.

2.4 Discussion

The extent of infiltrated mononuclear cells in different organs of mink is the most accurate measure of the severity of the disease in AMDV-infected mink (Henson et al.,

1976). To date, almost all of the published papers on histopathological evaluations of AMDV-infected mink were based on subjective visual methods (Leader et al., 1963; Henson et al., 1966; Farid and Ferns, 2011, 2017; Jensen et al., 2016), where the severities were evaluated based on a visual scoring method of zero to four. There is only one published report that applied a visual method for calculating the percentage of renal cortical tubules and interstitium replaced by plasma cells and lymphocytes on kidney slides stained with H&E from AMDV-infected mink (Jackson et al., 1996). There is also one report on the use of an automated digital evaluation on morphology and differential morphometry of glomerular parameters, and defining various forms of glomerulonephritis in the kidneys of AMDV-infected mink (Nieto et al. 1991). The current study is thus the first attempt to use an automated system to quantify the proportion of infiltrated cells in organs of AMDV-infected mink.

The failure to develop an algorithm for automated counting of infiltrated cells by the Image Pro Plus 7.0 in the current study was because the software was unable to distinguish between the nuclei of normal and infiltrated cells stained with the H&E. A similar result is reported by Rogers et al. (2016), who tried to measure percentage of infiltrated inflammatory cells using an automated DIA method on H&E stained mouse colon slides. To the best of our knowledge, there is only one published report on a successful usage of an image analysis system for counting infiltrated cells after H&E staining (Soltzberg et al., 2011), but the algorithm which was followed for the used DIA software was not reported. IHC stains are the preferred method in evaluating infiltrated cells using DIA (Prasad and Prabhu, 2012), but these methods are expensive ($123/slide, quoted from Animal Health Laboratory, University of Guelph, ON, January 2018)

compared with $12/slide when stained with H&E (NS Department of Agriculture,2017). The IHC staining methods are thus not used in routine evaluation of a large number of samples, similar to the current study. In addition, the histology laboratory at the NS Department of Agriculture is not equipped to perform IHC staining, because it requires antibodies against T cells (CD3, polyclonal), B cells (CD79a –monoclonal or CD20-polyclonal), and plasma cells (MUM-1) specific for mink (Dr. Josepha DeLay, Animal Health Laboratory, University of Guelph, On, Canada, personal communication). Shipment of samples to laboratories outside the province also requires additional expenses.

Although automated counting of the number of infiltrated and normal cells separately was not successful, automatic counting of total number of cells along with manual counting of infiltrated cells would be useful in calculating percentage of infiltrated cells. Even though this procedure required longer assessment time (approximately seven minutes per image), compared with the automatic method of counting each type of cells, yet, it was found to be a useful procedure for an accurate and reproducible evaluation of degree of severity of AD lesions.

The focus of this study then turned to developing an algorithm to use the automatic feature of the IPP 7.0 in order to count the total number of cells on each image, including infiltrated mononuclear cells and normal cells, which was needed for calculating the percentage of infiltrated mononuclear cells. There is no report on automatic counting of all cells on an image stained with H&E with the IPP 7.0. There are a few steps that are usually followed in cases where any type of cell is counted by a DIA software, namely conversion of RGB images to grayscale, using the Best-Fit tool and manual selection of greyscale thresholds, which were followed in the current study as well.

The red channel was selected for the conversion of original color images (RGB) in the current study because it showed the greatest maximum sensitivity, precision and F-score (Table 1.4.1) with the lowest degree of variations among images (Table 1.4.2), compared with green and blue channels. Another important factor that was considered in selecting the red channel was the occurrence of high estimates of sensitivity and precision at almost the same range scores in this color channel, presented as the degree of differences between sensitivity and precision estimates within each of the 23 range scores (Table 1.4.3). This feature is important because occurrence of the high values of sensitivity and precision in almost the same range scores, makes it easier to select a range score for counting the total number of cells by the software.

Most investigators who used H&E (Veta et al., 2013; Yin et al., 2013; Marcos-Graces et al., 2017) or other staining methods (Salinas-Navarro et al., 2009; McGinley and Thompson, 2011) converted RGB images to grayscale, because this procedure increases the contrast between the nuclei and other components of a tissue. The IPP 7.0 generates three grayscale colors, red, green and blue, which can be selected by the user. There is no published report, however, on the comparison among color channels for the accuracy of counting any specific type of cells. Those investigators who did not convert RGB to grayscale on H&E stained slides have not explained how contrast between cell nuclei and other components of tissues were improved (Soltzberg et al., 2011; Castro Souza Junior Neto et al., 2017).

The findings that the Best-Fit tool was beneficial for enhancing the contrast of image components and reducing variations among slides for estimated sensitivity, precision and F-score (Table 1.4.3) in different range scores, is in agreement with the report

of Marcos-Graces et al. (2017) who used the Best-Fit tool in IPP 7.0 software to evaluate slides stained with H&E, Masson's trichrome and Picrosirius red. Johansson et al. (2001) also found the useful effect of the Best-Fit tool for evaluating slides stained with IHC methods.

Each of the four organs had a specific best range score where the estimates of sensitivity, precision and F-score were high, and differences between sensitivity and precision were low (Table 1.4.5). The estimates of sensitivity, precision and F-score were the highest in the heart (>0.90) followed by the kidney and liver (>0.85), and were the lowest in the lungs, which is believed that were the result of differences in type and color of individual cells within each tissue. The performance of the software for the lung was lower than the other organs, which might be because of a naturally lower contrast between the cell nuclei and other tissue components in the lung images.

The opposite direction of changes in sensitivity and precision across range scores was because of the high failure rate of the software in counting the nuclei of cells at the starting range scores (high uncounted), although the ones which were counted were the correct nuclei (true positives) at these range scores. In contrast, at the higher range scores, the software was able to count a greater number of nuclei even though it counted non-nuclei objects as well (incorrectly counted or false positive). Both of these parameters are important when accurate estimates of the total number of cells on an image is needed. In the selected range scores, large estimates of sensitivity indicate that the software missed counting a relatively small number of cells (low false negative or uncounted), and the high estimates of precision indicated that the performance of the software in distinguishing cell

nuclei from other components of the tissues was high (low false positive or incorrectly counted).

Range scores (thresholds) were sometimes selected automatically by the DIA software (Kohlberger et al., 1999; Francisco et al., 2004), but this method cannot be a reliable method to select proper range scores unless the images have high contrast and brightness of color (Johansson et al., 2001). Thus, manually selecting range scores by the operator is a more common method. In some studies, the operator selects certain range scores only based on a visual comparison of the range score results and reference values (i.e. manually counted number of cells) (Soltzberg et al., 2011; Yin et al., 2013; Vasaturo et al., 2017). In other studies (Goedkoop et al., 2005; Prasad and Prabhu, 2012; Soendergaard et al., 2016), however, manually selected range scores are assessed more objectively, based on the degree of correlation between their results and the reference values in order to ensure more reliable outcomes. To the best of our knowledge, the current study is the only study in which 23 different range scores were assessed separately by calculating sensitivity, precision and F-score for each range score.

The rather high Spearman's rank correlation coefficients between the mean pixel values of the three different areas on each of the five kidney images proved that various areas of a slide were not significantly different in term of distribution of cells (Table 1.4.6). Yet, it is logical to recommend to measure three images from different areas of each slide for evaluating tissue slides by the software, because the differences among the three measurements can be used to identify and eliminate an outlier. This would improve the accuracy of slide assessment by DIA and only marginally increases the amount of time needed for evaluating each slide (two minutes for each slide).

New slide scanners that are used in some recent studies (Rizzardi et al., 2012; Laurinavicius et al., 2014; Eriksen et al., 2017) have the ability to scan the whole area of slides in a very short amount of time (Riber-Hansen et al., 2012), but such scanners were not available for this study. Thus, we had to use a high-quality microscope camera for taking images from the slides (Leica DM500-Microscope), which is the most common method of imaging (Brey et al., 2003; Francisco et al., 2004; Goedkoop et al., 2005; Ziabreva et al., 2006; Loughlin et al., 2007; Salinas-Navarro et al., 2009; McGinley and Thompson, 2011; Mostafa et al., 2012; López et al., 2014; von Diemen et al., 2016) because it is a more applicable and inexpensive method compared to automatic slide scanners. The protocols for using microscope cameras, however, should be standardized and identically followed for all of the slides.

Chapter 3. Relationships between the severity of histopathological and serological measurements in AMDV-infected mink.

3.1 Literature review

3.1.1 Aleutian disease in mink

Aleutian disease is a chronic and persistent viral infection of American mink (*Neovison vison*) caused by Aleutian Mink Disease Virus (AMDV), *Carnivore amdoparvovirus 1*, a member of the family *Parvoviridae*, subfamily *Parvovirinae*, genus *Amdoparvovirus* (Cotmore et al., 2014). The disease was first identified in the Aleutian coat color mink, which was a new color mutant of mink that happened unexpectedly on a mink ranch in the USA in the early 1940's (Best and Bloom, 2006). AMDV is a single-stranded DNA virus with a 4801 base pair genome that has similar structure to other autonomous parvoviruses. The virus can be transmitted horizontally via urine, feces and saliva or vertically from mother to kits (Bloom et al., 1994).

Two different forms of AD are defined based on the occurrence of the infection in newborn or adult mink. Clinical signs in neonatal mink appear in less than 14 days post-inoculation (dpi), including an acute interstitial pneumonia that results in lethal respiratory distress as a result of a huge amount of the virus in alveolar type II pneumocytes. The reason for that is the tendency of parvoviruses towards fast proliferating cells in the host, such as type II pneumocytes, during the viral replication stage. Type II pneumocytes are responsible for producing pulmonary surfactant thus, their infection by AMDV results in surfactant deficiency, dysfunction of the respiratory system and death in the neonatal mink (Bloom et al., 1994). Survivor kits, however, exhibit a different form of the disease, called the adult form. Maternal passive immunity also affects the form of the disease in infected

kits, meaning that the kits from seropositive dams show the adult form of the disease instead of the respiratory distresses (Bloom et al., 1994). The adult form, also called classical AD, is a pleomorphic disease mostly because of an intensive immune response of the animal to replication and sequestration of AMDV. The outcomes of the classical AD are influenced by the virus strain and the genotype of the infected mink, resulting in three different patterns of the disease, (a) progressive; (b) persistent, non-progressive; and (c) non-persistent, non-progressive infection. According to this classification, the infection does not always lead to a progressive disease, and some animals can either tolerate the virus or clean it from their body (Bloom et al., 1994). The pathogenicity of the virus influences the progression and severity of the AD, i.e. pathogenic strains replicate faster and result in the earlier progression of AD symptoms compared to less pathogenic strains (Oie et al., 1996; Stevenson et al., 2001). Susceptibility of the mink to the infection differs between Aleutian and non-Aleutian mink and also among individuals within the same color types (Bloom et al., 1975). Generally, the less susceptible genotypes to the progressive AMDV-infection are non-Aleutian genotypes (Johnson et al., 1975; Hadlow et al., 1983).

3.1.2 Mink immune response to AMDV-infection

The virus propagates and reaches a peak level by around 10 dpi (Bloom et al., 1994; Farid et al., 2015). In adult mink, macrophages and Kupffer cells of the liver are believed to be the primary sites of viral replication (Porter, 1986). Thus, the virus is concentrated in organs that are rich in macrophages such as lymph nodes, spleen and bone marrow (Bloom et al., 1994) and in the liver, where the Kupffer cells are located (Porter, 1986). Virus replication significantly decreases by around 60 dpi (Alexandersen et al., 1988), but the

virus is still detectible in most organs by PCR (Jensen et al., 2014). It is believed that in this stage the virus follows either a restricted type of replication or becomes sequestrated inside the infected macrophages, as it is found in the cytoplasm of the macrophages and not in the nucleus (Alexandersen et al., 1988). As a result of reduced virus replication, many infected mink are no longer viremic sometimes after infection, and the virus not detectable in their blood stream by polymerase chain reaction (PCR) (Jensen et al., 2014). One of the significant manifestations of AMDV-infection is plasma cell proliferation (plasmacytosis), which is the symbol of AD (Bloom et al., 1994). Mature plasma cells develop via two different pathways, either through a chain of cell differentiation in lymphoid organs or conversion of B-lymphocytes in various organs (Thomson, 1984). Plasma cells are terminally differentiated white blood cells (WBC) responsible for production and storage of antibodies (Minges Wols, 2005), and their presence in tissues is an indication of humoral immune response to an antigen. Generally, soon after the initiation of the infection and movement of an antigen from the site of infection to a lymph node, B-lymphocytes start producing antibodies against the antigen in that lymph node (Thomson, 1984). The B-lymphocytes then move from the lymph node to the target tissues via blood or lymph, where they differentiate to plasma cells and reside for life (Minges Wols, 2005). Various factors, such as tissue-specific adhesion molecules and chemokines, are believed to control migration and infiltration of the antibody secreting cells in tissues (Kunkel and Butcher, 2003).

Anti-AMDV antibodies are produced soon after infection and can be detected by counter-immunoelectrophoresis (CIEP). Reports on the time of early detection of Anti-AMDV antibodies differ among the studies, from five dpi (Best and Bloom, 2006) to two

to three week post-inoculation (wpi) (Farid et al., 2015; Jensen et al., 2016). Antibody titer then reaches a peak level by 6 to 8 wpi (Bloom et al., 1994). The kinetics of antibody production are influenced by several factors, including mink color type and virus strain. Thus, antibody titer may decrease, remain almost constant or increase in different mink (Bloom et al., 1994). Despite the high concentrations of circulating antibodies against AMDV, they are incapable of neutralizing the virus, rather, the virus and antibodies attach and form infectious immune complexes. These complexes block capillary arteries, cause inflammation and contribute to formation of a substantial portion of AD symptoms in infected mink. In contrast to most other viral diseases, antiviral antibodies can enhance the ability of AMDV to penetrate and infect macrophages by using their cellular Fc receptors, a process which is called antibody dependent enhancement of infection (Best and Bloom, 2006).

AMDV-infection also changes the blood protein profile of the mink. Electrophoretic separation of serum proteins (albumins, alfa-, beta- and gamma-globulin) from infected mink showed a progressive elevation in serum gamma-globulin levels during the course of the infection (Bloom et al., 1994), which is the hallmark of AD in adult infected-mink (Best and Bloom, 2006). Although the portion of anti-AMDV antibodies in the elevated gamma-globulins is not known, it is obvious that AMDV is the cause of overproduction of immunoglobulins (Table and Ingram, 1970). A relatively high coefficient of correlations between anti-AMDV antibody titer and gamma-globulin levels have been reported (Bloom et al., 1975; An and Ingram, 1977). In a study by Bloom et al, (1975) on inoculated sapphire and pastel mink, the coefficient of correlation between anti-AMDV antibody titers, measured by CIEP test, and serum gamma-globulin levels,

measured by electrophoresis on cellulose acetate, reported as good, which was 0.75. An and Ingram (1977), also, reported a high coefficient of correlation of 0.81 between the anti-AMDV antibody titers, measured by CIEP test, and serum gamma-globulin levels, measured by electrophoresis on cellulose acetate, of 74 naturally infected pastel mink. Serum gamma-globulin levels in the infected mink can rise to more than 30 mg/mL and account for 50% of total serum proteins (Best and Bloom, 2006). The increase in globulins is associated with a decrease in albumin in order to adjust the blood viscosity (Porter et al., 1980). Thus, the serum albumin:globulin ratio will drop from 1.3 g/100 mL in a normal mink to 0.6 g/100 mL in an infected mink.

The cellular (non-humoral) immune response of mink to AMDV-infection has not been properly defined because mink are outbred animals, and specific reagents for evaluating WBCs responsible for cellular immune response are restricted (Best and Bloom, 2006). In a review paper, Best and Bloom (2006) indicated that although the number of $CD4^+$ (helper) T cells in the body stays at the normal level during the infection period, the number of $CD8^+$ (cytotoxic) T cells increases and they infiltrate into tissues. $CD4^+$ T cells are responsible for helping B cells in detecting the virus and producing antibodies against it. $CD8^+$ T cells, and to lesser extent monocytes, are responsible for producing interferon (INF)-γ, a cytokine detectable in blood as early as two wpi. Other cytokines produced in response to AMDV-infection are interleukin (IL)-4 (produced by $CD8^+$ T), IL-8 (produced by monocytes) and IL-6 (produced by infected macrophages). Increment of IL-4 and IL-6 levels result in increased differentiation of B-lymphocytes to plasma cells and consequently the plasmacytosis.

For better understand the AD, attempts were made to compare the disease with other autonomous parvovirus infections in other species. B19 is the only autonomous parvovirus that can cause infection in humans, and its characteristics were compared with AMDV in a review by Best and Bloom (2005). They stated that the most remarkable similarity between AMDV and B19 infections is the important role of the humoral immune response in the pathogenesis of these diseases. The non-structural protein (NS1) of the B19 is capable of trans-activating the promoter of IL-6, which may have the same function in AMDV. In addition, the AMDV genome carries three copies of CTGGGA sequence, known as the IL-6 responsive enhancer element, which is believed to have an important role in IL-6 production. It has been hypothesized that the overproduction of IL-6 has a significant role in the development of plasmacytosis in AMDV-infected mink, the same situation as in Castleman's disease, caused by the Human Herpesvirus (HHV)-8, and in Cutaneous-Systemic Plasmacytosis (unknown etiology) in humans (Best and Bloom, 2006).

3.1.3 Gross and histopathological lesions of AD

As stated in a review paper by Henson at al. (1976), the general gross lesions in AMDV-infected mink include an intense emaciation because of a progressive body weight loss, lymphadenopathy, splenomegaly (abnormally enlarged spleen) and hepatomegaly (abnormally enlarged liver). Many pin-head size, pale gray concentrations of cellular infiltrates may be seen throughout the parenchyma of liver. A severely affected liver is also more difficult to cut (during the autopsy) as a result of fibrosis. For the kidneys, the gross lesions start when petechial hemorrhages appear on their surface, then they become

abnormally enlarged and swollen, and later they may become pale, shrunken, irregular in shape and difficult to cut during the autopsy. The gross lesions in the lymphoid system (lymph nodes and spleen) are detectable early after infection. Both the nodes and spleen become progressively enlarged and can be palpable during the examination of the live animal. Ulcers in the oral mucosa and gastrointestinal tract may be detectible as well. Gross lesions of nervous system are not very common, but can be seen in a small percentage of mink, as hemorrhage and infarction of the brain. AD may also cause development of white hair fibers (hair depigmentation) throughout the mink pelt (Farid and Ferns, 2011).

The gross lesions mentioned above can vary depending on the genotype of the mink, strain of the virus, type of the infection (naturally or experimentally infected), age of the mink at the time of exposure to the virus and the time elapsed after the infection. For example, in a recent study by Farid and Ferns (2017) on naturally infected mink with a low virulent strain of AMDV, only 0.9% of animals showed gross abnormalities, explained as enlarged, pale or yellowish and mottled kidneys; enlarged and hemorrhagic mesenteric lymph nodes; enlarged yellowish spleen; and yellowish livers with hemorrhagic spots. In another study by the same authors (Farid and Ferns, 2011), no gross lesions were observed in 17 naturally infected (~ six months old) black mink. No gross lesions were found in experimentally infected black and sapphire mink on 10 dpi (Farid et al., 2015). Jensen et al. (2016) reported gross lesions in experimental chronic AMDV-infection of mink as pale and congestive liver, enlarged spleen, and pale cortex and/or enlarged kidneys. Hadlow et al. (1983), compared the pathogenicity of four North American strains of AMDV (Utah-1, Ontario, Montana and Pullman) for experimentally infected Aleutian genotype and non-Aleutian genotype mink by evaluating AD gross lesions at necropsy. The lesions that were

considered as the signs of the disease were not declared in their study. They (Hadlow et al., 1983) concluded that all strains were equally pathogenic for sapphire mink. Pathogenicity of strains, however, was completely different for the pastel mink. Utah-1 strain showed the highest pathogenicity for the pastel mink, followed by Ontario and Montana strains. Pullman, however, was a lesser pathogenic strain for the pastel mink as no sign of AD was observed at the time of necropsy.

The general histopathological features of AD are characterized by drastic infiltration of plasma cells in various organs (plasmacytosis). Other types of WBCs, such as lymphocytes, plasmablasts and microphages are also present in organs of infected mink, which, along with the plasma cells, play a significant role in the inflammation process (Henson et al., 1976). Infiltration of WBCs and the consequent inflammation in different organs is the first histopathological manifestation of AD that can be easily detected by evaluating tissue slides stained with H&E under a light microscope. The types of infiltrated WBCs (plasma cells, lymphocytes and macrophages), however, can be distinguished from each other by immunohistochemical (IHC) staining methods (Mori et al., 1994).

The second cause of histopathological lesions in AMDV-infected mink is deposition of immune complexes in small arteries, glomerular capillaries and uvea, causing inflammation in those tissues, which are called arteritis, glomerulonephritis and uveitis, respectively (Best and Bloom, 2006). Immune complexes can be detected on tissue slides stained by IHC, specifically by the fluorescent antibody techniques, but lesions caused by deposition of those complexes can be observed on tissue slides stained by various methods, such as H&E, PAS, toluidine blue and silver-methenamine, depending on the organ and the intended form of the lesion that is studied (Henson et al., 1966, 1976; Nieto et al., 1991).

The liver, kidneys and lymphoid system (lymph nodes and spleen) are the first organs to show microscopic changes, including appearance of a small number of lymphocytes, macrophages and plasmablasts, which are followed by large masses of these cells in different organs in the later stages of the infection. Nevertheless, because of the normal cellularity of the lymph nodes and spleen, detection of the infiltrated mononuclear cells in those organs is not easy in the early stages of the disease (Henson et al., 1976). Mild AD lesions were observed on 10 dpi in the liver and kidneys of a few individuals (Farid et al., 2015), and interstitial nephritis was detected on 10 dpi in AMDV-infected sapphire mink (Mori et al., 1994). Histopathological lesions were noted between 7 and 11 wpi by Bloom et al. (1975), and on 45 dpi in liver, spleen and abdominal lymph nodes by Hadlow et al. (1985). Jensen et al. (2016) evaluated the presence and severity of the histopathological lesions of AD in seven organs of mink from two to 24 (2, 4, 8, 16 and 24) wpi. The first histopathological lesions that they observed were in the liver, spleen, brain and mesenteric lymph nodes by two wpi. Lesions in the lung and kidneys were observed by four wpi and in intestine by eight wpi. Contrary to other researchers (Henson et al., 1966, 1976), who believe that the AD lesions become more severe as the disease progresses, Jensen at al. (2016) observed a general decline in the severity of the lesions on the seven organs of inoculated mink from eight to 24 wpi.

Arteries of the vascular system in almost all organs, except the aorta, may show inflammation (arteritis). Organs with the greatest degree of arteritis, however, are coronary, hepatic, gastrointestinal, cerebral and renal arteries (Henson et al., 1966). Fluorescent antibody techniques indicated the early deposition of infectious immune complexes in arteries, suggesting that the arterial lesions in AD are the result of immune complex

deposition (Henson et al., 1976). Arteritis has been classified as acute and subacute, depending on its intensity (Porter et al., 1973). Subacute lesions in arteries are predominant with marked proliferation of endothelial cells, perivascular aggregation of plasma cells and lymphocytes, as well as fibrinoid necrosis of the media. Other lesions, which are in the minority, can be classified as extremely acute inflammatory lesions, consisting of infiltration of plasma cells, lymphocytes and polymorphonuclear leukocytes in the arterial wall and endothelial cell vacuolization (Porter et al., 1973). Changes in the arteries usually occur in the adventitial part of the media. The complete media, however, can be affected. Severe changes in the intima can also occur in the later stages of the disease (Henson et al., 1966).

Renal lesions in AMDV-infected mink are the main characteristic of the disease and result in renal failure, uremia and consequently death (Henson et al., 1976). The primary change in the kidneys due to AD is interstitial nephritis (Henson et al., 1976), resulting from cell-mediated immune response to infected epithelial cells of renal tubules in which the virus believed to replicate (Mori et al., 1994). This change is characterized by infiltration of mononuclear cells in the tubular part of the kidneys and around the arteries, which embraces perivascular accumulation of a small number of mononuclear cells, generally around small muscular arteries at the cortico-medullary junctions (Mori et al., 1994). These lesions can be observed on H&E stained tissues under a light microscope (Henson et al., 1976). A rapid increase in the total number of infiltrated cells occurs as the disease progresses, and it continues to the extent that a large number of mononuclear cells, mostly mature plasma cells, occupy the cortical and later the medullary interstitium. This causes different mechanical impacts on the surrounding tubular structure, such as

separation and rupture of tubules (tubulorrhexis), tubule necrosis, and proliferation of basement membrane of tubules (Henson et al., 1976), which may be the main cause of dysfunction of the kidneys (Bloom et al., 1994).

Glomerular changes are the other feature of renal lesions in AD and result from deposition of infectious immune complexes in glomerular capillaries (Mori et al., 1994), which are detectable by three wpi in the subendothelium and in the mesangial area of glomeruli. Glomerular lesions can be classified into different forms based on the location and intensity of the lesions i.e. focal and segmental, diffuse, mesangial, membranous and advanced sclerosing glomerulonephritis (Nieto et al., 1991). Various histopathological methods can be used for evaluating glomerular lesions depending on the type of the lesion. Light, fluorescent and electron microscopy, and various methods of staining, such as H&E, PAS, toluidine blue and silver-methenamine can be used based on the purpose of the study (Henson et al., 1976; Nieto et al., 1991). For example, the primary detectable glomerular lesions with light microscopy and H&E staining are enhanced cellularity, an increased amount of eosinophilic granular materials, and the size of the mesangial areas of glomeruli, which is called mesangial glomerulonephritis (Henson et al., 1976). The size of the mesangial areas progressively increases and degenerative alterations with hemorrhages are seen in some glomeruli. Consequently, interference with vascular flow, increased permeability of glomerular capillaries, loss of plasma components, and hemorrhage are the results of glomerulonephritis due to AMDV-infection and consequently the renal failure (Henson et al., 1966). Nieto et al. (1991) reported high degrees of association between the presence of different types of glomerulonephritis and interstitial nephritis. They did not, however, present any quantitative data regarding their findings.

Microscopic lesions in the liver result from arteritis in small hepatic arteries, and immune response to the presence of viral antigens in Kupffer cells and some hepatocytes in the portal areas, which can be detected in very early stages of AD (Henson et al., 1976). Infiltration of a small number of lymphocytes, plasmablasts and a few macrophage-like cells in periportal areas are the primary changes in the liver. The number of infiltrated cells in periportal areas increases simultaneously with the progression of the disease and mature plasma cells take over the majority of these cells as far as the whole area becoming occupied by them. Other alterations, such as proliferation of macrophages in the sinusoids, disruption of hepatic cords, emersion of large mononuclear-cell appearance and dilation and proliferation of bile ducts due to periportal infiltrations, could also occur (Henson et al., 1976).

In the spleen, the largest organ of the lymphoid system, detectable microscopic lesions include an increased number of plasma cells in the red pulp area, along with a mild to moderate reticuloendothelial hyperplasia. Lesions become more severe as the disease progresses. The reduced density of lymphoid cells in the red pulp of spleen may appear in some animals with advanced AD, as well as the presence of a large proportion of plasma cells and atrophic follicles (Henson et al., 1976). Lesions of the lymph nodes follow a similar pattern as in the spleen. They vary in severity from mild, characterized by a slight elevation in the number of plasma cells some of which contain Russell bodies only in medullary cords, to severe lesions, marked with an extreme increase in number of plasma cells and Russell bodies both in cortex and medulla. The diminished structure of nodes, loose appearance of the follicular pattern of the cortex, and a great decline in the number

of the mature lymphocytes are also factors that differentiate severe lesions from mild lesions in the lymph nodes (Henson et al., 1966, 1976).

Microscopic alterations in other organs are mainly the results of the changes that occur in the vascular system, as explained above. For example, in the gastrointestinal tract, ulcers of gastric mucosa might be due to pathologic arterial disorders, which cause hemorrhagic anemia and death (Henson et al., 1976). In the brain of AMDV-infected mink, mild meningeal mononuclear infiltration, perivascular accumulation of a few lymphocytes and histiocytes, and necrotizing arteritis have been observed (Henson et al., 1966). Dyer et al. (2000) reported an uncommon brain lesion, called nonsuppurative meningoencephalitis (inflammation of meninges and brain), in mink infected with a highly pathogenic strain of AMDV (AMDV-TH5). Later in 2010, Jahns et al. evaluated a total of 157 mink from four AMDV-infected farms (with an Irish strain of the virus) and one AMDV-free farm in Ireland for the presence of the nonsuppurative meningoencephalitis. It was found that none of the animals from the uninfected farm had the lesion in their brain, whereas 10 to 32 percent of those from the infected farms exhibited lymphocytic, plasmacytic and histiocytic infiltration in the meninges covering the ventral part of the brain (medulla, midbrain and thalamus), and to a lesser extent, in the meninges covering the frontal cortex, associated with the nonsuppurative meningoencephalitis. Jahns et al. (2010) concluded that the AMDV can cause nonsuppurative meningoencephalitis in mink. The lungs in adult mink can be affected by the arteritis as well, characterized by plasma cells infiltration, without any pathological disorders of parenchymal tissue (Henson et al., 1976). The AD lesions in the lungs of AMDV-infected adult mink, however, are either less severe compare to other organs (Henson et al., 1976; Jensen et al., 2016) or not observed (in great number of

AMDV-positive animals) at all (Farid and Ferns, 2017). Perivascular and peribronchial lymphoplasmatic infiltrations as well as the presence of a few infiltrated macrophages in alveoli of the lungs of ferret infected by AMDV is reported (Une et al., 2000). The heart is affected by AD the same way as in the gastrointestinal tract, brain and lungs, as a result of the systemic infection of vascular system. Coronary arteries of the heart are one of the first locations of mononuclear infiltration causing problems in delivering blood to the heart muscle cells. Other microscopic changes in the heart can be perivascular accumulation of mononuclear cells and necrotizing arteritis in other parts of the heart (Henson et al., 1976).

Histopathological lesions can vary in feature and severity depending on the genotype of the mink, strain of the virus, method of the infection (naturally or experimentally infected), age of the mink at the time of exposure to the virus and the time elapsed after the infection. For example, in Porter et al. (1969), it is reported that the experimentally infected Aleutian genotype (violet) mink died much earlier than the experimentally infected non-Aleutian genotype (pastel) mink as a result of the high amount of immune complexes deposited in the renal glomeruli and kidney failure. In the study of Johnson et al. (1975), the renal changes in experimentally infected Aleutian and non-Aleutian mink were examined at three week intervals for 24 wpi. Johnson et al. (1975) reported that the Aleutian mink is more susceptible to AD. They also reported that the Aleutian mink has a shorter life span and exhibits a more rapid progression of lesions when compared to non-Aleutian mink after experimental infection with AMDV. In that study (Johnson et al., 1975), Aleutian mink showed mild renal lesions as early as three wpi and severe renal lesions at 18, 21 and 24 wpi. Severe in their case referred to the occurrence of diffuse infiltration of plasma cells throughout the interstitium, a noticeable

glomerulonephritis along with presence of neutrophils and increase in glomerular PAS-positive material. Hadlow et al. (1985) evaluated 27 experimentally inoculated Pastel (non-Aleutian) mink, within 8 to 126 dpi. Three randomly selected animals were euthanized on each of nine examination days (8, 10, 12, 14, 28, 43, 70, 99 and 126 dpi) and the presence of AD was tested by evaluating the presence of infiltrated plasma cells in the liver, spleen and abdominal lymph nodes. They (Hadlow et al., 1985) reported that the emersion of the disease occurred at 43 dpi (one of three mink), which seemed unusually early for pastel mink inoculated with a low-virulence strain of AMDV (Pullman). In addition, they (Hadlow et al., 1985) found that two of the three mink on day 126 showed AD lesions. Hadlow et al. (1985) did not, however, compared the tissues for the severity of lesions. Mild histopathological lesions (infiltration of plasma cells) were found in the kidneys and liver of a few experimentally infected black (three of 47) and sapphire (one out of 14) mink 10 dpi (Farid et al., 2015). Farid et al. (2015) found no lesion in the heart tissues from the 61 experimentally infected black and sapphire mink 10 dpi. Farid and Ferns (2011) evaluated the severity of lesions in the kidneys, liver, heart, and brain in (six months old) naturally infected male and female black mink and found no differences between the two sexes in terms of distribution of lesion severity in any of the organs.

3.1.4 Measuring severity of histopathological lesions of AD

The severity of histopathological lesions of AD are often subjectively assessed under the light microscope. Leader et al. (1963) were among the pioneers of visually assessing the severity of histopathological lesions of AD stained with H&E and other histochemical methods of staining. They subjectively referred to the severity, location and

form of the hepatic, renal and arterial lesions, but did not score the severities. Henson et al. (1966) used 50 mink from two AMDV-infected ranches and visually evaluated the tissue samples from liver, kidney, spleen, lymph nodes, lungs, heart, urinary bladder, duodenum, colon, stomach, pancreas, brain, skeletal muscle, and skin stained with H&E, PAS, Wilder's reticulin, alcian blue-chromotrope 2R, toluidine blue, Weigert-Van Gieson and Pollak's trichrome. They (Henson et al., 1966) subjectively classified renal interstitial lesions and liver lesions into mild, moderate and severe based on the amounts of infiltrated mononuclear cells in those organs. Jackson et al. (1996) used 24 black and 26 brown mink in their study to evaluate the progression of AD in naturally and experimentally infected animals. They visually classified lesions on H&E stained kidney and liver slides based on the percentage of renal cortical tubules and interstitium replaced by plasma cells and lymphocytes, and the number of plasma cells surrounding portal areas, respectively. Jackson et al. (1996) found no relationships between severity of renal and hepatic lesions. A visual assessment of plasma cell infiltrations and related abnormalities in kidneys, liver, heart and brain, was performed on H&E stained samples under a light microscope by Farid and Ferns (2011), who scored lesion severity from 0 (no lesion) to 4 (very severe) in 17 naturally infected black mink and reported that the severity of the lesions in the liver was significantly lower than that in the kidneys. They also reported that the occurrence of very severe lesions (score 4) in the kidneys and heart was higher compared to the liver. In another study, Farid and Ferns (2017), performed the same visual histopathological evaluation on H&E stained brain, lung, liver, kidney and heart samples of 680 naturally infected and 132 non-infected mink. The objective of that study was to measure the severity of lesions (scoring 0 - 4) in mink selected for tolerance to AMDV-infection. They (Farid

and Ferns, 2017) reported that in AMDV-infected animals, first, the degrees of severity for the kidney and liver lesions were comparable; second, those two organs (kidneys and liver) seemed to be the most severely affected organs compared to the heart, brain and lungs; and third, the severity of the lesions in the kidneys, liver, heart and brain correlated to each other. Jensen et al. (2016) also visually classified lesion severity of the lung, liver, intestine, kidneys and brain based on the amount of infiltrated mononuclear cells into four groups of suspected, mild, moderate or massive. The spleen was evaluated based on (a) the degree of activation of lymphoid follicles with necrotic cells and macrophages; and (b) reduced density of lymphoid cells in lymphoid follicles, and/or diffusely in the spleen. In the mesenteric lymph nodes, the lesions were described as (a) reduced density of lymphoid cells in lymphoid follicles; (b) reduced density of lymphocytes in medulla and increased numbers of plasma cells in medulla and sinuses, and (c) increased numbers of macrophages, mainly in the medulla of the lymph node. This report (Jensen et al., 2016) did not compare the organs for the severity of the lesions but concluded that the frequency of the occurrence of hepatic lesions was more than that in the other organs. In the study of Johnson et al. (1975), renal glomeruli of experimentally infected Aleutian and non-Aleutian mink were visually evaluated by light, fluorescent and electron microscopy. Their (Johnson et al., 1975) evaluations consisted of determining the mean number of glomerular nuclei (within 10 glomeruli for each mink), the morphologic appearance of the glomeruli when stained by H&E, the presence and amount of PAS-positive material in the glomeruli (0-4 scale) and the presence of neutrophils in the glomeruli (0-4 scale). Johnson et al. (1975) evaluated presence of interstitial infiltration of plasma cells and arterial lesions in the kidneys as well.

3.1.5 Controlling Aleutian disease

3.1.5.1 Vaccine

All previous attempts for developing an effective vaccine against AMDV have failed or have created only partial protection (Porter et al., 1972; Aasted et al., 1998; Castelruiz et al., 2005). Porter et al. (1972) used a formalin-inactivated AMDV vaccine and reported a higher severity of lesions in vaccinated mink, compared to unvaccinated controls. Susceptibility to oral infection in the vaccinated mink by AMDV was also higher than in the unvaccinated animals. In another study, administration of capsid-protein-based vaccine increased the levels of serum gamma-globulin, CD8+ T-lymphocyte and mortality, but vaccination with non-structural protein provided partial immunity (Aasted et al., 1998). The use of NS1 DNA vaccine also provided partial protection against the AMDV in the study of Castelruiz et al. (2005).

3.1.5.2 Treatment

There is no effective treatment for AD. Supportive therapy, such as administration of electrolytes, antibiotics, and anti-inflammatory drugs, was suggested for preventing secondary infections in mink and ferret (Schuler, 2007). The immunosuppressive drug, cyclophosphamide (Cy), was examined by Cheema et al. (1972) for its effects on the immune response of mink to the AMDV-infection. Administration of Cy prevented anti-AMDV antibody response, reduced the serum gamma-globulin level, and prevented gross and microscopic lesions of AD, as well as the deposition of IgG in the kidneys. The effects of Cy treatment were, however, temporary and diminished two to three weeks after

termination of the therapy. The use of Cy showed several side effects such as anorexia, cyanosis, and leukopenia, and was not tolerated by mink at the dosages used. In addition, some common side effects of Cy in dogs and rats, such as necrosis and depletion of lymphoid tissues, hepatic degeneration, renal tubular epithelial necrosis, and necrotic or hemorrhagic cystitis, were observed in mink as well (Cheema et al., 1972).

3.1.5.3 Virus eradication

In the absence of a treatment or an effective vaccine, virus eradication has been the main method for combating AMDV worldwide. The iodine agglutination test (IAT) (Kirk, 1963; Greenfield et al., 1973), CIEP test (Cho and Ingram, 1973), and more recently, enzyme-linked immunosorbent assay (ELISA) (Chen et al., 2016) have been used for the detection and elimination of infected animals. Using CIEP for viral eradication in Nova Scotia started in the mid-1970s, but the infection has remained a major problem for the mink industry (Farid et al., 2012). Variability of the virus genome, false-negative CIEP test results, biosecurity failure, presence of infected wild animals in nature, and persistence of the virus on the farms were suggested as possible reasons for the ineffectiveness of the eradication strategies (Farid et al., 2012). Iceland is the only country where the virus has been successfully eradicated in farmed mink using CIEP since the early 1980s (except in one incident in a farm after 12 years) (Gunnarsson, 2001), whereas the virus still has not been eradicated from one region in Denmark, a country which has implemented a very vigorous viral eradication program since the mid-1970s (Themudo et al., 2011).

3.1.5.4 Selection for tolerance

Because of the unsuccessful virus eradication strategies, selection for tolerance has recently been adopted by mink farmers in several countries, including Canada, as the only viable option to control AD. This approach is based on the presence of some persistently infected mink that can tolerate the infection and show no or mild symptoms of the disease, such as hypergammaglobulinemia, high anti-AMDV antibody titers and histopathological lesions (Bloom et al., 1994). Forty-one of 140 AMDV-inoculated pastel mink (Larsen and Porter, 1975), 25 of 74 naturally infected pastel mink (An and Ingram, 1977), 24 of 30 feral mink and 6 of 24 naturally infected farmed mink (Cho and Greenfield,1978), 17 of 20 inoculated pastel mink (Hadlow et al., 1984) and 90 of 195 naturally infected wild-type farmed mink (Aasted and Hauch, 1988), are the examples of infected non-Aleutian type mink that showed non-progressive infection and have proven the existence of some mink tolerant to the AMDV-infection. Most recently, the effects of selection for tolerance on the severity of histopathological lesions in AMDV-infected mink were investigated by Farid and Ferns (2017). They (Farid and Ferns, 2017) investigated 116 animals (all CIEP-positive) from three farms that followed a selection for tolerance strategy for a long period of time and then compared them to 696 animals (CIEP-positive and -negative) from 25 farms that had not selected their animals for tolerance against the AMDV-infection. The spleen, brain, lungs, liver, kidneys, mesenteric lymph nodes and heart were examined for gross lesions such as enlargement, color abnormalities, inflammation and necrosis, and the brain, lung, liver, kidney and heart samples were evaluated for histopathological lesions associated with AD and scored based on the extent of infiltration of mononuclear cells. They reported that the tolerant animals showed significantly lower severe AD lesions despite being CIEP-positive. More importantly, it is believed that tolerance to AMDV-

infection is genetically controlled (Bloom et al., 1975; Aasted and Hauch, 1988; Farid and Ferns, 2017).

Tolerant animals are expected to have normal growth and reproductive performance (physical health) and mild histopathological lesions. Obviously, measuring histopathological lesions on live animals is not possible. Thus, measuring physical health seems to be the logical method of identifying tolerant animals. Nonetheless, animals need to be evaluated for health individually on a regular basis and for a long period of time, which is a time-consuming and non-practical method. For this reason, mink farmers have turned their focus to using various serological tests, hoping to find a more accurate tool for identifying healthy mink among their infected herd. To be effective, the test should have, first, a high degree of association with the severity of histopathological lesions and thus with the level of health; and second, it should be inexpensive, practical and ideally easy to use on the farm.

Positive relationships between serum gamma-globulin levels, measured by cellulose acetate electrophoresis technique or paper electrophoresis apparatus, and the presence or severity of gross and/or histopathological lesions have been reported. For instance, An and Ingram (1977) tested 74 naturally infected pastel mink between three weeks to 10 months after initial detection of infection and found that those with serum gamma-globulin levels (measured by cellulose acetate electrophoresis technique) of more than 25% of total serum proteins showed histopathological lesions, whereas those with less than 21% of serum proteins did not show any lesion. In the study by Henson et al. (1966), the severity of the histopathological lesions was found to be associated with serum gamma-globulin levels, measured by a paper electrophoresis apparatus. Hadlow et al. (1985)

studied levels of gamma-globulin, measured by cellulose acetate electrophoresis technique, and the presence of gross lesions in 27 pastel mink, sacrificed between 8 and 126 dpi, and observed that five of the 12 mink that were sacrificed after 43 dpi and showed lesions of AD, had serum gamma-globulin levels between 1.0 and 4.0 g/dL, whereas those which did not show any lesions, had serum gamma-globulin levels between 0.4 and 1.4 g/dL. Kenyon et al. (1963) evaluated 57 naturally infected pastel mink and reported a high degree of correlation between the level of serum gamma-globulin, measured by a paper electrophoresis apparatus, and the extent of plasma cell infiltration in kidneys, liver and spleen. They (Kenyon et al., 1963), however, did not present any data regarding the degree of that positive relationship.

Another method for measuring the serum gamma-globulin level in mink is the IAT, which is an easy, in-house and inexpensive serological test. Gamma-globulin binds with the iodine, causing agglutination and clots that can be visually assessed on a glass slide by the mink farmer. This test was originally proposed by Mallen et al. (1950) for detecting altered serum proteins in humans. They classified their results as: negative (-), weak positive (+), moderately positive (++), positive (+++) and strongly positive (++++), based on the size of the clots. The test was first used in mink by Henson et al. (1962) for detecting hypergammaglobulinemia, as a means of virus eradication (Gorham et al., 1976), but was abandoned for this purpose after the development of CIEP. Despite its relatively low specificity in detecting AMDV-infected mink (Greenfield et al., 1973), the IAT is being used as a measure of health by many mink farmers in Nova Scotia, Canada, and has shown promising results (Farid, 2010). There is only one published report on the relationships (92.3) between positive IAT results and the presence of AD gross lesions (Henson et al.,

1962). The relationships between IAT results and the presence or severity of histopathological lesions have not, however, been reported to date.

Positive relationships between high anti-AMDV antibody titers measured by CIEP and the presence or severity of gross and/or histopathological lesions are reported. An and Ingram (1977) reported that all the naturally infected pastel mink (46 out of 74) with antibody titers of greater than 512 showed histopathological lesions. Similarly, five of the 27-pastel mink with gross lesions had antibody titers of 256 and higher (Hadlow et al., 1985). Jackson et al. (1996), however, reported a low correlation (0.36) between antibody titer, measured by CIEP, and the severity of histopathological lesions in the kidneys (percentage of occupied tissue by infiltrated cells) and the liver (proportion of portal areas surrounded by plasma cells) in two groups of non-Aleutian mink. The latter is the only published paper reporting the association between intensity of AD lesions with antibody titers.

Using CIEP on serially diluted serum or plasma samples is a standard method for measuring the antibody titers in mink (Bloom et al., 1975; An and Ingram, 1977). Even though the test is highly specific and reasonably sensitive (Jackson et al., 1996), it is too expensive for routine antibody measurement because it should be performed on multiple dilutions of a sample. Recently, VP2 protein or AMDV-G based ELISA systems have been used by some farmers in Canada, USA and the Netherlands to identify animals with low anti-AMDV antibody titers which are expected to be tolerant to AMDV-infection. Despite its low cost, ELISA systems need some refinements before being used for measuring antibody titer since their accuracies are not high (Farid and Segervall, 2014; Farid and Rupasinghe, 2016).

3.2 Materials and methods

3.2.1 Source of animals and inoculation

Data on 120 male and 226 female (total of 346) black American mink, that varied in age between 6 months and 5 years, were used in this study (Table 3.2.1). The animals were intranasally inoculated with 600 ID_{50} of a spleen homogenate containing a local strain of AMDV (Farid et al., 2015), between October 2010 and September 2013 at the Aleutian Disease Research Center (ADRC). Anesthesia was performed prior to inoculation or blood sampling by intramuscular injection of ketamine hydrochloride (Ketalean, Bimeda-MTC Cambridge, ON, Canada) and xylazine hydrochloride (Rompun 20%, Bayer Health Care) at the rates of 10 mg/kg and 2 mg/kg of the body weight, respectively. All procedures were performed in accordance with the standards of the Canadian Council on Animal Care after approval by the institutional Animal Care and Use Committee. Apart from 47 animals which naturally died from 2011 to 2013, others (n=299) were euthanized by intracardial injection of sodium pentobarbital (Euthanyl, Bimedia_MTC) at the rate of 100 mg/kg of body weight or by CO_2 exposure. With a few exceptions, in the majority of cases, animals were six-months old when inoculated (Table 3.2.2). The durations of infection varied between less than six months to around 3.5 years (Table 3.2.1).

3.2.2 Animal sampling

Terminal samplings were performed during a 4-year period (2011-2014) at the ADRC. Blood samples were collected by heart puncture into heparinized tubes for plasma preparation for CIEP test and in plain tubes for serum preparation for the IAT. Samples

were kept in a refrigerator overnight and centrifuged at 1397 g (Porta Spin C826 centrifuge, UNICCO, Dayton, NJ, USA) for 10 minutes. One fresh plasma sample was used for CIEP testing and the rest of the plasma and serum samples were stored at -80˚C until use. Blood sampling was not performed on those mink which died naturally. Samples of kidneys, liver, heart, and lungs were collected from euthanized and naturally dead mink and kept in 10% formalin until use for histopathological examination. Tissues from the four organs were embedded in paraffin, sectioned at 5 μm thick using a Leica microtome RM2255 (Leica Biosystems, 2018), fixed on slides and stained with H&E at the Pathology Laboratory, Nova Scotia Department of Agriculture.

Table 3.2.1 Distribution of duration of infection in killed and naturally dead animals

Duration of infection (year)	Male		Female		Total
	Killed	Dead	Killed	Dead	
0.5 (0.1-0.5)	37	2	1	8	48
1.0 (0.6-1.0)	0	2	0	7	9
1.5 (1.1-1.5)	34	5	104	3	146
2.0 (1.6-2.0)	0	4	0	9	13
2.5 (2.1-2.5)	24	1	68	0	93
3.0 (2.6-3.0)	1	0	1	6	8
3.5 (3.1-3.2)	10	0	19	0	29
Total	106	14	193	33	346

Ranges of duration of infection are in brackets

Table 3.2.2 Joint distribution of termination age and duration of infection.

Age at the time of sampling (year)	Duration of infection (year)							Total
	0.5	1.0	1.5	2.0	2.5	3.0	3.5	

1.0 (0.5-1.0)	44	0	0	0	0	0	0	44
1.5 (1.1-1.5)	2	6	0	0	0	0	0	8
2.0 (1.6-2.0)	0	0	143	0	0	0	0	143
2.5 (2.1-2.5)	2	1	1	7	0	0	0	11
3.0 (2.6-3.0)	0	0	2	2	92	0	0	96
3.5 (3.1-3.5)	0	1	0	2	0	2	0	5
4.0 (3.6-4.0)	0	1	0	2	0	2	29	34
4.5 (4.1-4.5)	0	0	0	0	0	4	0	4
5.0 (4.6-4.8)	0	0	0	0	1	0	0	1
Total	48	9	146	13	93	8	29	346

Ranges of age are in brackets

3.2.3 Anti-AMDV antibody titers

Frozen plasma samples were thawed, two-fold serially diluted ten times (1/2 to 1/1024) and tested by CIEP. The CIEP test was performed at the Animal Health Laboratory of the Nova Scotia Department of Agriculture in Truro. Glass slides with the diameter of 75×50 mm, coated with 10 mL of 0.8% standard low-Mr agarose (BioRad) in barbital buffer (VWR), were utilized. Plasma samples were placed in anodal wells and antigen (Research Foundation of the Danish Fur Breeders Association, Glostrup, Denmark) were placed in cathodal wells along with a positive control on each plate. Gels were electrophoresed for 50 minutes at 80 volts, soaked overnight in 2% sodium chloride and scored under a stereoscope. Appearance of a visible greyish-white band in the agarose gel was the sign of anti-AMDV antibodies in the sample (Cho and Greenfield, 1978). Faint bands were reported as doubtful by the testing laboratory, which were due to low antibody titers. The reciprocal of the highest dilution of the plasma that showed a positive or doubtful result was recorded as the titer of anti-AMDV antibody.

3.2.4 Serum gamma-globulin levels

An iodine solution was prepared by mixing 20 grams of iodine and 40 grams of potassium iodine in distilled water to make a 300 mL solution, and was kept in a brown glass container (Henson et al., 1962). Frozen serum samples were thawed and one drop mixed with one drop of iodine solution on a glass slide and evaluated, approximately one minute after mixing the iodine solution and the serum, to determine the gamma-globulin level of each sample. Results were classified as follows: negative test (0), the mixture remained clear without any clots and only a change in color of the serum was observed which was because of the iodine; weak positive test (1), turbidity in the solution was the first sign and after rotation by hand a slight agglutination appeared; moderately positive test (2), the agglutination was more obvious than grade one; positive test (3), a heavy granular precipitate appeared; strongly positive test (4), a heavy shapeless precipitate appeared instantly (Appendix 2, Fig. A2.1, A2.2, A2.3, A2.4 and A2.5).

3.2.5 Measuring the severity of histopathological lesions

Tissue slides were optically assessed using the Leica DM500-Microscope (Leica Microsystems, 2018), to check the quality of the stained slides. Low-quality slides in terms of tissue fixation, H&E stain or stain debris were prepared again. An image was then captured from each of three randomly selected areas on each slide, using 10X magnification. The images were saved as digital files (.tif format) and transferred to the DIA software, Image Pro Plus (IPP) version 7.0 (http://www.mediacy.com/imageproplus). Infiltrated mononuclear cells (plasma cells, lymphocytes and macrophages) were counted using the manual feature of IPP 7.0, the total number of cells (infiltrated mononuclear cells

and normal tissue cells) were counted by the automatic feature of IPP 7.0 using the algorithm previously developed (explained in the chapter 2.0), and the percentage of infiltrated mononuclear cells was calculated.

3.2.6 Data Analyzing

Data were analyzed with the SAS 9.4 for Windows (SAS Institute Inc., Cary, NC). Associations between the three images on each slide within each organ were computed by the Spearman's rank correlation, and with intra-class correlation using the PROC MIXED with animals as the random effect. Percent infiltrated cells and number of total cells (mean of the three images on each slide) were analyzed using the PROC MIXED with Restricted Maximum Likelihood (REML) estimation method, Variance Components type for the covariance structure and Type 3 tests of fixed effects. Prior to the analysis, durations of infection were classified into four groups (0.5, 1.5, 2.5 and 3.5 years), because the number of observations in other classes were small (Table 3.2.1). The model included the fixed effects of organ (heart, kidneys, liver), duration of infection, sex, disposal method (naturally died or killed), and all two-way interactions. Interaction terms which were not significant (sex by organ, sex by duration of infection, sex by disposal methods) and those which resulted in non-estimable least-squares means (duration of infection by disposal method) were excluded from the final model. The random effect of individual mink was included in the model to take care of the correlation among organs of the same mink for the measurements. Age of animals at the time of termination was not included in the model because it was almost the same as the duration of infection (Table 3.2.2). Multiple

comparisons of the least-squares means were performed following the *post hoc* Tukey-Kramer's adjustments.

A stepwise regression model was used to determine the effects of linear and quadratic terms of antibody titer and duration of infection, as well as the interaction between antibody titer and duration of infection, sex and its interactions with antibody titer and duration of infection on percent infiltrated cells in killed animals within each organ. Linear term of antibody titer was forced to the model. Disposal method was not included in the models because antibody titer was not measured on dead animals. The log-transform values of antibody titer were used for analyses ($\log_2$(titer)=0 if titer=0 and $\log_2$(titer)+1 if titer>0). Because the sex effect and/or its interactions were significant, another stepwise regression analysis was performed within organ and sex. Data on percent infiltrated cells were re-analyzed after replacing antibody titers by gamma-globulin levels, measured by IAT.

3.3 Results

3.3.1 Percentage of infiltrated cells in different organs

Histopathological slides from the heart, liver and kidneys of 324 animals were available in this study. All three organs of 22 naturally dead animals and one or two organs of another 10 naturally dead animals could not be evaluated because of the severe post-mortem degenerations. Overall, three images from each of 322 heart, 317 kidney and 315 liver slides were evaluated in this study (total of 2,862 images). Descriptive statistics of the number of infiltrated cells which were counted manually, total number of cells counted by the IPP 7.0, and the calculated percentages of infiltrated cells on images of the three organs

are shown in Table 3.3.1. The sums of infiltrated cells manually counted on 966 heart images (322 slides), 951 kidney images (317 slides) and 945 liver images (315 slides) were 468,534, 605,793 and 361,146, respectively. The largest and the smallest numbers of infiltrated cells counted on an image were 38 in the liver and 6221 in the kidneys. The total number of cells automatically counted in the heart, kidneys and liver were 1,908,450, 4,415,071 and 3,456,594, respectively, and ranged between 1,165 in the heart and 8,681 in the kidneys. The lowest and highest percentages of infiltrated cells on an image were 1.11 and 91.25, respectively, which were both in the liver. The differences between minimum and maximum values (ranges) of all the three measurements were smaller in the heart images, compared to the kidney and liver images.

Means, medians, standard deviations, minimums, maximums, coefficient of variations and differences between means and medians of the number of infiltrated cells, total number of cells and percentage of infiltrated cells, averaged over the three images on each slide, of each organ are presented in Table 3.3.2. The highest means of average number of the infiltrated cells and the total number of cells per slide were in the kidneys. The highest mean of average percent infiltrated cells, however, was in the heart, followed by that in the kidneys and liver. Standard deviations of average number of infiltrated cells, total number of cells and percent infiltrated cells were lower in the heart, compared to those in the liver and kidneys. The heart also had the lowest coefficient of variations for the average number of infiltrated cells (28.6) and percent infiltrated cells (29.22), compared to the kidneys (106 and 84.31) and liver (107 and 82.81), which had a comparable coefficient of variation for those two measurements. In contrast, the coefficient of variation for the average of total number of cells were lower in the kidneys and liver, which were

comparable (11.61 and 12.60, respectively), compared to that in the heart (19.48). Differences between means and medians of average of number of infiltrated cells, total number of cells and percent infiltrated cells were the lowest in the heart, compared to those in the kidneys and liver. In particular, the difference between mean and median of average percent infiltrated cells in the heart was 4.5- and 2.5-fold lower than those in the kidneys and liver, respectively.

Table 3.3.1 Sum, minimum and maximum number of infiltrated cells, total number of cells and percentage of infiltrated cells on the three images on each slides of each organ.

Organ	Variable	Images	Sum	Minimum	Maximum
Heart	Infiltrated cells	966	468,534	101	1,046
	Total cells	966	1,908,450	1,165	3,996
	% Infiltrated	966	-------	4.92	60
Kidney	Infiltrated cells	951	605,793	113	6,221
	Total cells	951	4,415,071	3,021	8,681
	% Infiltrated	951	-------	2.45	89
Liver	Infiltrated cells	945	361,146	38	4,821
	Total cells	945	3,456,594	2,053	6,420
	% Infiltrated	945	-------	1.11	91.25

Table 3.3.2 Means, standard deviations (SD), minimums (Min), maximums (Max), medians, coefficients of variation (CV) and differences between means and medians (mean-median) of averages of infiltrated cells (Inf.), total number of cells (Tot.) and percent infiltrated cells (%inf.) of the three images on each slide of each organ.

Organ	Variable (Average)	No. of slides	Mean	SD	Min.	Max.	Median	CV	Mean-Median
Heart	Inf.	322	485	138	137	997	477	28.60	8
	Tot.	322	1,975	384	1,291	3,606	1,920	19.48	55
	%Inf.	322	25.13	7.34	5.6	52.58	24.61	29.22	0.69
Kidney	Inf.	317	637	679	159	4,838	451	106	186
	Tot.	317	4,642	539	3,278	7,802	4,632	11.61	10
	%Inf.	317	13.12	11	3.34	70.38	10	84.31	3.12
Liver	Inf.	315	382	409	68	4,236	293	107	89
	Tot.	315	3,657	460	2,634	5,863	3,687	12.60	-30
	%Inf.	315	10.21	8.4	2	87	8.5	82.81	1.71

3.3.2 Test of normality

Probabilities of deviation of the distributions of means of infiltrated cells, total number of cells and percentage of infiltrated cells of the heart, kidneys and liver from normality using the Kilmogorov-Smiranov test are shown in Table 3.3.3. All distributions significantly deviated from normality, except for means of infiltrated cells and percentage of infiltrated cells in the heart, and the mean of total number of cells in the liver. Log transformation did not improve the normality of any of the distributions.

Table 3.3.3 Probabilities of deviation of the distributions of means of infiltrated cells, total number of cells and percent infiltrated cells of heart, kidneys and liver from normality using Kilmogorov-Smiranov test.

Measurement	Heart	Kidney	Liver
No. of infiltrated cells	0.07	<0.01	<0.01
Total number of cells	<0.01	<0.01	0.15
Percent infiltrated cells	0.15	<0.01	<0.01

3.3.3 Correlations between three images within each slide in organs

Spearman's rank correlation coefficients between pairs of images on each slide for the numbers of infiltrated cells, total numbers of cells and percent infiltrated cells are shown in Table 3.3.4. The lowest correlation coefficients between pairs of images for the number of infiltrated cells, total number of cells and percent infiltrated cells were in the heart (0.61 to 0.86), and the kidneys and liver which had comparable correlation coefficients for the three measurements. Correlation coefficients between pairs of images on each slide for the total number of cells were the lowest (0.61 to 0.80) and for the number of infiltrated cells were the highest (0.77 to 0.94) in all organs.

Table 3.3.4 Spearman's rank correlation coefficients between pairs of images on each slide for the number of infiltrated cells, total number of cells and percentage of infiltrated cells in different organs.

Organ	Image	Infiltrated cells	Total cells	% Infiltrated cells
Heart	1 and 2	0.85	0.67	0.79
	1 and 3	0.77	0.61	0.72
	2 and 3	0.86	0.64	0.80
Kidney	1 and 2	0.93	0.80	0.92
	1 and 3	0.87	0.77	0.86
	2 and 3	0.93	0.76	0.91
Liver	1 and 2	0.94	0.76	0.90
	1 and 3	0.88	0.74	0.84
	2 and 3	0.91	0.76	0.90

Intra-class correlations for the three images on each slide for the numbers of infiltrated cells, total numbers of cells and percent infiltrated cells are shown in Table 3.3.5. Consistent with the results of Spearman's rank correlation coefficients, the heart images had lowest intra-class correlations for the three measurements compared to those in the kidney and liver images, which had comparable estimates. The highest intra-class correlation for the number of infiltrated cells was in the liver (0.95), whereas the highest intra-class correlation coefficients for the total number of cells (0.79) and percent infiltrated cells (0.93) were in the kidney images.

Table 3.3.5 Intra-class correlations for the number of infiltrated cells, total number of cells and percent infiltrated cells for the three images of each slide in different organs.

Organ	Infiltrated cells	Total cells	% Infiltrated cells
Heart	0.56	0.64	0.62
Kidney	0.93	0.79	0.93
Liver	0.95	0.77	0.92

3.3.4 Factors affecting percent infiltrated cells and total number of cells

The results of the Mixed model analyses showed that all the main effects (organ, duration of infection, disposal method and sex), as well as interactions between organs and durations of infection and between organs and disposal methods, were significant for percent infiltrated cells and number of total cells, except sex which did not have a significant effect on the number of total cells (Table 3.3.6). The magnitudes of the F-values suggest that disposal method and organs had the greatest effects on variations in percent infiltrated cells and number of total cells, respectively.

Table 3.3.6 F-values and probabilities of the main effects and interactions for percent infiltrated cells and number of total cells

Factor	Degrees of freedom	% Infiltrated cells		Number of total cells	
		F-value	Pr.	F-value	Pr.
Organ	2	31.5	0.000	962.6	0.000
Duration of infection (DI)	3	5.2	0.001	21.3	0.000
Disposal method (DM)	1	256.5	0.000	15.6	0.000
Sex	1	10.6	0.001	0.9	0.339
Organ*DI	6	7.8	0.000	2.5	0.023
Organ*DM	2	138.9	0.000	16.4	0.000

As a result of significant interaction between organs with the duration of infection and disposal method, the main effects, although significant, do not accurately explain the effects of these factors on percent infiltrated cells and number of total cells. Least-square means of percent infiltrated cells and number of total cells for the main effects and interactions are shown in Table 3.3.7. In the heart, percent infiltrated cells steadily increased as the duration of infection increased from 22.5% in animals which were infected for 0.5 years to 31.8% in those which were infected for 3.5 years, but only the latter was significantly greater than the others. Duration of infection did not have any significant

effect on percent infiltrated cells in the kidneys and liver. Percentages of infiltrated cells were the lowest in the liver, intermediate in the heart and the highest in the kidneys, regardless of the duration of infection, except in animals which were infected for 3.5 years where kidneys and heart had almost the same values. Percentages of infiltrated cells in the kidneys were 10.6%, 6.3%, 7.2% and 10.1% greater than those in the liver at 0.5, 1.5, 2.5 and 3.5 years after inoculation, respectively, and the differences were all significant. Percent infiltrated cells in the liver were also smaller than those in the heart, but differences were significant only in animals which were infected for 2.5 and 3.5 years. Percent infiltrated cells in the kidneys was significantly larger than that in the heart only in animals which were terminated after six months of infection (30.9% vs 22.5%).

In all organs, the number of total cells counted by the DIA steadily decreased as the duration of infection increased. Differences among the durations of infection were not significant within each organ, except in the liver and heart where animals that were infected for 3.5 years had significantly smaller numbers of total cells compared with those which had shorter durations of infection. Numbers of total cells in the kidneys were almost 2.5 times greater than those in the heart, and almost 1.5 times greater than those in the liver in every duration of infection, and the differences between pairs of organs in each duration of infection was significant. Numbers of total cells in the liver were almost twice as many as those in the heart, and differences between the two organs at each duration of infection was significant.

Percent infiltrated cells in the heart were comparable between naturally dead and killed animals, whereas the estimates in the kidneys and liver were almost four times greater in the dead than in the killed mink. Among dead animals, percent infiltrated cells

was significantly higher in the kidneys, followed by that in the liver and heart, which were not significantly different. The mink which were killed had the highest percent infiltrated cells in the heart, followed by those in the kidneys and liver, and the differences were all significant.

Table 3.3.7 Least-squares means ±standard errors of percent infiltrated cells and number of total cells for the main effects and interactions.

Main effect		Percent infiltrated cells	Number of total cells	Interaction	Percent infiltrated cells	Number of total cells
Organ	Heart	26.0±0.8^{a}	1,888±50^{a}	Heart*0.5y	22.5±1.1^{cde}	2,077±67^{a}
	Kidney	28.8±0.9^{b}	4,876±55^{b}	Heart*1.5y	24.4±0.9^{cd}	1,943±58^{a}
	Liver	20.2±0.9^{c}	3,722±58^{c}	Heart*2.5y	25.4±1.1^{bc}	1,915±68^{a}
				Heart*3.5y	31.8±1.4^{a}	1,617±88^{f}
DI	0.5y	24.6±0.8^{a}	3,668±46^{a}			
	1.5y	24.0±0.7^{a}	3,611±41^{a}	Kidney*0.5y	30.9±1.2^{a}	5,126±74^{e}
	2.5y	23.9±0.8^{a}	3,491±47^{b}	Kidney*1.5y	27.0±1.0^{abc}	5,017±61^{e}
	3.5y	27.6±1.0^{b}	3,211±59^{c}	Kidney*2.5y	26.7±1.1^{abc}	4,885±72^{e}
				Kidney*3.5y	30.6±1.4^{ab}	4,477±90^{b}
DM	Dead	34.7±1.2^{b}	3,633±67^{b}			
	Killed	15.4±0.3^{a}	3,357±19^{a}	Liver*0.5y	20.3±1.2^{de}	3,801±73^{cd}
				Liver*1.5y	20.7±1.0^{de}	3,872±66^{c}
Sex	Female	26.1±0.6^{a}	3,513±36^{a}	Liver*2.5y	19.5±1.2^{e}	3,674±75^{d}
	Male	24.0±0.7^{b}	3,478±43^{a}	Liver*3.5y	20.5±1.5^{de}	3,540±92^{d}
				Heart*Dead	26.4±1.5^{bc}	1,832±95^{a}
				Heart*Killed	25.7±0.5^{c}	1,944±30^{a}
				Kidney*Dead	45.8±1.7^{a}	5,215±105^{d}
				Kidney*Killed	11.8±0.5^{d}	4,537±30^{b}
				Liver*Dead	31.8±1.8^{b}	3,853±112^{c}
				Liver*Killed	8.7±0.5^{e}	3,590±30^{c}

DI=Duration of infection, DM=Disposal method, y=Year,
Least-squares means within each subclass followed by different letters are different at $P<0.05$ using the Tukey-Kramer test.

The number of total cells in the heart and liver were comparable between naturally dead and killed animals, whereas it was significantly greater in the kidneys of dead than

that in the killed animals. The number of total cells in the dead and killed animals were the highest in the kidneys, intermediate in the liver and the lowest in the heart, and the three organs were significantly different within each of the dead and killed groups. Females had a higher percent infiltrated cells and total number of cells than the males, but differences were significant only for the former.

3.3.5 Associations between anti-AMDV antibody titer and severity of histopathological lesion

The distribution of $\log_2$ of antibody titer by sex of mink are shown in Table 3.3.8. There was a significant difference between males and females for the distribution of observations in each antibody titer ($\chi^2_{(1)}$=31.95, P<0.00). A larger number of females (n=66, 34.2%) had antibody titers greater than 16 compared with males (28, 26.4%). Data on four females with antibody titers greater than 256 were combined with those with antibody titer of 256 prior to statistical analyses.

Table 3.3.8 Distribution of antibody titer and $\log_2$ of antibody titer[§] (in brackets) by sex

Sex	0 (0)	1 (1)	2 (2)	4 (3)	8 (4)	16 (5)	32 (6)	64 (7)	128 (8)	256 (9)	512 (10)	1024 (11)	Total
Female	16	14	23	28	27	19	20	30	6	6	3	1	193
Male	20	10	18	6	14	10	9	4	5	10	0	0	106
Total	36	24	41	34	41	29	29	34	11	16	3	1	299

[§]$\log_2$(titer)=0 if titer=0 and $\log_2$(titer)+1 if titer>0.

Stepwise regression models which included the linear and quadratic terms of antibody titer and duration of infection, the interaction between these two variables, sex and its interactions with antibody titer and duration of infection, were used to analyze percent infiltrated cells in killed animals within each organ. The results showed that the

best fitted models were different between the three organs (Table 3.3.9). More importantly, sex and the interaction between sex and duration of infection were significant for the heart, the interaction between antibody titer and sex was significant for the liver, and the interaction between duration of infection and sex was significant for the kidneys. Consequently, data were re-analyzed by stepwise regression models within each sex and organ.

Table 3.3.9 Regression coefficients (β) ± standard errors (SE) and P-values of factors affecting the percent infiltrated cells within the three organs of killed animals calculated by the stepwise procedure.

Factor[§]	Heart		Kidney		Liver	
	β±SE	P-value	β±SE	P-value	β±SE	P-value
Intercept	21.862±1.069	0.000	9.832±1.082	0.000	6.684±0.959	0.000
AbT	-2.4928±0.4747	0.060	-1.7097±0.5618	0.003	-.2610±0.3548	0.46
AbT^2	0.2783±0.0534	0.000	0.3302±0.0525	0.001	0.0864±0.0336	0.011
DI	.	.	.	.	1.0861±0.4581	0.018
DI^2	1.1879±0.1683	0.000	0.5186±0.1654	0.002	.	.
Sex	10.365±2.095	0.000	.	.	.	.
AbT*DI	.	.	-.3758±0.1436	0.009	-.1865±0.1026	0.070
AbT*Sex	.	.	.	.	0.2492±0.1103	0.025
DI*Sex	-3.6646±1.0150	0.000	0.8210±0.3751	0.029	.	.
R^2	0.243		0.202		0.092	

[§]AbT and DI are $\log_2$ of antibody titer and duration of infection (years), respectively

3.3.5.1 The effects of antibody titer and duration of infection on percent infiltrated cells in the heart

Both $\log_2$ antibody titer and duration of infection significantly affected percent infiltrated cells in the heart of females, and the fitted model explained 10.3% of the variations in percent infiltrated cells (Table 3.3.10). Percent infiltrated cells increased exponentially as the duration of infection increased. At no detectable level of antibody, predicted percent infiltrated cells were 28.41, 29.22, 30.82 and 33.23, at 0.5, 1.5, 2.5 and 3.5-year post-inoculation, respectively. These values show 0.80%, 1.61% and 2.41%

increase in percent infiltrated cells for the successive increases in the duration of infection, i.e. the rate of change in percent infiltrated cells doubled for each year increase in the duration of infection. The total change in percent infiltrated cells when the duration of infection increased from 0.5 to 3.5 years was 4.82. The same rates of change were observed at all levels of antibody titer, showing that the highest percent infiltrated cells within each level of antibody titer was observed at 3.5 years after infection (Fig. 3.3.1). The predicted percentages of infiltrated cells at $\log_2$ antibody titer of 9 were 28.99, 29.80, 31.40 and 33.81, at 0.5, 1.5, 2.5 and 3.5 years post inoculation, respectively, and 33.81% was the maximum predicted percent infiltrated cells.

The predicted percentages of infiltrated cells in the heart of female mink which were infected for 0.5 years were 28.41, 26.16, 24.49, 23.40, 22.88, 22.95, 23.59, 24.81, 26.61 and 28.99 at $\log_2$ antibody titers from zero to nine, respectively. These values showed -2.25%, -1.67%, -1.09%, -0.51%, 0.06%, 0.64%, 1.22%, 1.80%, 2.38% changes in percent infiltrated cells as the $\log_2$ of antibody titer increased by one unit (Fig. 3.3.1). At 0.5 years after inoculation, the minimum predicted value of 22.88% was observed at $\log_2$ antibody titer of 4, and the maximum value of 28.99% was just slightly (0.58%) above the predicted value at antibody titer of zero. The rates of change in percent infiltrated cells by successive increases in antibody titer at other durations of infection were the same as those for 0.5 years of infection (Fig. 3.3.1), showing that the lowest percent infiltrated cells were at $\log_2$ antibody titer of four at all durations of infection (22.88%, 23.69%, 25.29% and 27.70%) and the highest were at $\log_2$ antibody titer of 9 (28.99%, 29.80%, 31.40% and 33.81%).

Percent infiltrated cells in the heart of males was significantly affected by the linear and quadratic forms of $\log_2$ antibody titer and the duration of infection, and the model

explained a rather large proportion of variations (37.6%) in percent infiltrated cells (Table 3.3.10). At no detectable level of antibody, predicted percent infiltrated cells were 23.12, 23.10, 27.84 and 37.34 at 0.5, 1.5, 2.5 and 3.5-year post-inoculation, respectively. These values show a slight decline (-0.02) in percent infiltrated cells in animals which were infected for 1.5 years compared with those which were infected for 0.5 year. Percent infiltrated cells then increased by 4.74% and 9.50% as the duration of infection prolonged from 1.5 to 2.5 years, and from 3.5 to 2.5 years, respectively. i.e. a substantial increase in percent infiltrated cells in animals which were infected for more than 1.5 years. The rates of change in percent infiltrated cells by changes in the duration of infection at all other antibody levels were the same as those for no antibody titer, showing that the lowest and the highest percentages of infiltrated cells within each level of $\log_2$ antibody titer were at 1.5 and 3.5 years, respectively (Fig. 3.3.2). The total change in percent infiltrated cells when the duration of infection changed from 0.5 to 3.5 years was 14.22.

The predicted percentages of infiltrated cells in the heart of male mink which were infected for 0.5 years were 23.12, 21.43, 20.13, 19.21, 18.68, 18.52, 18.76, 19.37, 20.36 and 21.75 for $\log_2$ antibody titers from zero to nine, respectively. These values show -1.69%, -1.30%, -0.92%, -0.54%, -0.15%, 0.23%, 0.61%, 1.00% and 1.38% changes in percent infiltrated cells as the $\log_2$ of antibody titer increased by one unit from zero to nine, respectively (Fig. 3.3.2). In animals which were infected for 0.5 years, the minimum predicted value of 18.52% was observed at $\log_2$ antibody titer of 5, and the maximum value of 23.12% was at $\log_2$ antibody titer of zero. The total change in percent infiltrated cells when $\log_2$ antibody titer changed from zero to nine was -1.37%, suggesting a small decline in percent infiltrated cells at the highest antibody titer compared with those with no

detectable level of antibody. The rates of change in percent infiltrated cells by successive increases in $\log_2$ antibody titer at other durations of infection were the same as those for 0.5 years of infection (Fig. 3.3.2), showing that the lowest percent infiltrated cells were at $\log_2$ antibody titer of five at all durations of infection. The predicted percent infiltrated cells at 1.5-years post inoculation, which were the lowest among all durations of infection were 23.10, 21.41, 20.11, 19.19, 18.66, 18.50, 18.74, 19.35, 20.35 and 21.73 for $\log_2$ antibody titers from zero to nine, respectively. The corresponding values after 3.5 years of inoculation, which were the highest amounts, were 37.34%, 35.65%, 34.35%, 33.43%, 32.89%, 32.74%, 32.97%, 33.59%, 34.58% and 35.97%. The minimum predicted percent infiltrated cells was 18.50 which was reached at $\log_2$ antibody titer of 5 and duration of infection of 1.5 years, and the maximum value was at $\log_2$ antibody titer of zero and duration of infection of 3.5 years.

Table 3.3.10 Regression coefficient (β) ± standard error (SE) and P-values of $\log_2$ of antibody titer (AbT) and duration of infection (DI) on percent infiltrated cells in the heart of female and male animals.

	Female		Male	
Factor	β ±SE	P-value	β ±SE	P-value
Intercept	28.314±1.453	0.000	24.914±2.019	0.000
AbT	-2.5404±0.6520	0.000	-1.8775±0.7446	0.013
AbT^2	0.2894±0.0727	0.000	0.1917±0.0869	0.029
DI	.	.	-4.7790±2.6407	0.073
DI^2	0.4015±01498	0.008	2.3796±0.6794	0.001
R^2	0.103		0.376	

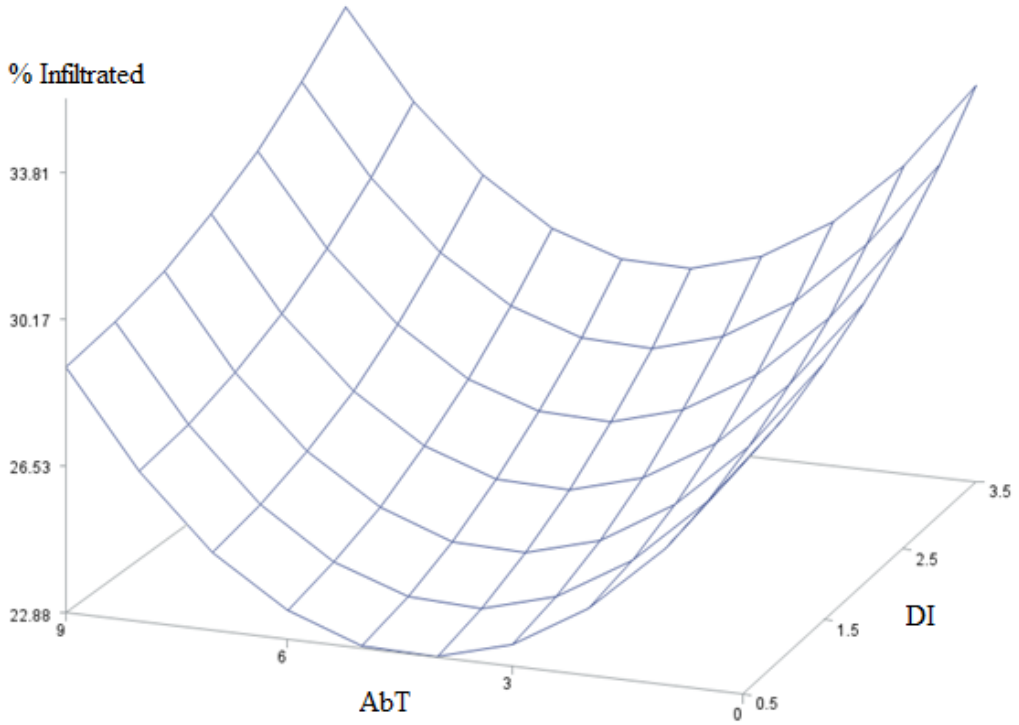

Figure 3.3.1 Effects of antibody titer (AbT) and duration of infection (DI) on percent infiltrated cells in the heart of female animals.

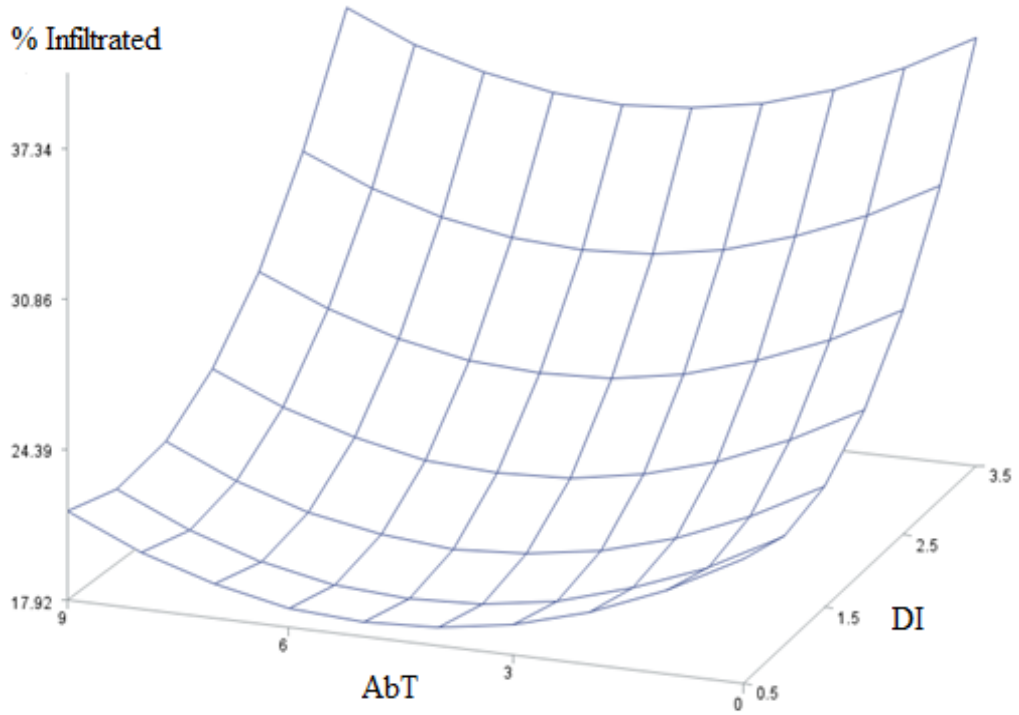

Figure 3.3.2 Effects of antibody titer (AbT) and duration of infection (DI) on percent infiltrated cells in the heart of male animals.

3.3.5.2 The effects of antibody titer and duration of infection on percent infiltrated cells in the kidneys

Percent infiltrated cells in the kidneys of females was significantly affected by the linear and quadratic forms of $\log_2$ antibody titer and the duration of infection (Table 3.3.11). The model explained 22.4% of variations in percent infiltrated cells. At no detectable level of antibody, predicted percent infiltrated cells were 16.85, 13.55, 14.28 and 18.95 at 0.5, 1.5, 2.5 and 3.5-years post-inoculation, respectively. These values show that percent infiltrated cells decreased by -3.31% as the duration of infection increased from 0.5 to 1.5 years, and then increased by 0.70% and 4.71% as the duration of infection prolonged from 1.5 to 2.5 years, and from 2.5 to 3.5 years, respectively. i.e. a large increase in percent infiltrated cells in animals which were infected for more than 2.5 years. The rates of change in percent infiltrated cells by changes in the duration of infection at all other $\log_2$ antibody titers were the same as those for no antibody titer, showing that the lowest and the highest percentages of infiltrated cells within each level of $\log_2$ antibody titer were at 1.5 and 3.5 years, respectively (Fig. 3.3.3). The total change in percent infiltrated cells when the duration of infection changed from 0.5 to 3.5 years was 2.10.

The predicted percentages of infiltrated cells in the kidneys of female mink which were infected for 0.5 years were 16.85, 14.35, 12.62, 11.66, 11.46, 12.04, 13.39, 15.50, 18.39 and 22.04 for $\log_2$ antibody titers from zero to nine, respectively. These values show -2.50, -1.73, -0.96, -0.19, 0.58, 1.35, 2.12, 2.89 and 3.66 changes in percent infiltrated cells as the $\log_2$ of antibody titer increased by one unit from zero to nine, respectively (Fig. 3.3.3). In animals which were infected for 0.5 years, the minimum predicted value of 11.46% was observed at $\log_2$ antibody titer of four, and the maximum value of 18.39% was at $\log_2$ antibody titer of nine. The total change in percent infiltrated cells when $\log_2$ antibody

titer changed from zero to nine was 5.19%. The rates of change in percent infiltrated cells by successive increases in $\log_2$ antibody titer at other durations of infection were the same as those for 0.5 years of infection (Fig. 3.3.3), showing that the lowest percent infiltrated cells were at $\log_2$ antibody titer of four at all durations of infection. The predicted percent infiltrated cells at 1.5-year post inoculation, which were the lowest among all durations of infection were 13.55, 11.04, 9.31, 8.35, 8.16, 8.73, 10.08, 12.20, 15.08 and 18.74 for $\log_2$ antibody titers from zero to nine, respectively. The corresponding values after 3.5 years of inoculation, which were the highest amounts, were 18.95, 16.45, 14.72, 13.75, 13.56, 14.14, 15.48, 17.60, 20.48 and 24.14. The minimum predicted percent infiltrated cells was 8.16 which was reached at $\log_2$ antibody titer of 4 and duration of infection of 1.5 years, and the maximum value (24.14) was at $\log_2$ antibody titer of nine and duration of infection of 3.5 years. The relationships between percent infiltrated cells and $\log_2$ antibody titer in the kidneys of male mink was curvilinear. The predicted percent infiltrated cells was 11.09% at $\log_2$ antibody titer of zero, declined to 8.06% at $\log_2$ antibody titer of 3.2 (-b/2a), then increased to 17.97% at $\log_2$ antibody titer of nine. This model explained only 15.3% of variations in percent infiltrated cells.

Table 3.3.11 Regression coefficient (β) ± standard error (SE) and P-values of $\log_2$ of antibody titer (AbT) and duration of infection (DI) on percent infiltrated cells in the kidneys of the female and male animals.

	Female		Male	
Factor	β ±SE	P-value	β ±SE	P-value
Intercept	20.008±4.520	0.000	11.088±1.333	0.000
AbT	-2.8873±0.5704	0.000	-1.8925±0.7661	0.015
AbT^2	0.3849±0.0636	0.000	0.2953±0.0862	0.001
DI	-7.3100±4.1441	0.079	.	.
DI^2	2.0023±0.8924	0.026	.	.
R^2	0.224		0.153	

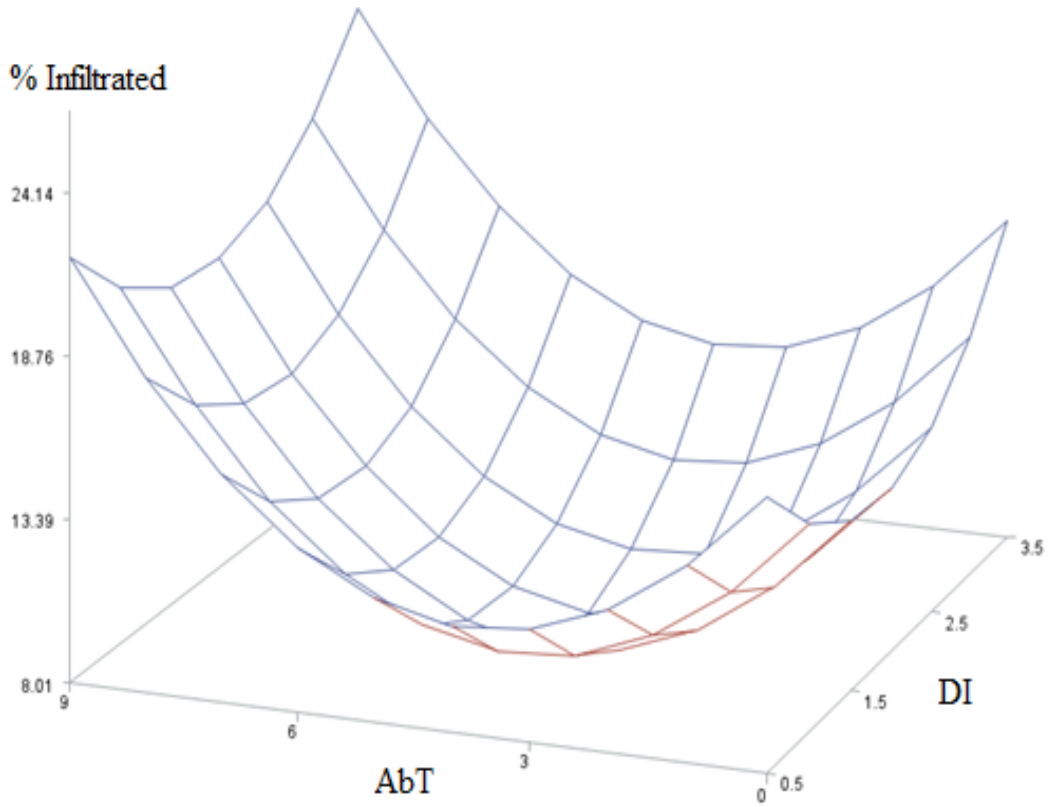

Figure 3.3.3 Effects of antibody titer (AbT) and duration of infection (DI) on percent infiltrated cells in the kidneys of female animals.

3.3.5.3 The effects of antibody titer and duration of infection on percent infiltrated cells in the liver

The relationships between percent infiltrated cells and $\log_2$ antibody titer in the liver of female mink was curvilinear, and the fitted model explained 10.8% of variations in percent infiltrated cells (Table 3.3.12). The predicted percent infiltrated cells was 9.90% at $\log_2$ antibody titer of zero, declined to a minimum of 8.09 at $\log_2$ antibody titer of 3.2 (-b/2a), then increased to 13.81% at $\log_2$ antibody titer of nine. The $\log_2$ antibody titer had a linear and significant effect on percent infiltrated cells in the liver of male mink. Each unit increase in $\log_2$ antibody titer resulted in 0.22% increase in percent infiltrated cells, and only 3.9% of variations in percent infiltrated cells was explained by this equation.

Table 3.3.12 Regression coefficient (β) ± standard error (SE) and P-values of log_2 of antibody titer (AbT) and duration of infection (DI) on percent infiltrated cells in the liver of female and male animals.

	Female		Male	
Factor	β ±SE	P-value	β ±SE	P-value
Intercept	9.909±0.824	0.000	7.745±0.497	0.000
AbT	-1.1227±0.4198	0.008	0.2218±0.1078	0.042
AbT^2	0.1729±0.0467	0.000	.	.
R^2	0.108		0.039	

3.3.5.4 The effects of antibody titer on percent infiltrated cells within sex and organs

The effect of log_2 antibody titer, excluding the duration of infection, was tested on percent infiltrated cells within each organ and sex, because the exact time of establishment of infection is not known on farms. These analyses were performed only for percent infiltrated cells in the heart of males and females and in the kidneys of females, because the duration of infection did not enter the fitted models in the kidneys of males and the liver of males and females (Tables 3.3.11 and 3.3.12). Antibody titer did not have any significant effect on percent infiltrated cells in the heart of male mink (Table 3.3.13), but the relationships between percent infiltrated cells and log_2 antibody titer in the heart and kidneys of female mink were curvilinear, explaining 6.98% and 16.29% of variations of percent infiltrated cells, respectively. The predicted percent infiltrated cells in the heart of females was 30.17% at no detectable level of antibody, reached a minimum value of 24.70% at log_2 antibody titer of 4.47 (-b/2a), then increased to 30.32% at log_2 antibody titer of nine. In the kidneys of females, the predicted percent infiltrated cells was 14.41 at log_2 antibody titer of zero, declined to a minimum value of 9.05% at log_2 antibody titer of 3.80, and increased to 19.07 at log_2 antibody titer of nine.

Table 3.3.13 Linear (b) and quadratic (a) regression coefficients ± standard errors and P-values of antibody titer on percent infiltrated cells within organs and sex.

Organ	Intercept	b±SE	Pr.	a±SE	Pr.	R^2
Heart						
Male	24.328±1.124	-0.3883±0.2434	0.11	.	.	0.239
Female	30.169±1.298	-2.4464±0.6616	0.000	0.2737±0.0736	0.000	0.689
Kidney						
Female	14.414±1.154	-2.8193±0.5879	0.000	0.3707±0.0654	0.000	0.163

3.3.6 Associations between serum gamma-globulin levels and severity of histopathological lesion

The number of male and female mink in various classes of IAT scores were comparable ($\varkappa^2_{(1)}$ =4.69, P=0.32) (Table 3.3.14). The Spearman's rank correlation between antibody titers and IAT scores was intermediate and significant (r=0.37, P<0.001). The results of stepwise regression analyses within organs, which included the linear and quadratic terms of IAT score, duration of infection and their interaction, sex, and its interactions with IAT score and duration of infection are shown in Table 3.3.15. Sex had a significant effect on percent infiltrated cells in the heart and kidneys, and the interaction between sex and gamma-globulin levels was significant in the liver. Thus, the data were re-analyzed within sex and organ using stepwise regression models.

3.3.6.1 The effects of serum gamma-globulin level and duration of infection on percent infiltrated cells in the heart

Percent infiltrated cells in the heart of female mink was significantly affected by the linear and quadratic forms of serum gamma-globulin level and the quadratic form of the duration of infection (Table 3.3.16). The predicted percentages of infiltrated cells at IAT score of zero were 23.6, 24.4, 25.9 and 28.2 for 0.5, 1.5, 2.5 and 3.5 years of infection,

respectively. The predicted values at all durations of infection increased as IAT scores increased, reached peaks at the score of 2 (26.1%, 26.8%, 28.3% and 30.6%, respectively), then declined to 22.3%, 23.1%, 24.6% and 26.9% at IAT score of 4.0. These values show that as the duration of infection increased from 0.5 to 1.5 years, percent infiltrated cells increased by 0.75%, and the rates of increase were 1.50% and 2.26% for the other incremental changes in the durations of infection (Table 3.3.17, Fig. 3.3.4). These changes were the same across all levels of gamma-globulin, and suggest that increases in percent infiltrated cells at all levels of serum gamma-globulin were more pronounced as the duration of infection became longer.

Table 3.3.14 Distribution of serum gamma-globulin levels (IAT score) by sex.

	IAT score					
Sex	0	1	2	3	4	Total
Female	69	80	20	16	8	193
Male	87	34	11	12	2	106
Total	116	114	31	28	10	299

Table 3.3.15 Regression coefficients (β) ± standard errors (SE) and P-values of factors affecting the percent infiltrated cells within the three organs of killed animals calculated by the stepwise procedure.

Factors[§]	Heart		Kidney		Liver	
	β±SE	Pr	β±SE	Pr	β±SE	Pr
Intercept	21.711±1.813	0.000	12.642±1.788	0.000	8.005±0.311	0.000
IAT	1.87533±0.97906	0.056	3.72048±1.14048	0.001	1.05299±0.47783	0.028
IAT^2	-0.43301±0.28840	0.134	0.78757±0.27040	0.004	.	.
DI	-4.35319±2.17427	0.046	-7.11334±1.92994	0.000	.	.
DI^2	2.08320±0.57744	0.000	2.26289±0.46209	0.000	.	.
IAT*DI	.	.	-2.21122±0.40343	0.000	-0.29187±0.18613	0.118
SEX	10.41502±2.42725	0.000	2.16873±0.83119	0.010	.	.
IAT*SEX	.	.	.	.	0.78021±0.33208	0.020
DI*SEX	-3.63681±1.11091	0.001	.	.	.	.
R^2	0.196		0.214		0.809	

[§]IAT and DI are gamma-globulin level and duration of infection (years), respectively.

At 0.5 years after inoculation, the predicted percent infiltrated cells in the heart of females were 23.6, 25.6, 26.1, 25.0 and 22.3 at IAT scores of 0, 1, 2, 3 and 4, respectively. The value at IAT of 4 (22.3%) was the minimum predicted percent infiltrated cells. The corresponding values at 3.5 years of infection increased to 28.2%, 30.1%, 30.6%, 29.5% and 26.9%, respectively. The predicted value of 30.6% at IAT score of 2 and duration of infection of 3.5 years was the maximum predicted value of percent infiltrated cells. The rate of increase in percent infiltrated cells was 1.98% when the gamma-globulin level increased from zero to one, followed by 0.44%, -1.1% and -2.6% changes for incrementally higher levels of gamma-globulin, which reflect the curvilinear natures of changes in percent infiltrated cells as gamma-globulin levels increased (Fig. 3.3.4). Total changes in percent infiltrated cells for the duration of infection from 0.5 to 3.5 years was 4.52%, and for the IAT score from 0 to 4 was -1.3% (Table 3.3.17).

Table 3.3.16 Regression coefficient (β) ± standard error and P-values of serum gamma-globulin level and duration of infection (DI) on percent infiltrated cells in the heart of female and male mink.

Factor[§]	Female		Male	
	β±SE	P-value	β±SE	P-value
Intercept	23.548±1.044	0.000	23.388±1.903	0.000
IAT	2.7473±1.2304	0.027	0.7329±0.5633	0.196
IAT^2	-0.7678±0.3513	0.030	.	.
DI	.	.	-6.7100±2.4021	0.006
DI^2	0.3761±0.1552	0.016	2.7282±0.6522	0.000
R^2	0.053		0.344	

[§]IAT and DI are gamma-globulin level and duration of infection (years), respectively.

Table 3.3.17 Predicted changes in percent infiltrated cells in the heart of male and female mink by differences between consecutive durations of infection at various levels of gamma-globulin (IAT score), and differences between consecutive gamma-globulin levels at different durations of infection.

Difference between durations of infection, years	IAT score (0,1,2,3,4)		Difference between IAT scores	Duration of infection (0.5, 1.5. 2.5, 3.5 years)	
	Female	Male		Female	Male
1.5 – 0.5	0.75	-1.25	1-0	1.98	0.73
2.5 – 1.5	1.50	4.20	2-1	0.44	0.73
3.5 – 2.5	2.26	9.66	3-2	-1.09	0.73
			4-3	-2.63	0.73
3.5 – 0.5	4.52	12.61	4-0	-1.30	2.92

The effects of the level of serum gamma-globulin on percent infiltrated cells in the heart of male mink was positive but non-significant, but the duration of infection showed a significant quadratic relationship with percent infiltrated cells (Table 3.3.16). At the gamma-globulin level of zero, the predicted percentages of infiltrated cells were 20.7, 19.5, 23.7 and 33.3 at 0.5, 1.5, 2.5 and 3.5 years of infection, respectively. These values steadily increased by 0.73% as the gamma-globulin levels increased by one unit, and reached 23.6%, 22.4%, 26.6% and 36.3% at gamma-globulin level of 4. The rate of change in percent infiltrated cells by each unit increase in IAT score (0.73%) was the same for changes in every duration of infection (Table 3.3.17, Fig. 3.3.5).

Predicted percent infiltrated cells after 0.5 years of infection in the heart of male mink were 20.7, 21.4, 22.2, 22.9 and 23.6, for the IAT scores of 0, 1, 2, 3 and 4, respectively. These values declined by 1.25% at all levels of IAT scores to 19.5%, 20.1%, 20.9%, 21.7% and 22.4%, respectively, at 1.5 years of infection. The predicted values then increased by 4.2% from 1.5 to 2.5 years of infection, and by 9.66% (Table 3.3.17) to 33.3%, 34.1%, 34.7%, 35.5% and 36.3% after 3.5 years of infection at IAT score of 4. The minimum predicted percent infiltrated cells was 19.5% at IAT score of zero and duration

of infection of 1.5 years, and the maximum predicted value was 36.3% at the IAT score of 4 and duration of infection of 3.5 years. Total changes in percent infiltrated cells for the duration of infection from 0.5 to 3.5 years was 12.6%, and for the IAT score from 0 to 4 was 2.9% (Table 3.3.17). A small proportions of variations in percent infiltrated cells in the heart was explained by the regression model in females (R^2=5.3%), but it was considerably higher in males (R^2=34.4%).

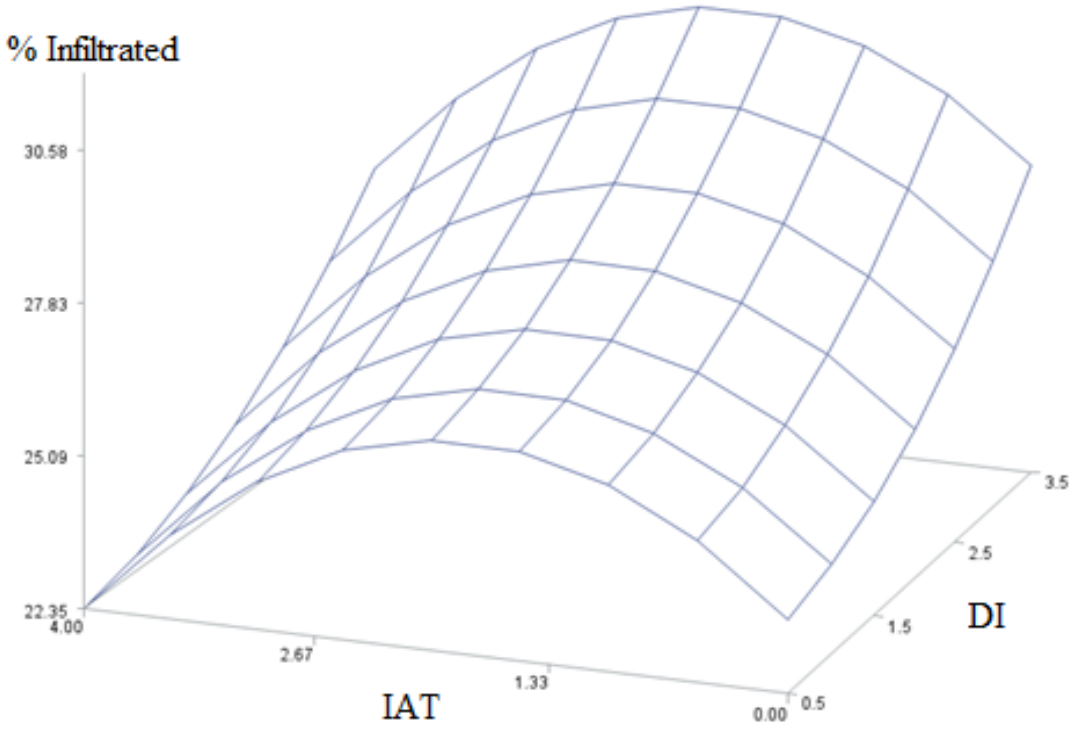

Figure 3.3.4 Effects of serum gamma-globulin level (IAT) and duration of infection (DI) on percent infiltrated cells in the heart of female animals.

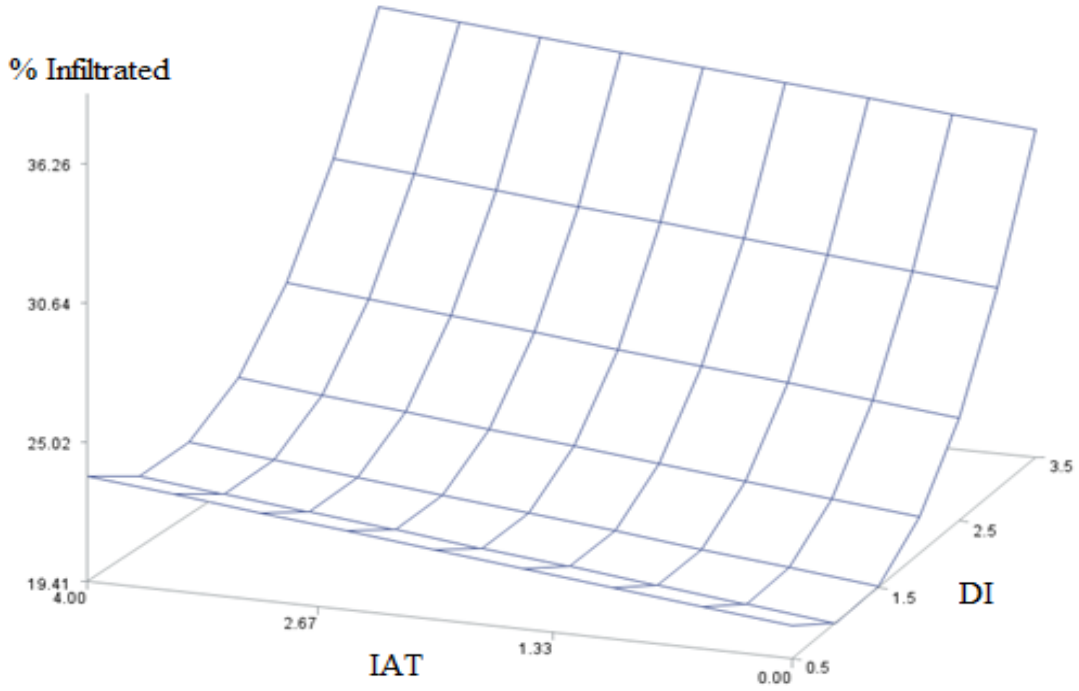

Figure 3.3.5 Effects of serum gamma-globulin level (IAT) and duration of infection (DI) on percent infiltrated cells in the heart of male animals.

3.3.6.2 The effects of serum gamma-globulin level and duration of infection on percent infiltrated cells in the kidneys

Percent infiltrated cells in the kidneys of female mink was significantly influenced by the linear and quadratic forms of gamma-globulin level and duration of infection, as well as the interaction between gamma-globulin level and duration of infection (Table 3.3.18), suggesting a complex association among the variables (Fig. 3.3.6). The minimum predicted value of percent infiltrated cells was 9.0, which was observed at IAT score of zero and duration of infection of 1.5 years, and the maximum value of 42.6% was attained at IAT score of 4 and duration of infection of 0.5 year. As the duration of infection increased from 0.5 to 1.5 years, predicted percent infiltrated cells decreased at all levels of IAT scores at an increasing rate, ranging from -5.04% at IAT score of zero to -16.22% at the IAT score of 4 (Table 3.3.19). The increase in the duration of infection from 1.5 to 2.5

years resulted in a small increase (1.64%) in percent infiltrated cells at IAT score of zero, but percentages of infiltrated cells declined in accelerated rates as IAT scores increased. Almost the same situation was observed when duration of infection increased from 2.5 to 3.5 years, showing 8.33% increase in percent infiltrated cells at IAT score of zero, followed by 5.54%, 2.76%, -0.26% and -2.81% at incremental levels of IAT scores. Total predicted changes from 0.5- to 3.5-year duration of infection ranged from 4.93% at IAT score of zero to -28.48% at the IAT score of 4 (Table 3.3.19).

At all durations of infection, predicted percent infiltrated cells increased as the levels of gamma-globulin increased, and the rates of changes were positive and large at 0.5 years of infection (4.35% to 9.93%), and became smaller and mostly negative at 3.5 years of infection (Table 3.3.20, Fig. 3.3.6). Total changes in percent infiltrated cells as IAT score changed from zero to 4 was 28.55% at 0.5-years of infection, followed by 17.42%, 6.28% and -4.85% at subsequent durations of infection.

Table 3.3.18 Regression coefficient (β) ± standard error and P-values of serum gamma-globulin level and duration of infection (DI) on percent infiltrated cells in the kidneys of female and male mink.

Factor[§]	Female		Male	
	β±SE	P-value	β±SE	P-value
Intercept	19.074±4.670	0.000	8.541±0.882	0.000
IAT	4.8105±1.7077	0.005	4.6494±1.0223	0.000
IAT^2	0.9298±0.3079	0.003	.	.
DI	-11.7260±4.2716	0.007	.	.
DI^2	3.3421±0.9273	0.000	.	.
IAT*DI	-2.7838±0.6364	0.000	-1.3724±0.4137	0.001
R^2	0.213		0.169	

[§]IAT and DI are antibody titer and duration of infection (years), respectively.

Table 3.3. 19 Predicted changes in percent infiltrated cells in the kidneys of female mink by increases in the duration of infection at various levels of gamma-globulins (IAT score).

Difference between duration of infection, years	IAT score				
	0	1	2	3	4
1.5 – 0.5	-5.04	-7.83	-11.0	-13.1	-16.22
2.5 – 1.5	1.64	-1.14	-3.91	-6.70	-9.49
3.5 – 2.5	8.33	5.54	2.76	-0.26	-2.81
3.5 – 0.5	4.93	-3.42	-11.77	-20.13	-28.48

The effect of serum gamma-globulin level on percent infiltrated cells in the kidneys of male mink was linear and significant, as was the interaction between serum gamma-globulin levels and duration of infection (Table 3.3.18). The minimum predicted percent infiltrated cells of 7.93% was observed at IAT score of 4 and duration of infection of 3.5 years. This value showed small increases to 8.08%, 8.23%, 8.39% and 8.54% as IAT scores declined to 3, 2, 1 and zero, respectively (Fig. 3.3.7), i.e. increase in IAT scores from zero to 4 resulted in a total of 0.61% decrease in percent infiltrated cells when animals were infected for 3.5 years (Table 3.3.21). The maximum percent infiltrated cells was attained at IAT score of 4 and duration of infection of 0.5 years. This value decreased to 20.43%, 16.47%, 12.50% and 8.51% as the IAT score decreased to 3, 2, 1 and zero, respectively. i.e. increase in IAT score from zero to 4 resulted in a total of 15.85% increase in percent infiltrated cells when animals were infected for 0.5 years (Table 3.3.21).

Table 3.3.20 Predicted changes in percent infiltrated cells in the kidneys of female mink by increases in the level of gamma-globulin (IAT score) at various durations of infection.

Difference between IAT scores	Duration of infection, years			
	0.5	1.5	2.5	3.5
1-0	4.35	1.56	-1.20	-4.00
2-1	6.21	3.42	0.64	-2.14
3-2	8.07	5.28	2.50	-0.28
4-3	9.93	7.14	4.36	1.58
4-0	28.55	17.42	6.28	-4.85

Changes in percent infiltrated cells in the kidneys of male mink were the same between consecutive durations of infection, i.e., 1.5-0.5, 2.5-1.5 and 3.5-2.5 years at each level of gamma-globulin (Table 3.3.21). At the IAT score of zero, there was no change in percent infiltrated cells when the durations of infection changed from 0.5 to 3.5 years, but the differences in percent infiltrated cells decreased from -1.3% to -5.49% as IAT scores increased by one unit from 1 to 4, respectively. A similar pattern, although larger in magnitude, was observed when duration of infection changed from 0.5 to 3.5 years and IAT scores changed from 0 to 4 (Table 3.3.21, Fig. 3.3.7). Changes in percent infiltrated cells were also the same at each duration of infection when IAT scores changed by one unit. The amount of change in percent infiltrated cells was the largest (3.96%) at duration of infection of 0.5 year, and steadily decreased as the duration of infection prolonged (Table 3.3.21). The total changes in percent infiltrated cells when IAT changed from zero to 4 was 15.85% after 0.5 years of infection, and this value reduced to -0.61% after 3.5 years of infection. The above values imply the presence of different effects of gamma-globulin levels on percent infiltrated cells in recently infected animals compared with those which were infected for a longer time. Considerable proportions of variations among percent infiltrated cells were explained by the regression equations, i.e. 21.3% in females and 16.9% in males.

Table 3.3.21 Predicted changes in percent infiltrated cells in the kidneys of male mink by increases in the duration of infection at various levels of gamma-globulins (IAT score), and increases in the gamma-globulin levels at various durations of infection.

Durations of infection, years	IAT score	Change in % infiltrated cells	IAT score	Duration of infection, years	Change in % infiltrated cells
Difference	0	0.0	Difference	0.5	3.96
between all	1	-1.3	between all	1.5	2.59
consecutive	2	-2.7	consecutive	2.5	1.22
years	3	-4.1	IAT scores	3.5	-0.15
	4	-5.49			
3.5 – 0.5	0	0.0	4-0	0.5	15.85
	1	-4.12		1.5	10.36
	2	-8.24		2.5	4.87
	3	-12.35		3.5	-0.61
	4	-16.47			

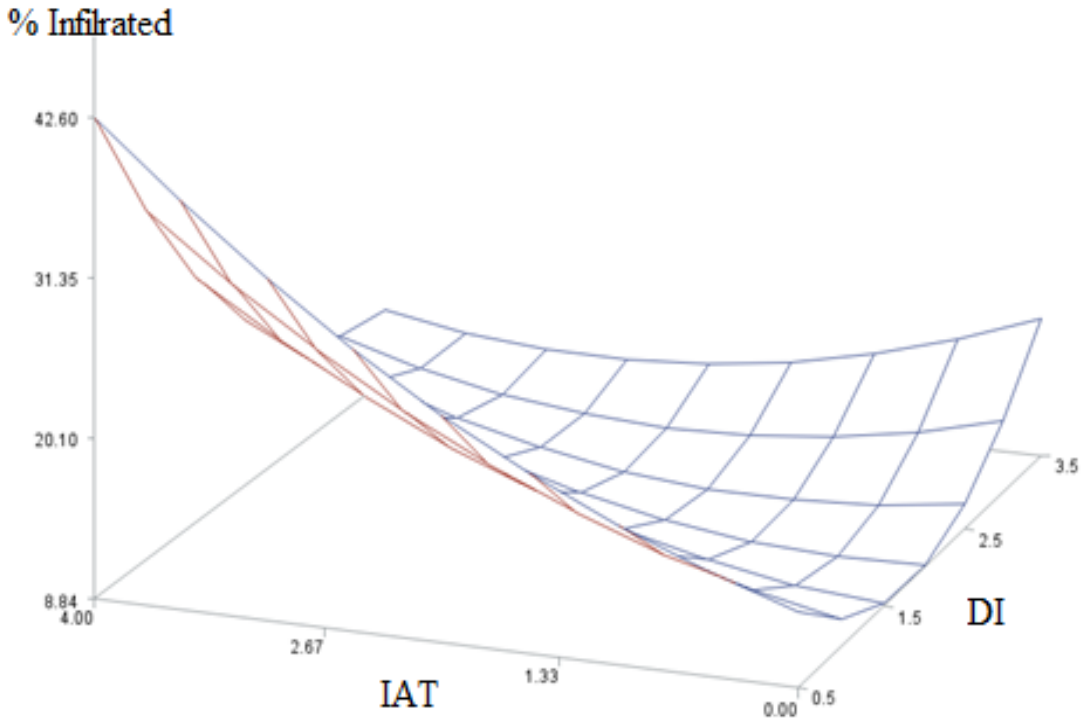

Figure 3.3. 6 Effects of serum gamma-globulin level (IAT) and duration of infection (DI) on percent infiltrated cells in the kidneys of female animals.

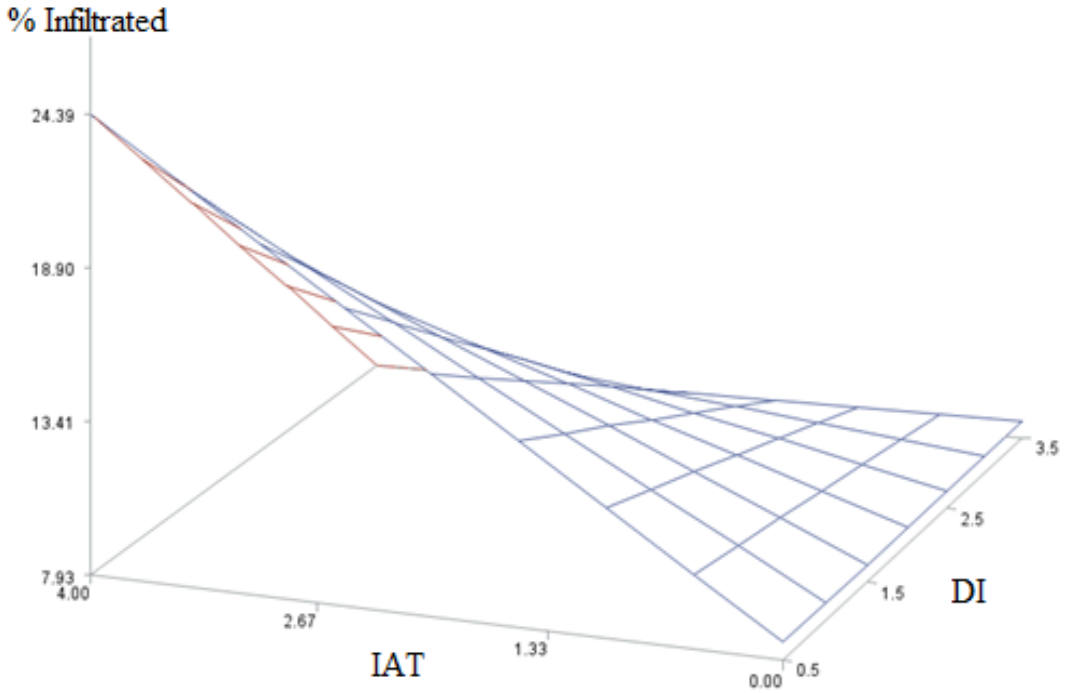

Figure 3.3.7 Effects of serum gamma-globulin level (IAT) and duration of infection (DI) on percent infiltrated cells in the kidneys of male animals.

3.3.6.3 The effects of serum gamma-globulin level and duration of infection on percent infiltrated cells in the liver

Percent infiltrated cells in the liver of female mink were significantly affected by the serum gamma-globulin, duration of infection and the interaction between gamma-globulin level and duration of infection (Table 3.3.22), and the model explained 11.5% of variations in percent infiltrated cells. The minimum predicted percent infiltrated cells was 7.65, which was observed at IAT score of zero and duration of infection of 1.5 years, and the maximum value of 23.35% was observed at IAT score of 4 and duration of infection of 0.5 years (Fig. 3.3.8). At the IAT score of zero, predicted percent infiltrated cells were 10.17, 7.65, 7.79 and 10.58 for 0.5, 1.5, 2.5 and 3.5 years of infection, respectively. These values changed by 3.27%, 2.08%, 0.87% and -0.34% for each unit increase in the IAT

score at 0.5, 1.5, 2.5 and 3.5 years of infection, respectively, indicating that changes in percent infiltrated cells for each unit increases in IAT score were the same within each year of infection, and was the greatest at 0.5 years and the smallest after 3.5 years of infection.

Table 3.3.22 Regression coefficient (β) ± standard error and P-values of serum gamma-globulin levels and duration of infection (DI) on percent infiltrated cells in the liver of female and male mink.

Factor[§]	Female		Male	
	β±SE	P-value	β±SE	P-value
Intercept	12.422±3.326	0.000	7.780±0.413	0.000
IAT	3.9007±1.0913	0.000	0.5989±0.2879	0.040
DI	-5.1697±3.0820	0.095	.	.
DI^2	1.3269±0.6691	0.049	.	.
IAT*DI	-1.2114±0.4625	0.010	.	.
R^2	0.115		0.040	

[§]IAT and DI are antibody titer and duration of infection (years), respectively.

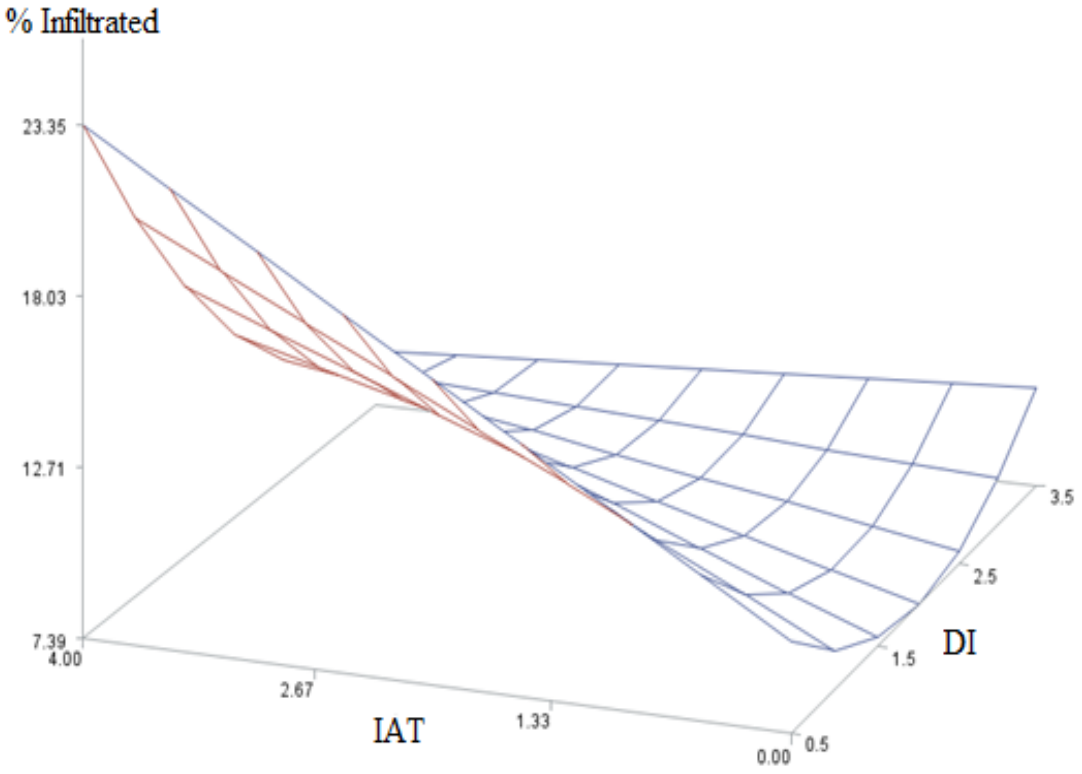

Figure 3.3.8 Effects of serum gamma-globulin level (IAT) and duration of infection (DI) on percent infiltrated cells in the liver of female animals.

After 0.5 years of infection, percent infiltrated cells were 10.17, 13.46, 16.76, 20.05 and 23.39 for IAT scores of 0, 1, 2, 3 and 4, respectively. As the duration of infection increased from 0.5 to 3.5 years, percent infiltrated cells changed by 0.41%, -3.22%, -6.83%, -10.52% and -14.14% at IAT scores of 0, 1, 2 ,3 and 4, respectively (Table 3.3.23), showing sharper declines in percent infiltrated cells at higher IAT scores. Changes in percent infiltrated cells between subsequent durations of infection were also greater in higher IAT scores (Table 3.3.23). Percent infiltrated cells in the liver of male mink was significantly affected by the linear IAT values, which explained 4% of variations in percent infiltrated cells (Table 3.3.22). Each unit increase in IAT score resulted in 0.5989% increase in percent infiltrated cells.

Table 3.3.23 Predicted changes in percent infiltrated cells in the liver of female mink by increases in the duration of infection at various levels of gamma-globulins (IAT score).

Difference between duration of infection, years	IAT score				
	0	1	2	3	4
1.5 – 0.5	-2.52	-3.73	-4.90	-6.20	-7.36
2.5 – 1.5	0.14	-1.07	-2.30	-3.51	-4.71
3.5 – 2.5	2.79	1.58	0.37	-0.81	-2.05
3.5 – 0.5	0.41	-3.22	-6.83	-10.52	-14.12

3.3.6.4 The effects of serum gamma-globulin level on percent infiltrated cells

The results of linear and quadratic regression of gamma-globulin levels, excluding the duration of infection, on percent infiltrated cells within each organ and sex are shown in Table 3.3.24. Gamma-globulin level had a linear and significant effect on percent infiltrated cells in the heart, kidneys and liver of male mink, as well as on the liver of female mink. Each unit increase in the level of gamma-globulin resulted in 1.80%, 1.94% and

0.60% increase in percent infiltrated cells in the heart, kidneys and liver of male mink, respectively, explaining 7.2%, 8.0% and 4.0% of variations in percent infiltrated cells. Each unit increase in the level of gamma-globulin resulted in 1.1% increase in percent infiltrated cells in the liver of female mink, and explained 6.9% of variations in percent infiltrated cells.

The relationships between percent infiltrated cells and gamma-globulin levels in the heart and kidneys of female mink were curvilinear. The predicted percent infiltrated cells in the heart of female mink was 25.23% at IAT score of zero, reached a peak of 27.77% at IAT score of 1.92 (-b/2a), then declined to 24.79% at IAT score of 4. This model explained only 2.3% of variations in percent infiltrated cells. Predicted percent infiltrated cells in the kidneys of female mink was 10.70% at IAT score of zero, slightly declined to a minimum value of 10.48% at IAT score of 0.57 (-b/2a) and elevated to 18.7% at IAT score of 4. This model explained 8.6% variations in percent infiltrated cells.

Table 3.3.24 Linear (b) and quadratic (a) regression coefficients ± standard errors and P-values of gamma-globulin level on percent infiltrated cells within organ and sex.

Organ	Intercept	b±SE	P-value	a±SE	P-value	R^2,%
Heart						
Male	21.226±0.909	1.8046±0.6342	0.005	.	.	7.2
Female	25.231±0.790	2.6475±1.2454	0.035	-0.6892±0.3543	0.053	2.3
Kidney						
Male	8.736±0.922	1.9378±0.6428	0.003	.	.	8.0
Female	10.704±0.716	-0.7989±1.1291	0.48	0.6971±0.3212	0.031	8.6
Liver						
Male	7.780±0.413	0.5989±0.2879	0.040	.	.	4.0
Female	8.227±0.426	1.0678±0.2849	0.000	.	.	6.9

3.4 Discussion

The current study is the only one in which a large number of AMDV-infected mink, with a broad range of durations of infection (six months to 3.5 years), were used for evaluating the severity of histopathological lesions of AD, using a DIA software (IPP 7.0). Over 1.4 million infiltrated cells were manually counted on 2,862 histopathology images from the heart, liver and kidneys of 324 AMDV-inoculated mink (Table 3.3.1). There is only one published report where severity of histopathological lesions of kidney samples from AMDV-infected mink were evaluated using a DIA software, and morphological and differential morphometrical methods for evaluation of glomerular parameters were developed (Nieto et al. 1991). Although the algorithm which was developed for IPP 7.0 in chapter 2.0 of the current study can be used for counting the total number of cells on the kidneys, liver, heart and lung slide images, it was decided to exclude the lung samples from this study. Similarities in the shape and color of the infiltrated mononuclear cells and the normal cellularity of lung tissue made it difficult to distinguish between these two types of cells in the lung tissue, which was the main reason for this decision. In addition, previous studies have shown that the lung lesions in adult mink are not necessarily due to AD and can be caused by pathogens other than the AMDV (Farid and Ferns, 2017), such as *Pseudomonas aeruginosa, Escherichia coli* (Hildebrandt, 2014a) and Influenza virus (Hildebrandt, 2014b).

3.4.1 Differences among organs for response to AMDV-infection

It is logical to assume that the total number of cells automatically counted by the DIA, as well as the proportion of infiltrated cells, were influenced by the function and microscopic structure of the organs that were evaluated in this study. No doubt the inflammation caused by AMDV-infection influences all organs of the body of an infected mink, primarily via arteries of the vascular system (arteritis), but the extents of AD lesions are different among organs as a result of differences in the structure and function of organs and their responses to infection. Widespread AD lesions in the body and differences in the intensity of AD lesions in different organs in AMDV-infected mink have been previously reported (Jackson et al., 1996; Farid and Ferns, 2011, 2017; Jensen et al., 2016).

3.4.1.1 The heart

The heart is pumping the blood into the vascular system by performing spontaneous rhythmic contractions. The inner layer of the heart, endocardium, is incessant with the tunica intima of the large blood vessels leaving and entering the heart. The contractile muscular layer is called the myocardium, which is the middle layer and composed mostly of cardiac muscle cells that joint together and create layers of muscle tissue with different directional arrangements around different chambers of the organ (ventricles and atriums). Pericardium is the outer layer of the heart, which is a comparatively thin layer of tissue, consisting of a covering mesothelium and a thin underlying layer of loose connective tissue that combines with the connective tissue layers of the myocardium. The loose connective tissue supports the blood vessels and nerves that supply the heart. The thickness of the heart wall varies from location to location. For example, the outer wall of a ventricle is significantly thicker than the outer wall of the atrium, and the outer wall of the left ventricle

is thicker than the outer wall of the right ventricle. The thickness of the heart wall at a specific location is determined by the amount of force it must develop during its contraction (Dellmann and Brown, 1981). Different structural compositions in different parts of the heart, high numbers of chambers and blood vessels in the heart, which cause the appearance of hollow spaces on the slides, along with the different orientations (longitudinal and/or transverse) of muscle fibers on various areas of the heart slides, resulting in non-uniform distribution of tissues across the slides (personal observation) (Appendix 3, Fig. A3.5 and A3.6). It can be assumed that it is the main reason for the high variations among the heart slides for the total number of cells.

The heart is affected by AD as a result of the systemic inflammation of the vascular system. Mononuclear infiltration into coronary arteries of the heart causes arteritis and problems in delivering blood to the heart muscle cells (Henson et al., 1976). Other microscopic changes in the heart can be perivascular accumulation of mononuclear cells and necrotizing arteritis in other parts of the heart (Henson et al., 1976). The AD lesions observed in the heart of animals in this study were caused by the arteritis in the great number of arteries of this organ (Henson et al., 1966) (Appendix 3, Fig. A3.7).

3.4.1.2 The kidneys

The kidneys have excretory and conservational functions by removing waste products and reserving proteins, carbohydrates and electrolytes, keeping hemostasis in the body and providing a constant internal environment for the animal by secreting urine. The complex functions performed by the kidneys require a close array of renal tubules with

blood vessels (Dellmann and Brown, 1981). The main tissue arrangement of the kidneys is similar to that of a gland with highly adapted secretory units and highly specified ducts. The histological structure of the kidneys, visible under a light microscope, is consisted of (1) a tough fibrous capsule made of a dense connective tissue for protecting the organ, (2) a granular cortex in the outer region, which is densely filled with filtration units, called nephrons, consisted of glomeruli and convoluted renal tubules, (3) a medulla in the inner region, which has a striated appearance because of the presence of straight renal tubules, and (4) arteries and veins that are responsible for providing blood flow to and from the kidneys and appear as oval hollow areas within the tubular structure of the cortex or medulla (Dellmann and Brown, 1981). Apart from the minor differences between the appearance of tubules and glomeruli structures as well as the presence of a few hollow areas related to blood vessels on different areas of kidney slides, the kidney tissue had generally a constant and uniform structure (Appendix 3, Fig. A3.1), shown by small coefficient of variation for total number of cells (Table 3.3.2).

The kidneys are one of the first organs to show microscopic changes, including appearance of a small number of lymphocytes, macrophages and plasmablasts (Mori et al., 1994; Farid et al., 2015), which are followed by large masses of these white blood cells in the later stages of the infection (Henson et al., 1966, 1976). Although kidneys show arteritis as a result of general inflammation of the vascular system (Henson et al., 1976), the primary change in kidneys is interstitial nephritis (Henson et al., 1976; Mori et al., 1994), resulting from cell-mediated immune response to infected epithelial cells of renal tubules in which the virus is believed to replicate (Mori et al., 1994). This change is characterized by infiltration of mononuclear cells in the tubular part of the kidneys and around the arteries

(Mori et al., 1994) (Appendix 3, Fig. 3.2). Renal lesions in AMDV-infected mink are the main characteristic of the disease and result in renal failure, uremia and consequently death (Henson et al., 1976). Deposition of immune complexes in the renal glomeruli also contribute to renal failure (Johnson et al., 1975; Henson et al., 1976).

3.4.1.3 The liver

Liver, as the largest gland of the body, has several complex functions such as excreting waste products, secreting bile, storing lipids, vitamins A and B, and glycogen, synthesis of fibrinogen, globulins, albumin and prothrombin, detoxification of drugs, conjugation of toxic substances and steroid hormones, esterification of free fatty acids to triglycerides, and metabolism of proteins, carbohydrates, fats, hemoglobin and drugs. Liver has a dual blood supply. The portal vein brings food-laden blood from the intestine and associated organs, and the hepatic artery supplies the liver cells with oxygenated blood. Branches of these two vessels follow the ramifying connective tissue, providing an extensive network, in which the liver cells are never more than a few millimeters far from any branch of these blood vessels (Dellmann and Brown, 1981). The structural and functional units of the liver are called lobules which are arranged alongside each other. Each lobule is surrounded by 6 portal tracts and settled on the centrolobular vein, which is a terminal branch of the hepatic vein. The portal vein ramifications in the portal tracts give off a series of branches between adjacent portal tracts, which in turn give rise to sinusoids draining blood towards the center of the lobule. Basically, the microscopic structure of liver consists of the following components: (1) parenchyma, which is represented by hepatocytes (liver cells) and Kupffer cells (phagocytic cells) that are arranged in one-cell-thick plates, (2) stroma, which consists of connective tissue and contains the vessels. The

connective tissue of the stroma is type III collagen (reticulin), which forms a meshwork that provides integrity for the hepatocytes and sinusoids, (3) sinusoids, which are capillaries travelling between hepatocytes, and (4) spaces of Disse (perisinusoidal spaces), which are located between the hepatocytes and the sinusoids (Dellmann and Brown, 1981). All these components are arranged in a uniform fashion, resulting in the liver appearing as a uniform tissue under microscope that does not have notable variations in different areas of the slides (Appendix 3, Fig. A3.3). This uniformity in the structure of the liver was evident by the small coefficient of variation for total number of cells (Table 3.3.2).

The liver is also one of the first organs to show microscopic changes as a result of AMDV-infection, including the appearance of a small number of lymphocytes, macrophages and plasmablasts (Bloom et al., 1975; Henson et al., 1976; Farid et al., 2015; Jensen et al., 2016), which are followed by large masses of these cells in the later stages of infection (Henson et al., 1966, 1976) (Appendix 3, Fig. A3.4). Microscopic lesions in the liver result from arteritis in small hepatic arteries, as well as the immune response to the presence of viral antigens in Kupffer cells and some hepatocytes in the portal areas, which can be detected in very early stages of AD (Henson et al., 1976).

3.4.2 Correlations between the three images of each slide within the organs

Three images on randomly selected areas of each slide were analyzed to increase the accuracy of the measurements because, as explained above, the cells were not uniformly scattered across the slides. The lowest Spearman's rank correlation coefficients and intra-class correlation between the three images on each slide for the number of infiltrated cells, total number of cells and percent infiltrated cells were observed in the heart

(Tables 3.3.4, 3.3.5). The reasons for the low associations among the three images in the heart slides could have been the result of high numbers of chambers and blood vessels in the heart, which cause the variable number of hollow spaces on the images. In addition, different orientations of muscle fibers (longitudinal and/or transverse) on various areas of the heart images, which resulted in a high number of heart muscle cells on some areas of the images where cells had transverse orientations, as explained above. The Spearman's rank correlation coefficients and intra-class correlation among images of the kidney and liver slides were comparable and greater than those in the heart, implying that the distribution of cells across these two organs was more uniform. There is no published information to which these observations can be compared. It can be concluded that visual assessment of the proportion of infiltrated cells on one area of a slide is less accurate in the heart than in the kidneys and liver.

3.4.3 Normality of the distributions of average measurements of the three images of each slide

The differences between means and medians of the distributions of average number of infiltrated cells, total number of cells and percent infiltrated cells within each organ (Table 3.3.2), were the reflection of deviations of some of the measurements from normality, which were also confirmed by the Kilmogorov-Smiranov test (Table 3.3.3). Deviation from normality measured by the Kilmogorov-Smiranov tests generally agreed with the magnitude of differences between means and medians. For instance, the observation that the differences between means and medians of percent infiltrated cells in the heart were lower than those in the kidneys and liver was in line with the non-significant

Kilmogorov-Smiranov test results for this trait in the heart. Deviations from normality were mainly caused by a small number of observations with large values (positively skewed distributions), which are also depicted in greater estimates of means than medians (Table 3.3.2). Because the severity of AD lesions varies greatly among individual mink, the number and percent infiltrated cells were very large in some individuals which were severely affected by the disease, shown by large ranges of values (Table 3.3.1) and coefficients of variation (Table 3.3.2), causing positively skewed distributions. The reasons for positively skewed total number of cells in the heart was the presence of small areas with a large number of transversally cut cells. Although the Box-Cox power transformations suggested that log transformation was the most proper method of normalizing the distribution, log transformation did not make the distribution normal. Because distributions deviated from normality, the non-parametric Spearman's rank correlation was used to compute correlations between measurements, but the assumption of normality was deviated for the MIXED model analyses. Analysis of variance, however, is not very sensitive to moderate deviations from normality (Harwell et al. 1992, Lix et al. 1996).

3.4.4 Factors affecting the total number of cells

Because percent infiltrated cells, which is the measure of severity of AD lesions, is a function of the total number of cells which were counted by the IPP 7.0, statistical analysis was performed to understand the factors that affect this measurement. The observation that the organs significantly interacted with the durations of infection and disposal methods for the total number of cells (Table 3.3.6) suggests that the cellularity of

the organs changed differently by the duration of infection and the health status of the animals. Necrosis (death of cells) is one of the final results of inflammation process in any organ (Jones et al., 1997). It can be hypothesized that the steady reduction in the total number of cells in all organs, particularly in the heart and kidneys of the infected mink during the course of the disease (Table 3.3.7) was the result of necrosis and loss of the cells. The kidneys had a significantly higher density, as measured by the total number of cells, than the liver, and the heart had the smallest number of total cells at all durations of infection, yet the heart lost a higher number of total cells from 0.5 to 3.5 years after infection (22.0%) compared to the kidneys (12.7%) and the liver (8.9%), which was the reason for the significant interaction between organs and duration of infection.

The findings that the difference between dead and euthanized animals for the total number of cells in the heart was small and non-significant, whereas dead animals had greater numbers of total cells in their kidneys (13.0%, $P<0.05$) and liver (6.8%) compared with those in euthanized animals (Table 3.3.7), are contrary to the expectation that dead animals had fewer total cells because of necrosis. There is no published data to compare these results with, and further research is needed to verify these findings. It may be concluded that differences among the organs in cell density need to be taken into account when visually inspecting slides for the degree of cell infiltration in AD infected mink.

3.4.5 Factors affecting percent infiltrated cells

The current study was a retrospective investigation where measurements were taken on mink which were selected for health and reproductive success for more than three

years, and those whose performances were at the lower end of the herd were euthanized and sampled, and the results should be interpreted accordingly. The current experiment is thus unique and the results cannot always be directly compared with published reports. The significant interactions between the organs and durations of infection and disposal methods for percent infiltrated cells suggest that the severity of the AD lesions changed differently in different organs as the duration of infection prolonged, as well as in dead and euthanized animals. The finding that the percent infiltrated cells in the heart steadily increased as the duration of infection increased from 0.5 to 3.5 years was likely because of the gradual increase in accumulation of infiltrated cells in the cardiovascular system, which resulted in a significantly high percentage of infiltrated cells at the later stages of the disease. This finding is in agreement with the report of Henson et al. (1966) in naturally infected Aleutian mink that the infiltration of the mononuclear cells in the heart, and generally in the vascular system, increased as the duration of infection increased over five months. The finding that the effects of duration of infection on percent infiltrated cells were not significant in the kidneys and liver was in agreement with the report of Jensen et al. (2016) who found no statistically significant difference in the number of histological symptoms in the liver, kidneys, lung and brain of non-Aleutian mink from 8 to 24 weeks after infection. Other published reports indicate that the severity of histopathological lesions in the kidneys (Henson et al., 1966, 1976; Johnson et al., 1975; Mori et al., 1994) and liver (Henson et al., 1966, 1976) had a positive relationship with the duration of infection. In addition to the genotype of the mink, the strain of the virus (Hadlow et al., 1983) also contribute to the severity of lesions in various organs.

The significantly higher percent infiltrated cells in the kidneys during the first six months after infection compared with that in the heart and liver at this stage of infection might be explained by the fact that the primary infiltration of mononuclear cells in the kidneys occurs as a result of a fast replication of AMDV in renal tubular cells during the early stages of AD (Johnson et al., 1975; Henson et al., 1976). There are, however, other reports indicating that the microscopic lesions of AD were usually detectable on the liver at the same time or earlier than on the other organs (Porter et al., 1969; Henson et al., 1976; Farid et al., 2015; Jensen et al., 2016). The finding that the kidneys and heart had comparable percent infiltrated cells in animals which were infected for 1.5 years and longer may be the result of changes in the severity of AD symptoms in the kidneys of animals that survived beyond one year of age.

Comparing the naturally dead and the euthanized animals for the percent infiltrated cells in their organs may point to the fact that the degree of infiltration of mononuclear cells in the heart did not affect the health status of the infected mink, whereas the kidneys and liver of naturally dead animals were more severely damaged than those in mink which survived, shown by the significantly greater number of infiltrated cells in these organs in dead animals (Table 3.3.7). The significantly greater number of infiltrated cells in the kidneys of dead animals compared with that in those which survived the infection is logical, because death of AMDV-infected mink is mostly the result of kidney lesions (Porter et al., 1969). The significantly greater number of infiltrated cells in the liver of naturally dead animals compared with those which were euthanized suggests that the liver of the former was severely affected by the infection at the time of death. Although degenerated liver cells in the AMDV-infected mink undergo the regeneration process to help the liver to maintain

its functionality (Valdovska and Pilmane, 2011), there was likely no time for dead animals to adequately recover from the disease. As explained above, the kidneys and liver have more complex functionalities compared to the heart, and it is logical to assume that the effects of infiltration of mononuclear cells on a small number of the complex functions of kidneys and liver will result in serious health problems in the mink.

The current study is also one of the very few (Farid and Ferns, 2011) in which male and female mink were compared for the severity of histopathological lesions of AD. The finding that the females showed a significantly higher percent infiltrated cells than the males, may be because females are more susceptible to stress and are prone to different types of diseases during their reproductive cycle (Gilbert and Bailey, 1968). This is, however, contrary to the report of Farid and Ferns (2011) in a small number of AMDV-infected mink who found that the female and male mink showed comparable degrees of severity of AD lesions.

3.4.6 Associations between anti-AMDV antibody titer, gamma-globulin level and severity of histopathological lesion

Anti-AMDV antibody titer was determined by the CIEP using serially diluted plasma, which is the gold standard and has been used extensively (Bloom et al., 1975, 1982; An and Ingram, 1977; An et al., 1978; Aasted and Cohn, 1982; Hadlow et al., 1983, 1984; Hahn and Hahn, 1983; Farid and Segervall, 2014; Farid and Rupasinghe, 2016). An interesting observation was the significantly larger number of females than males which showed high antibody titers (Table 3.3.8). The results of the current study may indicate that females respond to infection more severely than males, as indicated by the significantly

greater percent infiltrated cells (Table 3.3.7) and greater number of animals with high antibody titer. It is difficult to speculate about the reasons for the higher antibody titers in females than males because of the absence of any published information on this topic. Any of the elements in the large array of differences between males and females, such as body weight and sex hormones, could influence animals' response to infection, including antibody profiles. It is also possible that males were generally healthier than females because of the higher selection pressure which was applied to males at the time of keeping replacement animals.

IAT is a low-cost on-farm test, which is not specific for AMDV-infection (Greenfield et al., 1973), but has been successfully used to establishing a tolerant mink herd in Nova Scotia (Farid, 2010). The major problem with IAT is that it can be elevated when animals are infected with pathogens other than AMDV as well (Farid et al., 2018), and thus IAT is primarily a measure of general health, rather than animal response to AMDV-infection. Contrary to the result of antibody titer, the distribution of gamma-globulin levels was comparable between males and females (Table 3.3.14), which could be explained by the moderate Spearman's rank correlation coefficient between antibody titers and gamma-globulin levels (r=0.37). This estimate is lower than the correlation coefficients between antibody titer, measured by CIEP, and serum gamma-globulin concentration, measured by cellulose acetate electrophoresis, of 0.75 in experimentally inoculated sapphire and pastel mink (Bloom et al., 1975), and 0.81 in naturally infected and experimentally inoculated pastel and Aleutian mink (An and Ingram, 1977). It may be concluded that the association between serum gamma-globulin concentration and antibody titer is moderate to high, and the smaller correlation coefficient in the current study,

compared with the previous reports, is because of the different method used for measuring serum gamma-globulin level (IAT) in the current study compared to those reports (cellulose acetate electrophoresis).

Stepwise regression models were fitted to the data within organs, because percent infiltrated cells were significantly different among organs (Table 3.3.7). The observation that the best fitted regression models for percent infiltrated cells were different in different organs, and that sex had a significant effect on percent infiltrated cells in the heart, and interacted with antibody titer in the liver, and with duration of infection in the heart and kidneys (Table 3.3.9), which were also observed when gamma-globulin was replaced by antibody titer in the regression models (Table 3.3.15), demonstrates the complexity of factors that influence the severity of the AD lesions in different organs. Females had a significantly higher percent infiltrated cells (Table 3.3.7) and higher antibody titer (Table 3.3.8) compared with males, which points out the higher sensitivity of females in response to the infection. Although more research is needed to verify the result of the current study, it may be safe to suggest that males and females need to be judged differently for their response to AMDV-infection. Because animals which were used in the current study were selected on the basis of health and reproductive success, it may be concluded that the females can cope with higher degrees of severity of AD lesions and higher antibody titer than males. Again, this statement is just a speculation and requires further study.

3.4.6.1 The effects of antibody titer, gamma-globulin level and duration of infection on percent infiltrated cells in the heart

The curvilinear effect of the duration of infection on percent infiltrated cells in the heart of males and females when antibody titer (Table 3.3.10) or gamma-globulin levels (Table 3.3.16) were analyzed revealed that there was a small decline in percent infiltrated cells from 0.5 to 1.5 years after inoculation, but percent infiltrated cells increased at a much faster rate as the duration of infection increased beyond 1.5 years, and reached the highest level in animals which were infected for 3.5 years (Fig. 3.3.1, 3.3.2, 3.3.4, 3.3.5). The increase in severity of AD lesions by the duration of infection was the same at all levels of antibody titer and gamma-globulin, and the results were the same as those previously reported when data were analyzed by the MIXED model (Table 3.3.7, Section 3.3.4). One unexpected observation that deserves attention was that the animals which were infected for 3.5 years had the highest percent infiltrated cells in their hearts, at all levels of antibody titer and gamma-globulin. This was unexpected because severe AD lesions are known to reduce survival rate, and thus tolerant mink should show less severe lesions. One possible explanation is that the animals which were used in this study were healthy and had minor AD lesions in previous years when they were retained for breeding, but their health status and/or reproductive performances declined in the year when they were culled and were subsequently sampled. Alternatively, because animals were selected solely based on health and reproductive success, some with severe AD lesions in their hearts with varying levels of antibody titer and gamma-globulins, were able to live healthy and productive lives.

The association between antibody titer and percent infiltrated cells in the hearts of male and female mink was somewhat unexpected. Contrary to general expectation, the lowest predicted percent infiltrated cells in the heart of female mink was observed at the antibody titer of 8 ($\log_2$ of 4) at all durations of infection (Fig. 3.3.1) and the lowest percent

infiltrated cells in the heart of males was observed at the antibody titer of 16 (log_2 of 5) regardless of the duration of infection (Fig. 3.3.2). A plausible explanation for these observations is that percentages of infiltrated cells at low levels of antibody titers, from zero to 16, were almost the same, but percent infiltrated cells rapidly increased when antibody titers rose above 16. Histopathological lesions in the heart has rarely been investigated. An alternative explanation is that low levels of anti-AMDV antibody titer (up to 16) had some beneficial effects on the severity of AD lesions, possibly by suppressing viral replication. It has been reported that viral replication is reduced or ceased by antibody in some mink (Alexandersen et al., 1988).

Regardless of the reasons for the curvilinear relationship between antibody titer and percent infiltrated cells in the heart, the results implied that antibody titers higher than 16 were associated with more severe AD lesions in the heart. The combination of antibody titer and duration of infection in the best fitted regression model explained 10.3% and 37.6% of variations in percent infiltrated cells in the heart of females and males, respectively (Table 3.3.10). These estimates, particularly in females, were low, suggesting that large amounts of variations in percent infiltrated cells were not accounted for by the antibody titer and duration of infection. Regression equations without duration of infection showed no relationship between antibody titer and severity of AD lesions in males, suggesting that most of the variations in percent infiltrated cells which were explained by the regression model were the result of differences in the duration of infection. In the heart of females, where a small amount of variations in percent infiltrated cells was explained by the duration of infection and antibody titer in the regression model (10.3%), antibody titer alone explained more of the variation (6.89%) than the duration of infection. The

lowest predicted percent infiltrated cells in the heart of females reached at $\log_2$ antibody titer of 4.47, which is close to 4 in the full model.

The effect of gamma-globulin level on percent infiltrated cells in the heart of male mink was not significant when the duration of infection was in the regression model (Table 3.3.16, Fig. 3.3.5). Percent infiltrated cells increased linearly and significantly as the IAT score increased when the duration of infection was ignored (Table 3.3.24), although only a small amount of variations in percent infiltrated cells (7.2%) was explained by the IAT scores. These results suggested that most of the variations in percent infiltrated cells in the heart of male mink were caused by the duration of infection, as was the case when antibody titer was in the model. Gamma-globulin levels were not thus an accurate indicator of the severity of AD lesions in the heart of male mink. The relationship between percent infiltrated cells and gamma-globulin levels in the heart of females was unexpected, because percent infiltrated cells increased as IAT score increased from zero to two, reached the peak at IAT score of two, and then declined (Fig 3.3.4). The regression equation explained a small amount of variation in percent infiltrated cells (5.3%, Table 3.3.16), yet a smaller amount (2.3%, Table 3.3.24) was explained by the regression equation when the duration of infection was ignored.

The overall conclusion is that (i) the associations between the severity of AD lesions and antibody titer and serum gamma-globulin levels in the heart of AMDV-infected male and female mink were weak, (ii) the results highlighted the potential importance of duration of infection and sex on the severity of AD lesions in the heart. Duration of infection can be substituted by age, assuming that all animals in a herd were infected at approximately the same time. To the extent that the heart is the indicator of animal health,

it may be concluded that animals of the same sex which were born in the same year should be compared for antibody titer and gamma-globulin level.

3.4.6.2 The effects of antibody titer, gamma-globulin level and duration of infection on percent infiltrated cells in the kidneys

The observation that the lowest estimated percentages of infiltrated cells in the kidneys of females at all levels of antibody titers were in those animals which were infected for 1.5 years (Fig. 3.3.3), could be because animals which were retained for breeding around six months after inoculation had less severe AD lesions in their kidneys than those which were culled and sampled. Animals which were sampled after 1.5 years of infection were, therefore, those which were selected because they had low AD lesions in previous years. The sharp increase in percent infiltrated cells in the kidneys of female mink from 2.5 to 3.5 years after inoculation, which resulted in animals that were infected for 3.5 years to show the greatest percent infiltrated cells in their kidneys (Fig. 3.3.3), was similar to the effect of duration of infection on percent infiltrated cells in the heart. As explained in the case of the heart (Section 3.4.6.1), these mink were possibly healthy with minor AD lesions in previous years when they were selected for breeding, but their health status and reproductive performances deteriorated in the following year, and were thus culled and sampled. The results suggest that some tolerant mink could become sick at older ages when their immune system declines. A less plausible explanation is that the high percent infiltrated cells at 3.5 years after inoculation was the result of selection of animals based on health and reproductive success, enabling some animals with moderate AD lesions in their kidneys to live healthy and productive lives.

The observation that the minimum predicted percentages of infiltrated cells in the kidneys of females were at the antibody titer of 8 (log_2 of four), increased as antibody titer increased, and reached their maximum values at antibody titer of 256 (log_2 of nine) at all durations of infection (Fig. 3.3.3) was the same trend as that observed for the heart (Section 3.4.6.1). The effect of antibody titer on percent infiltrated cells in the kidneys of male mink was almost similar to that in females, except having no association with the duration of infection, i.e. the predicted percent infiltrated cells decreased as antibody titer increased from zero to 4 (log_2 antibody titer of 3.2), and then increased to the maximum value of 17.97% at antibody titer of 256 (log_2 of 9). As hypothesized in the case of heart, the reason was that percentages of infiltrated cells at low levels of antibody titers (0 to 8) were almost the same, but increased rapidly in response to increases in antibody titers beyond 8. Alternatively, low levels of anti-AMDV antibody titer had some beneficial effects on keeping the severity of AD lesions at low levels, possibly by suppressing viral replication. The same results were reported by Jackson et al. (1996), who showed that all of the naturally infected brown mink that had antibody titers of 64 or less had no lesions, and concluded that the low levels of antibody titer have suppressive effects on AMDV replication during the early stages of the infection. An and Ingram (1977) evaluated 74 naturally infected pastel mink for five months and observed low levels of histopathological lesions in the kidneys, liver, spleen and mesenteric of mink with antibody titers of 256 or lower, and increased histopathological lesions in those with antibody titer of 512 or higher. Mori et al. (1994) evaluated sapphire and pastel female mink inoculated by a highly pathogenic strain of AMDV (Utah 1) and observed that all sapphire mink which had moderate and strong kidney lesions had antibody titers of 1024 and higher at 60 dpi. In

addition, four of the five pastel mink in their study that had weak kidney lesions had antibody titers of 256 or lower.

The effects of duration of infection on percent infiltrated cells in the kidneys of female mink when gamma-globulin level was in the regression model was complex, because not only was the relation curvilinear; but the duration of infection interacted with gamma-globulin level (Table 3.3.18), and resulted in the degree of changes in percent infiltrated cells to vary differently at different durations of infection at each gamma-globulin level (Table 3.3.19, Fig. 3.3.6). The interesting observation was that at low gamma-globulin levels, predicted percent infiltrated cells was minimum in female mink which were infected for 1.5 years, similar to that in the previous analysis where antibody titer was in the regression mode. At the high gamma-globulin levels, however, a different picture emerged. At six months after inoculation, animals which had the highest gamma-globulin level showed the maximum percent infiltrated cells; very likely these animals were not healthy and were culled at an early age. This result is comparable to the report of Hadlow et al. (1985) that five of the 12 female pastel mink that showed lesions of AD in their lymphoid system, kidneys, liver and small intestine on 43 dpi, had higher serum gamma-globulin levels (1.0 to 4.0 g/dL) than those that did not have any lesions (0.4 and 1.4 g/dL). Our results showed that, at 3.5 years after inoculation, animals which had the highest level of gamma-globulin had the lowest predicted percent infiltrated cells, implying that low levels of kidney lesions were crucial for infected animals to survive to old ages, despite the fact that some of them had high gamma-globulin levels at the time of sampling. Duration of infection had no effect on percent infiltrated cells in the kidneys of male mink when antibody titer was used in the stepwise regression model, but interestingly gamma-

globulin level significantly interacted with the duration of infection (Table 3.3.18), as was the case in the kidneys of females with almost the same results (Table 3.3.21, Fig. 3.3 7), i.e. at six months after inoculation, animals which had the highest gamma-globulin level showed the maximum percent infiltrated cells, and at 3.5 years after inoculation, animals which had the highest level of gamma-globulin had the lowest predicted percent infiltrated cells. There is no published information to compare the results with, although the presence of histopathological lesions in the kidneys, liver, spleen and mesenteric lymph nodes of AMDV-infected mink with gamma-globulin levels higher than 25% were reported (An and Ingram, 1977).

The combination of antibody titer and duration of infection in the best fitted regression models explained 22.4% and 15.3% of variations in percent infiltrated cells in the kidneys of female and male mink, respectively (Table 3.3.11), and 21.3% and 16.9% when gamma-globulin replaced antibody titer (Table 3.3.18). These estimates suggest that moderate amounts of variations in percent infiltrated cells were explained by the duration of infection and antibody titer or gamma-globulin levels, and that the amounts of variations explained by the regression models were greater in females than males. When duration of infection was ignored, the predicted percent infiltrated cells in the kidneys of female mink decreased as antibody titer increased from zero to eight ($\log_2$ of 3.8), and then increased to the maximum value of 19.07% at antibody titer of 256 (Table 3.3.13), almost the same trend as that in the males. The results suggested that the effect of antibody titer on percent infiltrated cells was substantial, shown by R^2 of 16.29%, which was just 6.11% smaller that that in the model that included the duration of infection. Our result is comparable with the report of Jackson et al. (1996) who observed a correlation coefficient of 0.36 between the

severity of renal lesions and antibody titers in naturally infected brown mink. Although gamma-globulin level had significant effect on percent infiltrated cells in the kidneys of male and female mink, the models explained only 8.0% and 8.6% of variations in percent infiltrated cells, respectively (Table 3.3.24), suggesting that the duration of infection had a more pronounced effect than gamma-globulin level alone in explaining variations in percent infiltrated cells in the kidneys. Our result is in agreement with the report of Henson et al. (1966), that the severity of renal lesions in naturally infected Aleutian type mink were related to the level of gamma-globulin. Kenyon et al. (1963) also reported a high degree of correlation between the serum gamma-globulin level and amounts of mononuclear infiltration in kidneys of naturally infected pastel mink. The exact values of correlations were not reported by Henson et al. (1966) or Kenyon et al. (1963).

The overall conclusions from the above analyses are that (i) the associations between the severity of AD lesions and antibody titer and serum gamma-globulin levels in the kidneys of AMDV-infected male and female mink were moderate when the duration of infection is known, (ii) severity of AD lesions in the kidneys were more strongly associated with antibody titer than with serum gamma-globulin, (iii) antibody titer had a stronger association with percent infiltrated cells than the duration of infection, (iv) the effects of gamma-globulin level, measured by IAT, on percent infiltrated cells depended on the duration of infection, and was the strongest in mink which were infected for six-months.

3.4.6.3 The effects of antibody titer, gamma-globulin level and duration of infection on percent infiltrated cells in the liver

Contrary to the heart and kidneys, duration of infection did not have a significant effect on percent infiltrated cells in the liver of male or female mink (Table 3.3.12). The results are in agreement with the MIXED model in which differences among durations of infection were small and non-significant (Table 3.3.7). The ability of the liver to regenerate its damaged cells (Valdovska and Pilmane, 2011) could be the reason for the lack of association between percent infiltrated cells and the duration of infection. Comparable with the observation in the kidneys of male and female mink, and with the heart of female mink, the minimum percent infiltrated cells in the liver of females was at antibody titer of 4 ($\log_2$ antibody titer of 3.2) and then increased as antibody titer increased. As hypothesized in the cases of heart and kidneys, low antibody titers could have had no effects on percent infiltrated cells, but increases in antibody titer beyond 8 resulted in rapid increases in percent infiltrated cells. Weak associations between low antibody titers and histopathological lesions in various organs of AMDV-infected mink have been reported (An and Ingram, 1977; Mori et al., 1994). The associations between percent infiltrated cells and antibody titers were weak in the liver, and explained 10.8% and 3.9% of variations in percent infiltrated cells in females and males, respectively.

The association between percent infiltrated cells and gamma-globulin level in the liver of male mink was almost identical to that of the effect of antibody titer in this organ (Table 3.3.22), i.e. no association with the duration of infection and a significant and positive linear association with gamma-globulin. The effects of duration of infection on percent infiltrated cells in the liver of female mink, when gamma-globulin level was in the regression model, was similar to that in the kidneys of male mink, i.e. a curvilinear relationship with interaction between the duration of infection and gamma-globulin levels

(Table 3.3.22). Similar to the relationship between percent infiltrated cells and gamma-globulin in the kidneys of female mink, predicted percent infiltrated cells at low gamma-globulin levels was minimum in the liver of females which were infected for 1.5 years. At the high gamma-globulin levels, however, the maximum percent infiltrated cells was observed at six months after infection, whereas animals which had the highest level of gamma-globulin, had the lowest predicted percent infiltrated cells at 3.5 years after inoculation (Fig. 3.3.8). Similar to the case of the kidneys of females, young animals with high levels of gamma-globulin had severe AD lesions, and were culled, but at older ages those animals which survived had low AD-symptoms, because healthy liver was needed for animals to survive. There is no published report to compare these results with, but lack of a relationship between AD lesions and low levels of gamma-globulins, and positive associations at high levels of gamma-globulins have been reported (An and Ingram, 1977; Hadlow et al., 1985).

The difference between males and females in the trend of association between gamma-globulin level and percent infiltrated cells could be the result of overall differences between sexes, or the fact that males were more severely selected for health status than females. The best fitted regression model of gamma-globulin level and duration of infection on percent infiltrated cells explained 11.5% of variations in the liver of female mink (Table 3.3.22), and almost half of this value (6.9%) was explained by the linear regression of gamma-globulin level on percent infiltrated cells (Table 3.3.24), suggesting a weak association between gamma-globulin and percent infiltrated cells in the liver of both males and female.

The overall conclusions from the above analyses are that (i) the associations between the severity of AD lesions and antibody titer and serum gamma-globulin levels in the liver of AMDV-infected mink were weak, particularly in the males, (ii) the effects of antibody titer and gamma-globulin level on severity of AD lesions were very similar, (iii) antibody titer and gamma-globulin level had stronger associations with percent infiltrated cells than the duration of infection, (iv) the effects of gamma-globulin level, measured by IAT, on the severity of AD lesions was the strongest in mink which were infected for six-months.

Chapter 4. Conclusion

Severity of AD lesions in various organs of AMDV-infected mink is an accurate measure of the degree of tolerance to the disease, which is an important criterion in selection programs for tolerance. Severity of AD lesions is always assessed by estimating the proportion of infiltrated mononuclear cells in the organs of infected mink, under the light microscope, which is a subjective and non-reproducible method. A digital image analysis software (Image Pro Plus 7.0) was tested for developing an accurate and objective measure of severity of AD lesions. The software was not able to accurately distinguish infiltrated cells from normal cells on images of the H&E stained slides, and thus accurate automatic counting of infiltrated cells was not possible. Manual counting of the infiltrated cells and automatic counting of total cells was an alternative strategy for the quantification of the proportion of infiltrated mononuclear cells, as a measure of severity of AD lesions. In the first part of this study, an objective, reproducible and reliable method for calculating the percentage of infiltrated mononuclear cells in different organs was developed.

It is important to accurately predict severity of AD lesions on live animals using serum parameters. The relationships between percent infiltrated cells assessed by the Image Pro Plus 7.0 on H&E stained slides of the kidneys, liver and heart of AMDV-infected mink, and anti-AMDV antibody titer and serum gamma-globulin level, were evaluated. Data of the percent infiltrated cells and serum parameters on 299 black mink, inoculated with a local strain of AMDV and euthanized between six months and 3.5 years after inoculation, were analyzed. The results showed that:

- The associations between percent infiltrated cells in the heart, kidneys and liver with antibody titer and gamma-globulin levels were generally weak, making these

blood parameters unreliable tools for the identification of tolerant mink, particularly when the time of infection is unknown.

- The associations between percent infiltrated cells and antibody titer and gamma-globulin levels were stronger in the kidneys than those in the heart and liver.
- The association between antibody titer and severity of AD lesions in the kidneys was almost twice as strong as that with gamma-globulin level.
- Severity of AD lesions in all organs was significantly affected by sex.
- Duration of infection was more strongly associated with the severity of AD lesions in the heart, and its effect in the liver was the lowest.
- The effects of gamma-globulin level on percent infiltrated cells in the kidneys of male and female mink, and the effect of antibody titer in the liver of female mink were the strongest in animals which were infected for six months, and the weakest in animals after 3.5 years of infection.

The use of antibody titer and gamma-globulin level in predicting the severity of AD lesions should be performed within sex and duration of infection. Duration of infection can be substituted by age, assuming that all animals in a herd were infected at approximately the same time, i.e. animals of the same sex which were born in the same year should be compared for antibody titer and gamma-globulin level.

Bibliography

Aasted B., Alexandersen S., and Christensen J., 1998. Vaccination with Aleutian mink disease parvovirus (AMDV) capsid proteins enhances disease, while vaccination with the major non-structural AMDV protein causes partial protection from disease. Vaccine, 16(11-12),1158–1165.

Aasted, B. and Cohn, A., 1982. Inhibition of precipitation in counter current electrophoresis. A sensitive method for detection of mink antibodies to Aleutian Disease Virus. Acta. Path. Microbiol. Immunol. Scand. C., 90(1), 15-19.

Aasted, B. and Hauch, H., 1988. Studies on the progression of Aleutian disease in mink. Acta. Vet. Scand., 29(3-4), 315-21.

Alexandersen, S., Bloom, M.E. and Wolfinbarger, J., 1988. Evidence of restricted viral replication in adult mink infected with Aleutian disease of mink parvovirus. J. Virol., 62(5), 1495-1507.

Altman, D.G. and Bland, J.M., 1983. Measurement in medicine: The analysis of method comparison studies. The Statisticians, 32, 307-317.

Altman, D.G. and Bland, J.M., 1994. Diagnostic tests 1: Sensitivity and specificity. Brit. Med. J., 308(6943), 1552-1553.

An, S.H. and Ingram, D.G., 1977. Detection of inapparent Aleutian disease virus infection in mink. Am. J. Vet. Res., 38(10), 1619-1624.

An, S.H., DePauli, F.J., Wright, P. and Ingram, D.G. 1978. Characteristics of inapparent Aleutian disease virus infection in mink. Res. Vet. Sci., 24(2), 200-2004.

Araujo, P., 2009. Key aspects of analytical method validation and linearity evaluation. J. Chromatography B, 877(23), 2224-2234. doi: 10.1016/j.jchromb.2008.09.030

Aronson, J.K., 2005. Biomarkers and surrogate endpoints. Brit. J. Clin. Pharmacol., 59(5) 491-494. doi: 10.1111/j.1365-2125.2005.02435.x

Baratloo, A., Mosseini, M., Negida, A. and Ashal, G.E., 2015. Part1: Simple definition and calculation of accuracy, sensitivity and specificity. Emergency, 3(2), 48-49.

Best, S.M. and Bloom, M.E., 2005. Pathogenesis of Aleutian mink disease parvovirus and similarities to B19 infection. J. Vet. Med. B, 52(7-8), 331-334.

Best, S.M. and Bloom, M.E., 2006. Aleutian mink disease parvovirus. London. Hodder Arnold Publication, Chap. 32, 457-471.

Bland, J.M. and Altman, D.G., 1990. A note on the use of the intraclass correlation coefficient in the evaluation of agreement between two methods of measurement. Comput. Biol. Med., 20(5), 337-340.

Bland, J.M. and Altman, D.G., 1999. Measuring agreement in method comparison studies. Stat. Meth. Med. Res., 8(2), 135-160.

Bland, J.M. and Altman, D.G., 2010. Statistical methods for assessing agreement between two methods of clinical measurement. Intern. J. Nurs. Stud., 47(8), 931-936.

Bloom, M.E., Kanno, H., Mori, S. and Wolfinbarger, J.B., 1994. Aleutian mink disease: Puzzles and paradigms. Infect. Agent. Dis., 3(6), 279–301.

Bloom, M.E., Race, R.E. and Wolfinbarger, J.B., 1982. Identification of a nonvirion protein of Aleutian disease virus: mink with Aleutian disease have antibody to both virion and nonvirion proteins. J. Virol., 43(2), 608-616.

Bloom, M.E., Race, R.E., Hadlow, W.J. and Chesebro B., 1975. Aleutian disease of mink: the antibody response of sapphire and pastel mink to Aleutian disease virus. J. Immun., 115(4), 1034-1037.

Brey, E.M., Lalani, Z., Johnston, C., Wong, M., McIntire, L.V., Duke, P.J. and Patrick Jr, C.W., 2003. Automated selection of DAB-labeled tissue for immunohistochemical quantification. J. Histochem. Cytochem., 51(5), 575-584.

Castelruiz, Y., Blixenkrone-Moller, M. and Aasted, B., 2005. DNA vaccination with the Aleutian mink disease virus NS1 gene confers partial protection against disease. Vaccine, 23(10), 1225-1231.

Castro Souza Junior Neto, J.D., de Moura Estevão, L.R., Baratella-Evêncio, L., Feitosa Vieira, M.G., Simões, R.S., Florencio-Silva, R., Evêncio- Luz, L. and Evêncio-Neto, J., 2017. Mast cell concentration and skin wound contraction in rats treated with *Ximenia Americana L.* Acta Cir. Bras., 32(2), 148-156.

Cheema, A., Henson, J.B. and Gorham, J.R., 1972. Aleutian disease of mink: Prevention of lesions by immunosuppression. Am. J. Pathol., 66(3), 543-556.

Chen, X., Song, C., Liu, Y., Qu, L., Liu, D., Zhang, Y. and Liu, M., 2016. Development of an ELISA based on fusion VP2332-452 antigen for detecting antibodies against Aleutian mink disease virus. J. Clin. Micro., 54(2), 439-442.

Cho, H.J. and Greenfield, J., 1978. Eradication of Aleutian disease of mink by eliminating positive counterimmunoelectrophoresis test reactors. J. Clin. Micro., 7(1), 18-22.

Cho, H.J. and Ingram, D.G., 1973. Antigen and antibody in Aleutian disease in mink: II. The reaction of antibody with the Aleutian disease agent using immunodiffusion and immunoelectrophoresis. Can. J. Comp. Med., 37(3), 217-222.

Churukian, C.J. and Schenk, E.A., 1981. A toluidine blue method for demonstrating mast cells. J. Histotech., 4(2), 85-86. doi: 10.1179/his.1981.4.2.85

Clarke, E.L. and Treanor, D., 2017. Colour in digital pathology: A review. Histopathol., 70(2), 153-163. doi: 10.1111/his.13079

Cotmore, S.F., Agbandje-McKenna, M., Chiorini, J.A., Mukha, D.V., Pintel, D.J., Qiu, J., Soderlund-Venermo, M., Tattersall, P. and Tijssen, P., 2014. The family Parvoviridae. Arch. Virol., 159(5), 1239–1247. doi: 10.1007/s00705-013-1914-1.

De Noronha Santos Netto, J., Pires, F.R., Da Fonseca, E.C., Silva, L.E. and De Queiroz Chaves Lourenco, S., 2012. Evaluation of mast cells in priapical cysts, dentigerous cysts, and keratocystic odontogenic tumors. J. Oral Pathol. Med., 41(8), 630-636. doi: 10.1111/j.1600-0714.2012.01126.x

Dellmann, H. and Brown, E.M., 1981. Textbook of veterinary histology, second edition. Philadelphia, PA. Lea & Febiger.

Doumas, B.T., 1997. The evolution and limitations of accuracy and precision standards. Clinica. Chimica. Acta, 260(2), 145-162.

Dyer, N.W., Ching, B. and Bloom, M.E., 2000. Nonsuppurative meningoencephalitis associated with Aleutian mink disease parvovirus infection in ranch mink. J. Vet. Diagn. Invest., 12(2), 159-162.

Eriksen A.C., Andersen J.B., Kristensson, M., deport Christensen, R., Hansen, T.F., Kjær-Frifeldt, S. and Sorensen, F.B., 2017. Computer-assisted stereology and automated image analysis for quantification of tumor infiltrating lymphocytes in colon cancer. Diagn. Pathol., 12(1), 65. doi: 10.1186/s13000-017-0653-0

Eusebi, P., 2013. Diagnostic accuracy measures. Cerebrovascular Diseases., 36(4), 267-272. doi: 10.1159/000353863

Farid, A.H. and Ferns, L.E., 2011. Aleutian mink disease virus infection may cause hair depigmentation. Scientifur, 35(4), 55-59.

Farid, A.H. and Ferns, L.E., 2017. Reduced severity of histopathological lesions in mink selected for tolerance to Aleutian mink disease virus infection. Res. Vet. Sci., 111, 127-134.

Farid, A.H. and Rupasinghe, P.P., 2016. Accuracy of enzyme-linked immunosorbent assays for quantification of antibodies against Aleutian mink disease virus. J. Viro. Meth., 235, 144-151.

Farid, A.H. and Segervall, J., 2014. A comparison between ELISA and CIEP for measuring antibody titres against Aleutian mink disease virus. Virol. Mycol., 3(137), 2161-0517. doi: 10.4172/2161-0517.1000137

Farid, A.H., 2010. Selection for low blood gamma globulin in mink naturally exposed to the Aleutian mink disease virus. 9th World Cong. Genet. Apple. Lives. Prod., Leipzig, Germany. http://www.kongressband.de/wcgalp2010/assets/pdf/0780.pdf

Farid, A.H., Daftarian, P.M. and Fatehi, J., 2018. Transmission dynamics of Aleutian mink disease virus on a farm under test and removal scheme. J. Vet. Sci. Med. Diagn., 7, 2. doi: 10.4172/2325-9590.1000253

Farid, A.H., Hussain, I. and Arju, I., 2015. Detection of Aleutian mink disease virus DNA and antiviral antibody in American mink (Neovison vison) 10 days postinoculation. J. Vet. Diag. Inve., 27(3), 287-294.

Farid, A.H., Zillig, M.L., Finley, G.G. and Smith, G.C., 2012. Prevalence of the Aleutian mink disease virus infection in Nova Scotia, Canada. Prev. Vet. Med., 106(3-4), 332-338.

Francisco, J.S., de Moraes H.P. and Dias, E.P., 2004. Evaluation of the Image-Pro Plus 4.5 software for automatic counting of labeled nuclei by PCNA immunohistochemistry. Braz. Oral Res., 18(2), 100-104.

Gilbert, F.F. and Bailey, E.D., 1968. Visual isolation and stress in female ranch mink particularly during the reproductive season. Can. J. Zool., 47(2), 209-212.

Goedkoop, A.Y., de Rie, M.A., Teunissen, M.B.M., Picavet, D.I., van der Hall, P.O., Bos, J.D., Tak, P.P. and Kraan, M.C., 2005. Digital image analysis for the evaluation of the inflammatory infiltrate in psoriasis. Arch. Dermatol. Res., 297(2), 51-59.

Gorham, J.R., Henson, J.B., Crawford, T.B. and Padgett, G.A., 1976. The epizootiology of Aleutian disease. Front Biol., 44, 135-158.

Greenfield, J., Walton, R. and Macdonald, K.R., 1973. Detection of Aleutian disease in mink: Serum-plate agglutination using iodine compared with precipitation by agar-gel electrophoresis. Res. Vet. Sci., 15(3), 381-383.

Gunnarsson, E., 2001. Documenting freedom from disease and re-establishing a free status after a breakdown Aleutian disease (Plasmacytosis) in farmed mink in Iceland. Acta. Vet. Scand., 42(Suppl. 1), S87.

Gurcan, M.N., Boucheron, L.E., Can, A., Madabhushi, A., Rajpoot, N.M. and Yener, B., 2009. Histopathological image analysis: A review. IEEE Rev. Biomed. Engi., 2, 147-171. doi: 10.1109/RBME.2009.2034865

Hadlow, W.J., Race, R.E. and Kennedy, R.C., 1983. Comparative pathogenicity of four strains of Aleutian disease virus for pastel and sapphire mink. Infect. Immun., 41(3),1016-1023.

Hadlow, W.J., Race, R.E. and Kennedy, R.C., 1984. Royal pastel mink respond variously to inoculation with Aleutian disease virus of low virulence. J. Virol., 50(1), 38-41.

Hadlow, W.J., Race, R.E. and Kennedy, R.C., 1985. Temporal replication of the Pullman strain of Aleutian disease virus in royal Pastel mink. J. Virol., 55(3), 853-856.

Hahn, E.C. and Hahn, P.S., 1983. Autoimmunity in Aleutian disease: Contribution of antiviral and anti-DNA antibody to hypergammaglobulinemia. Infect. Immun., 41(2), 494–500.

Hansen, M. and Lund, E., 1988. Pregnancy Rate and foetal mortality in Aleutian disease virus infected mink. Acta. Vet. Scand., 29(2), 271–2.

Harwell, M.R., Rubinstein, E.N., Hayes, W.S. and Olds, C.C., 1992. Summarizing Monte Carlo results in methodological research: The one-and two-factor fixed effects ANOVA cases. J. Edu. Stat., 17(4), 315–339.

Henson, J.B, Gorham, J.R., McGuire, T.C. and Crawford, T.B., 1976. Pathology and pathogenesis of Aleutian disease. Front. Biol., 44, 175-205.

Henson, J.B., Gorham, J.R. and Leader, R.W., 1962. A field test for Aleutian disease. National Fur News, 34, 8-26.

Henson, J.B., Leader, R.W., Gorham, J.R. and Padgett, G.A., 1966. The sequential development of lesions in spontaneous Aleutian disease of mink. Pathol., Vet., 3(4), 289-314.

Hildebrandt, H., 2014a. Bacterial diseases of mink In: Kahn CM, Line S, Aiello SE, editors. The Merck veterinary manual [online]. Whitehouse Station, NJ: Merck and Co; 2014. Available at: https://www.merckvetmanual.com/exotic-and-laboratory-animals/mink/bacterial-diseases-of-mink

Hildebrandt, H., 2014b. Viral diseases of mink In: Kahn CM, Line S, Aiello SE, editors. The Merck veterinary manual [online]. Whitehouse Station, NJ: Merck and Co; 2014. Available at: https://www.merckvetmanual.com/exotic-and-laboratory-animals/mink/viral-diseases-of-mink

International Organization for Standardization, 1994. Guide 8402: Quality Vocabulary. ISO, Geneva. https://www.iso.org/standard/20115.html

Jackson, M.K., Ellis, L.C., Morrey, J.D., Li, Z. and Barnard, D.L., 1996. Progression of Aleutian disease in natural and experimentally induced infection of mink. AJVR, 57(12), 1753-1758.

Jahns, H., Daly, P., McElroy, M.C., Sammin, D.J., Bassett, H.F. and Callanan, J.J., 2010. Neuropathologic features of Aleutian disease in farmed mink in Ireland and molecular characterization of Aleutian mink disease virus detected in brain tissues. J. Vet. Diagn. Invest., 22(1), 101-105.

Janowczyk, A. and Madabhushi, A., 2016. Deep learning for digital pathology image analysis: A comprehensive tutorial with selected use cases. J. Pathol. Info., 7.

JCGM200, 2008. International vocabulary of metrology- Basic and general concepts and associated terms (VIM). International Organization for Standardization Geneva ISBN 3.

Jensen, T.H., Chriel, M. and Hansen, M.S., 2016. Progression of experimental chronic Aleutian mink disease virus infection. Acta. Vet. Scand., 58(1), 35. doi: 10.1186/s13028-016-0214-7

Jensen, T.H., Hammer, A.S. and Chriél, M., 2014. Monitoring chronic infection with a field strain of Aleutian mink disease virus. J. Vet. Micro., 168(2-4), 420-427.

Johansson, A.C., Visse, E., Widegren, B., Sjogren, H.O. and Siesjo, P., 2001. Computerized Image Analysis as a tool to quantify infiltrating leukocytes: A comparison between high- and low-magnification images. The Journal of Histochem. Cytochem., 49(9), 1073-1079.

Johnson, M.I., Henson, J.B. and Gorham, J.R., 1975. The influence of genotype on the development of glomerular lesions in mink with Aleutian disease virus. Am. J. Pathol., 81(2), 321-336.

Jones, T.C, Hunt, R.D. and King, N.W., 1997. Veterinary pathology, sixths edition. Baltimore, MD. Williams & Wilkins.

Kenyon, A.J., Trautwein, G. and Helmboldt, C.F., 1963. Characterization of blood serum proteins from mink with Aleutian disease. Am. J. Vet. Res., 24, 168-73.

Kirk, R.J., 1963. Some aspects of the iodine-blood serum test and Aleutian disease. Fur Trade Journal of Canada, 40, 11-13.

Kohlberger, P.D., Breitenecker, F., Kaider, A., Losch, A., Gitsch, G., Breitenecker, G. and Kieback, D.G., 1999. Modified true-color computer-assisted image analysis versus subjective scoring of estrogen receptor expression in breast cancer: a comparison. Anticancer Res., 19(3), 2189-2193.

Kratz, A., Bengtsson, H.I., Casey, J.E., Keefe, J.M., Beatrice, G.H., Grzybek, D.Y., Lewandrowski, K.B. and Van Cott, E.M., 2005. Performance evaluation of the CellaVision DM96 system. Am. J. Clin. Pathol., 124(5), 770-781.

Kunkel, E.J. and Butcher, E.C., 2003. Plasma-cell homing. Nat. Rev. Immunol., 3(10), 822-829. doi: 10.1038/nril203.

Larsen, A.E. and Porter, D.D., 1975. Pathogenesis of Aleutian disease of mink: Identification of nonpersistent infections. Infect. Immun., 11(1) 92-94.

Laurinavicius, A., Laurinaviciene, A., Dasevicius, D., Elie, N., Plancoulaine, B., Bor, C. and Herlin, P., 2012. Digital image analysis in pathology: Benefits and obligation. Anal. Cell. Pathol., 35(2), 75-78. doi: 10.3233/ACP-2011-0033

Laurinavicius, A., Plancoulaine, B., Laurinavicius, A., Herlin, P., Meskauskas, R., Balrtusaityte, I., Besusparis, J., Dasevicius, D., Elie, N., Iqbal, Y., Bor, C. and Ellis, I.O., 2014. A methodology to ensure and improve accuracy of Ki67 labelling index estimation by automated digital analysis in breast cancer tissue. Breast Cancer Research, 16(2), R35. doi: 10.1186/bcr3639

Leader, R.W., Wagner, B.M., Henson, J.B. and Gorham, J.R., 1963. Structural and histochemical observations of liver and kidney in Aleutian disease of mink. Am. J. Pathol., 43, 33-53.

Leica Biosystems, 2018. https://www.leicabiosystems.com/histology-equipment/microtomes/products/leica-rm2255/

Leica Microsystems, 2018. https://www.leica-microsystems.com/applications/education/details/product/leica-dm500/.

Lix, L.M., Keselman, J.C. and Keselman, H.J., 1996. Consequences of assumption violations revisited: A quantitative review of alternatives to the one-way analysis of variance " F" test. Rev. Edu. Res., 66(4), 579–619.

López, C., Callau, C., Bosch, R., Korzynska, A., Jaen, J., Gracia-Rojo, M., Bueno, G., Salvado, M.T., Alvaro, T., Onos, M., delMilagro Femandez-Carrobles, M., Llobera, M., Baucells, J., Orero, G. and Lejeune, M., 2014. Development of automated quantification methodologies of immunohistochemical markers to determine patters of immune response in breast cancer: A retrospective cohort study. BMJ Open, 4(8) e005643. doi: 10.1136/bmjopen-2014-005643

Loughlin, P.M., Cooke, T.G., George, W.D., Gray, A.J., Stott, D.I. and Going, J.J., 2007. Quantifying tumor-infiltrating lymphocyte subsets: A practical immune-histochemical method. J. Immunol. Meth., 321(1-2), 32-40.

Mallen, M.S., Ugalde, E.L., Balcazar, M.R., Bolivar, J.I. and Meyran, S., 1950. Precipitation of abnormal serum by Lugol's solution. Am. J. Clin. Pathol., 20(1), 39-45.

Marcos-Graces, V., Harvat, M., Aguilar, P.M., Izquierdo, A.F. and Ruiz-Sauri, A., 2017. Comparative measurement of collagen bundle orientation by Fourier analysis and semiquantitative evaluation: Reliability and agreement in Masson's trichrome, Picrosirius red and confocal microscopy techniques. J. Micros., 267(2), 130-142.

McDonald, J.H., 2014. Handbook of biological statistics. Retrieved from http://www.biostathandbook.com/spearman.html.

McGinley, J.N., and Thompson, H.J., 2011. Quantitative assessment of mammary gland density in rodents using digital image analysis. Biological Procedures Online, 13(1), 4. doi: 10.1186/1480-9222-13-4

Minges Wols, H.A., 2005. Plasma cells. In: eLS. John Wiley & Sons Ltd, Chichester. http://www.els.net [doi: 10.1002/9780470015902.a0004030.pub2]

Mori, S., Nose, M., Miyazawa, M., Kyogoku, M., Wolfinbarger, J.B. and Bloom, M.E., 1994. Interstitial nephritis in Aleutian mink disease, possible role of cell-mediated immunity against virus-infected tubular epithelial cells. Am. J. Pathol., 144(6), 1326-1333.

Mostafa, S., Seamon, V. and Azzarolo, A.M., 2012. Influence of sex hormones and genetic predisposition in Sjogren's syndrome: A new clue to the immunopathogenesis of dry eye disease. Experimental Eye Research, 96(1), 88-97. doi: 10.1016/j.exer.2011.12.016

Muller-Peddinhaus, R. and Trautwein, G., 1983. Studies on the pathogenesis of Aleutian disease of mink. Abl. Vet. Med. B, 30, 487-501.

Nieto, J.M., Alvarez, C., Flores, J.M. and Romano, J., 1991. Glomerular lesions in Aleutian disease of mink (Mustela vison): A morphological and differential morphometrical study. Histopathol., 6, 141-148.

Noutsias, M., Patil, V.J. and Maisch, B., 2012. Cellular immune mechanisms in myocarditis. Herz, 37(8), 830-835. doi: 10.1007/s00059-012-3700-3

NS Department of Agriculture, 2017. https://novascotia.ca/agri/programs-and-services/lab-services/pathology-lab/.

Oie, K.L., Durrant, G., Wolfinbarger, J.B., Martin, D., Costello, F., Perryman, S., Hogan, D., Hadlow, W.J. and Bloom, M.E., 1996. The relationship between capsid protein (VP2) sequence and pathogenicity of Aleutian mink disease parvovirus (ADV): A possible role for raccoons in the transmission of ADV infection. J. Virol., 70(2), 852-861.

Paton, D., Faragher, B., Mustaffa, K.M.F., Szestak, T., Barrett, S.D. and Craig, A.G., 2011. Automated counting for *Plasmodium Falciparum* cytoadherence experiments. Malaria Journal, 10 (1), 91.

Porter, D.D, Larsen, A.E. and Porter, H.G., 1973. The pathogenesis of Aleutian disease of mink, III. Immune complex arteritis. Am. J. Pathol., 71(2), 331-338.

Porter, D.D., 1986. Aleutian disease: A persistent parvovirus infection of mink with a maximal but ineffective host humoral immune response. Prog. Med. Virol., 33, 42-60.

Porter, D.D., Larsen, A.E. and Porter, H.G., 1969. The pathogenesis of AD of mink. I. In vivo viral replication and the host antibody response to viral antigen. J. Exp. Med., 130(3), 575-589.

Porter, D.D., Larsen, A.E. and Porter, H.G., 1972. The pathogenesis of Aleutian disease of mink: II. Enhancement of tissue lesions following the administration of a killed virus vaccine or passive antibody. J. Immu., 109(1), 1-7.

Porter, D.D., Larsen, A.E. and Porter, H.G., 1980. Aleutian disease of mink. Adv. Immunol., 29, 261-286.

Powers, D., 2011. Evaluation: From precision, recall and F-measure to ROC, informedness, markedness and correlation. Journal of Machine Learning Technologies, 2(1), 37-63. doi: 10.1.1.214.9232

Prasad, K. and Prabhu G.K., 2012. Image analysis tools for evaluation of microscopic views of immunohistochemically stained specimen in medical research-a review. J. Med. Syst., 36(4), 2621-2631. doi: 10.1007/s10916-011-9737-7

Råberg, L., Sim, D., and Read, A.F., 2007. Disentangling genetic variation for resistance and tolerance to infectious diseases in animals. Science. 318(5851), 812-814. doi: 10.1126/science.1148526

Riber-Hansen, R., Vainer, B. and Steiniche, T., 2012. Digital image analysis: a review of reproducibility, stability and basic requirements for optimal results. APMIS, 120(4), 276-289. doi: 10.1111/j.1600-0463.2011.02854.x.

Rintoul, L., Panayiotou, H., Kokot, S., George, G., Cash, G., Frost, R., Bui, T. and Fredericks, P., 1998. Fourier transform infrared spectrometry: A versatile technique for real world samples. Analyst, 123(4), 571-577.

Rizzardi, A.E., Johnson, A.T., Isaksson Vogel, R., Pambuccian, S.E., Henriksen, J., Skubitz, A.P.N., Metzger, G.J. and Schmechel, S.C., 2012. Quantitative comparison of immunohistochemical staining measured by digital image analysis versus pathologist visual scoring. Diagn. Pathol., 7(1), 42.

Rogers, R., Eastham-Anderson, J., DeVoss, J., Lesch, J., Yan, D., Xu, M., Solon, M., Hotzel, K., Diehl, L. and Webster, J.D., 2016. Image analysis-based approaches for scoring mouse models of colitis. Vet. Pathol., 53(1), 200-210. doi: 10.1177/0300985815579998

Sackett, D.L., 1992. A primer on the precision and accuracy of the clinical examination. JAMA, 267(19), 2638-2644.

Salinas-Navarro, M., Jimenez-Lopez, M., Valiente-Soriano, F.J., Alarcon-Martinez, L., Aviles-Trigueros, M., Mayor, S., Holmes, T., Lund, R.D., Villegas-Perez, M.P. and Vidal-Sanz, M., 2009. Retinal ganglion cell population in adult albino and pigmented mice: A computerized analysis of the entire population and its spatial distribution. Vision Research, 49(6), 637-647.

Schuler, J., Pennick K.E. and Latimer K.S., 2007. An overview of Aleutian disease in ferrets. Veterinary clinical pathology clerkship program, www.vet.uga.edu/vpp/clerk/schuler/index.php

Sheethal, H.S., Uma, K., Rao, K., Priya, N.S., Umadevi, H.S. and Smitha, T., 2014. A quantitative analysis of mast cells in inflammatory periapical and gingival lesions. J. Contemp. Dent. Pract., 15(3), 300-305.

Soendergaard, C., Nielsen, O.H., Skak, K., Ropke, M.A., Seidelin, J.B. and Kvist, P.H., 2016. Objective qualification of immune cell infiltrates and epidermal proliferation in psoriatic skin: A comparison of digital image analysis and manual counting. App. Immunohistochem. Molec. Morphol., 24(6), 453-458.

Soltzberg, J., Frischmann, S., Heecheren, C.V., Brown, N., Caplan, A., and Bonfield, T.L., 2011. Quantitative microscopy in murine models of lung inflammation. Anal. Quant. Cytol. Histol., 33(5), 245-252.

Somanathan S., Schyna, T.M., Siegel, A.J. and Berezney, R., 2001. Targeting of PCNA to site of DNA replication in the mammalian cell nucleus. Journal of Cellular Biochemistry, 81(1), 58-67.

Statistics Canada, 2015. CANSIM - 003-0015 - Supply and disposition of mink and fox on fur farms. Retrieved February 5, http://www5.statcan.gc.ca/cansim/a47.

Stevenson, M.A., Fox, J.M., Wolfinbarger, J.B. and Bloom, M.E., 2001. Effect of a valine residue at codon 352 of the VP2 capsid protein on in vivo replication and pathogenesis of Aleutian disease parvovirus in mink. Am. J. Vet. Res., 62(10), 1658-63.

Table, H. and Ingram, D.G., 1970. The immunoglobulines in Aleutian disease of mink: Different types of hypergamaglobulinemias. Can. J. Comp. Med., 34(4), 329-332.

Themudo, G.E., Ostergaard, J. and Ersboll, A.K., 2011. Persistent spatial clusters of plasmacytosis among Danish mink farms. Prev. Vet. Med., 102(1), 75-82.

Thomson, R.G., 1984. General veterinary pathology, second edition. Philadelphia, PA. W.B. Saunders. Chap. 4, 163-188.

Uebersax, J., 2010. Kappa coefficients: A critical appraisal. Retrieved from http://john-uebersax.com/stat/kappa.htm#refer.

Une, Y., Wakimoto, Y., Nakano, Y., Konishi, M. and Nomura, Y., 2000. Spontaneous Aleutian disease in ferret. J. Vet. Med. Sci., 62(5), 553-555.

Valdovska, A. and Pilmane, M., 2011. Relation between serum enzymes and liver histopathology in mink with hepatitis. Papers on Anthropology, 20, 412-422.

Vasaturo, A., Di Blasio, S., Verweij, D., Blokx, W.A.M., van Krieken, J.H., de Vries I.J.M. and Figdor, C.G., 2017. Multispectral imaging for highly accurate analysis of tumor-infiltrating lymphocytes in primary melanoma. Histopathol., 70(4), 643-649. doi: 10.1111/his.13070

Veta, M., Van Diest, P.J., Kornegoor, R., Huisman, A., Viergever, M.A and Pluim, J.P., 2013. Automatic nuclei segmentation in H&E stained breast cancer histopathology images. Plos One 8(7), e70221. doi 10.1371/Journal.pone.0070221

von Diemen, V., Trindade, E.N. and Trindade, M.R.M., 2016. Hiatal hernia and gastroesophageal reflux: Study of collagen in the phrenoesophageal ligament. Surgical Endoscopy, 30(11), 5091-5098. doi: 10.1007/s00464-016-4858-1

Wang, C.J., Zhou, Z.G., Holmqvist, A., Zhang, H., Li, Y., Adell, G. and Sun, X.F., 2009. Survivin expression quantified by Image Pro-plus compared with visual assessment. App. Immunohistochem. Molec. Morphol., 17(6), 530-535.

Went, P., Mayer, S., Oberholzer, M. and Dirnhofer, S., 2006. Plasma cell quantification in bone marrow by computer-assisted image analysis. Histol. Histopathol., 21(7/9), 951-956. doi: 10.14670/HH-21.951

Westgard, J.O. and Hunt, M.R., 1973. Use and interpretation of common statistical tests in method-comparison studies. Clinical Chemistry, 19(1), 49-57.

Yin, L., Xu, S., Cheng, J., Zheng, D., Limmon, G.V., Leung N.H.N., Rajapakse, J.C., Chow, V.T.K., Chen, J. and Yu, H., 2013. Spatiotemporal quantification of cell dynamics in the lung following influenza virus infection. J. Biomed. Opt., 18(4), 046001. doi: 10.1117/1.JBO.18.4.046001

Ziabreva, I., Perry, E., Perry, R., Minger, S.L., Ekonomou, A., Przyborski, S. and Ballard, C., 2006. Altered neurogenesis in Alzheimer's disease. J. Psychosom. Res., 61(3), 311-316. doi: 10.1016/j.jpsychores.2006.07.017

Appendix 1. Digital Image Analysis

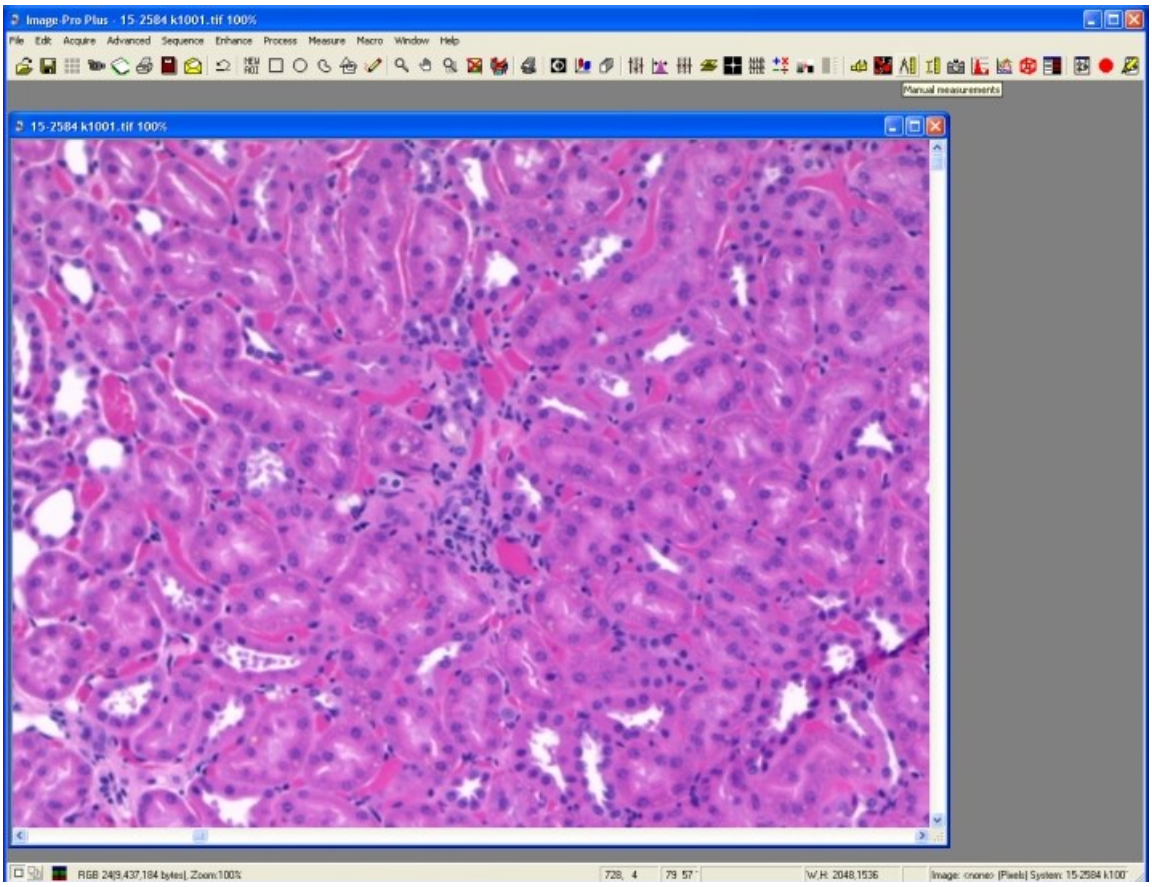

Figure A1.1 A typical RGB image from a kidney slide, in the IPP 7.0 software environment.

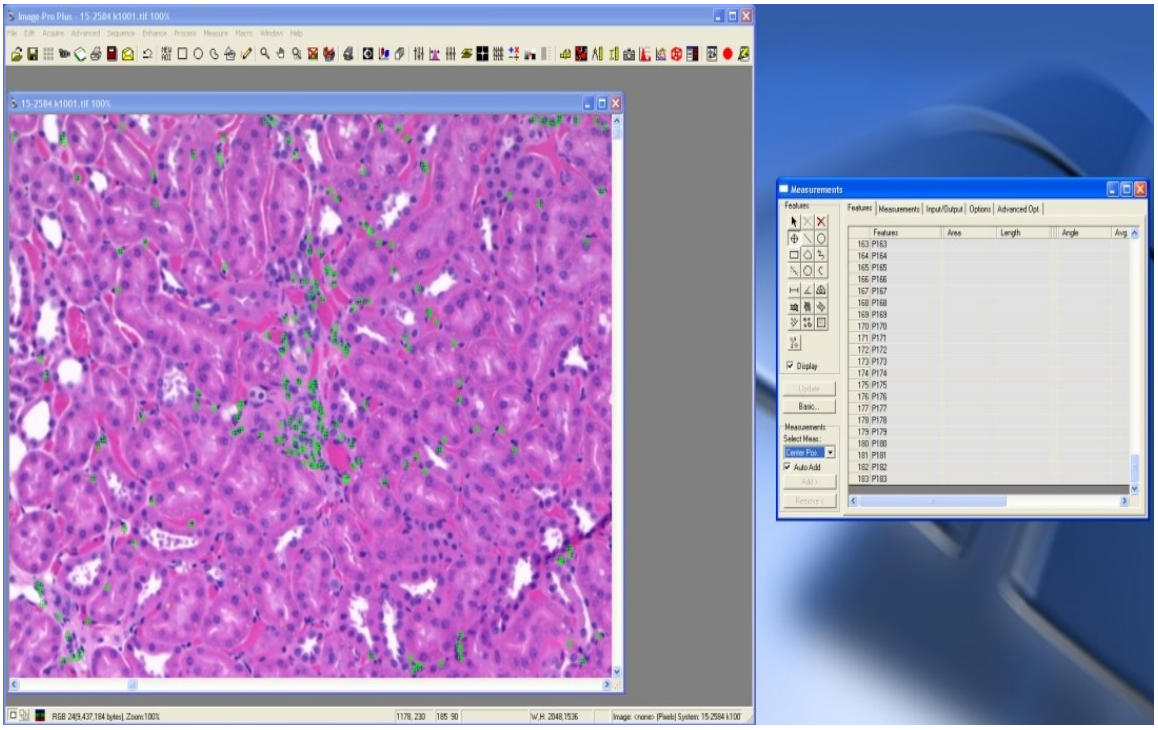

Figure A1.2 Using the “Measurements” option on the main tool bar menu of the software to manually count the infiltrated cells.

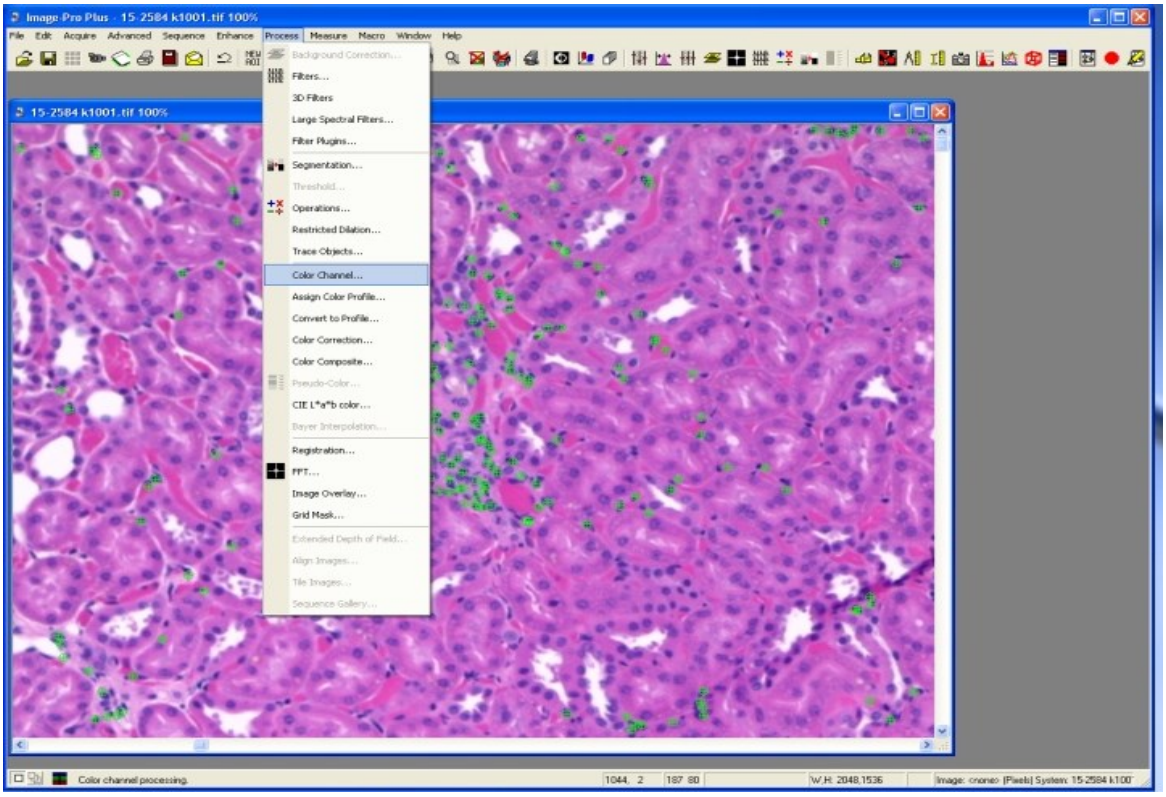

Figure A1.3 Opening the “Color Channel “option under the “Process” menu.

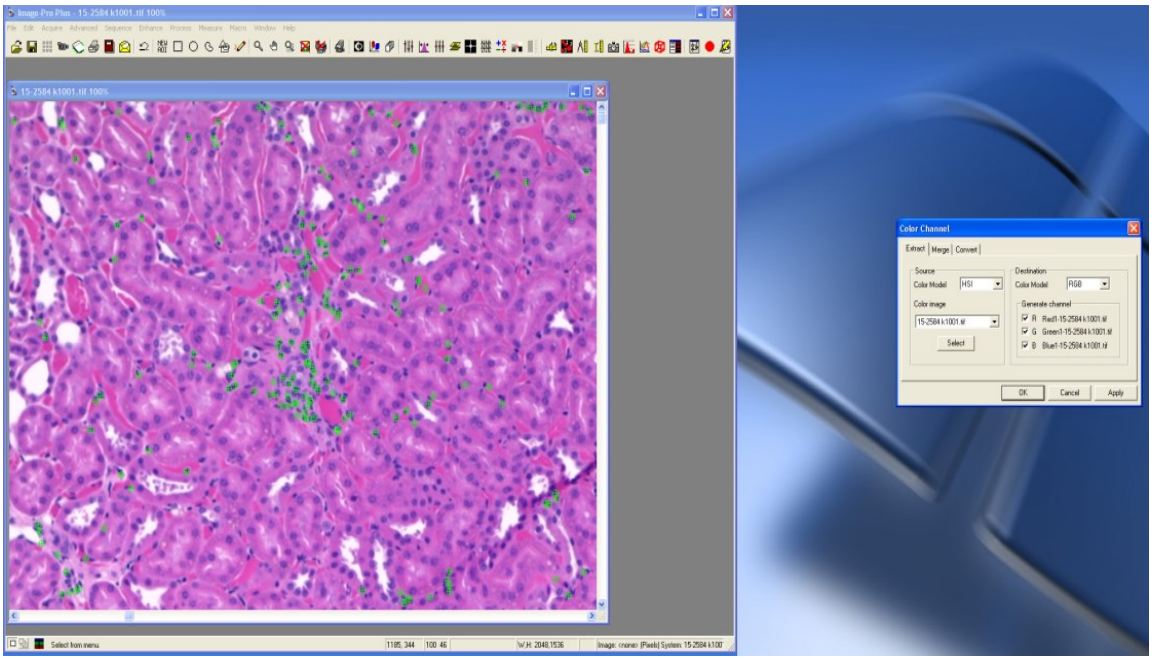

Figure A1.4 Selecting the color channels to convert the RGB images.

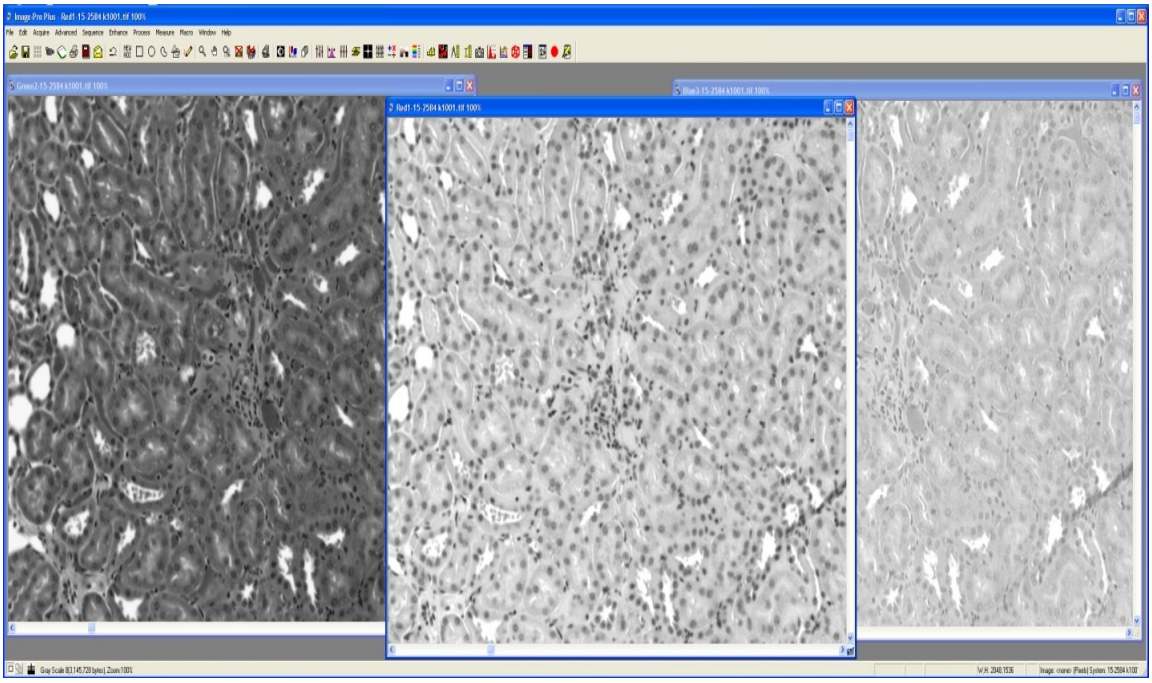

Figure A.1.5 An RGB image converted to three grayscale images based on the three color channels of red, green and blue.

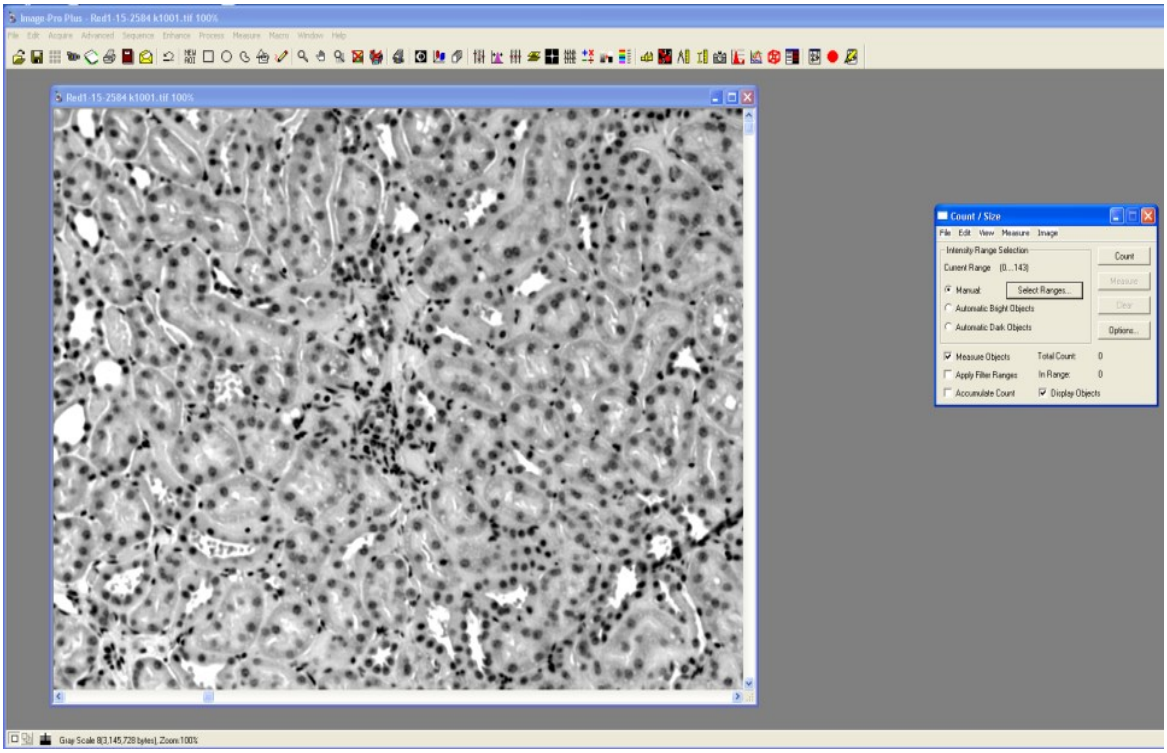

Figure A1.6 Opening the "Count/Size" option on the main tool bar menu of the software and then pressing the "Selected Ranges" button.

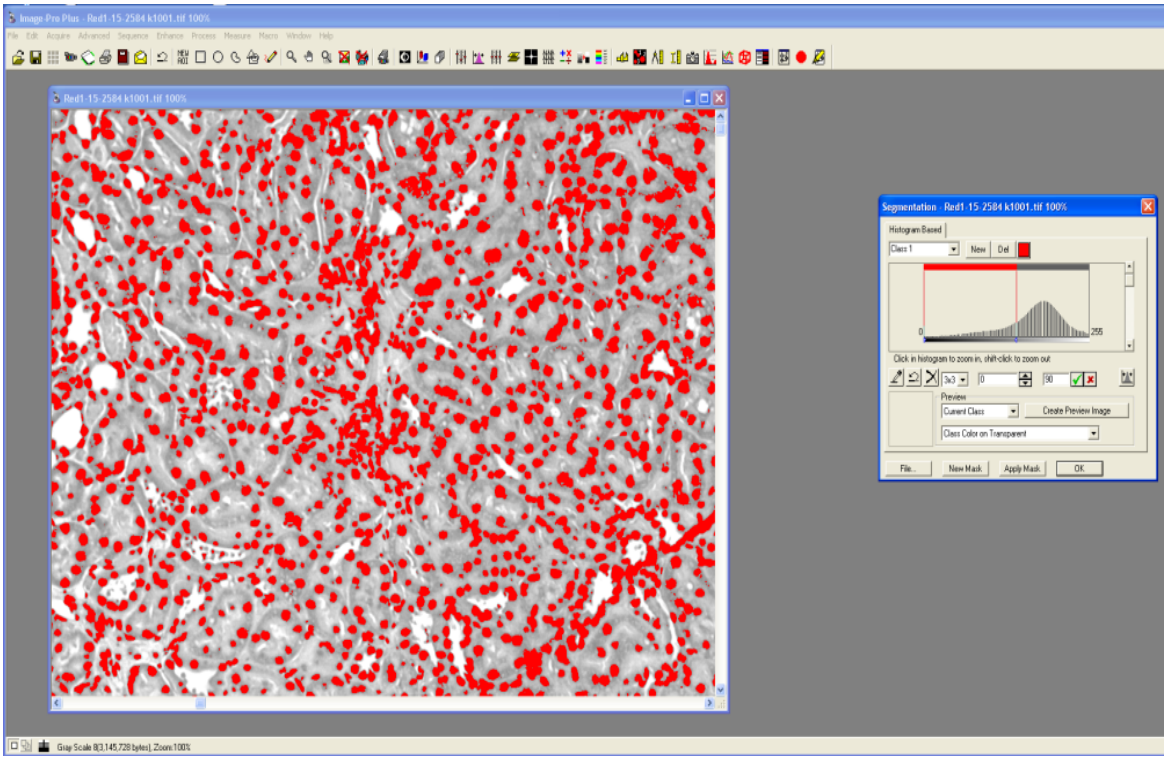

Figure A1.7 Segmentation window where the operator can choose between different range scores.

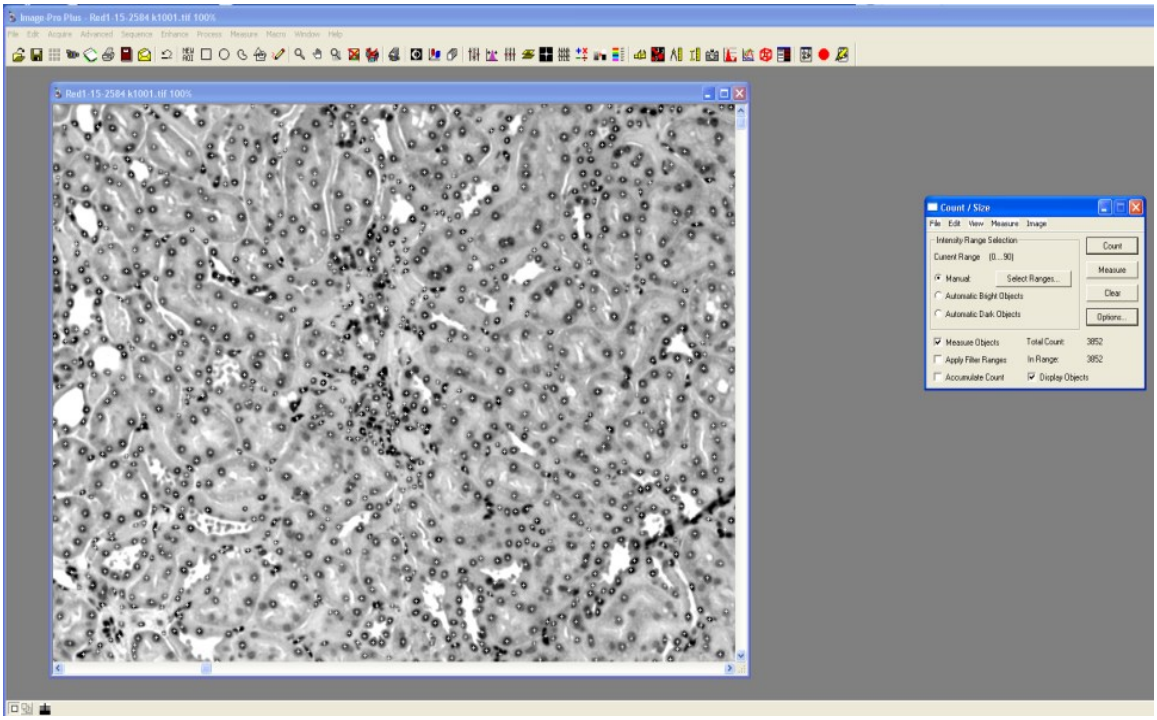

Figure A1.8 Counted nuclei based on the selected range score, indicated by white dots.

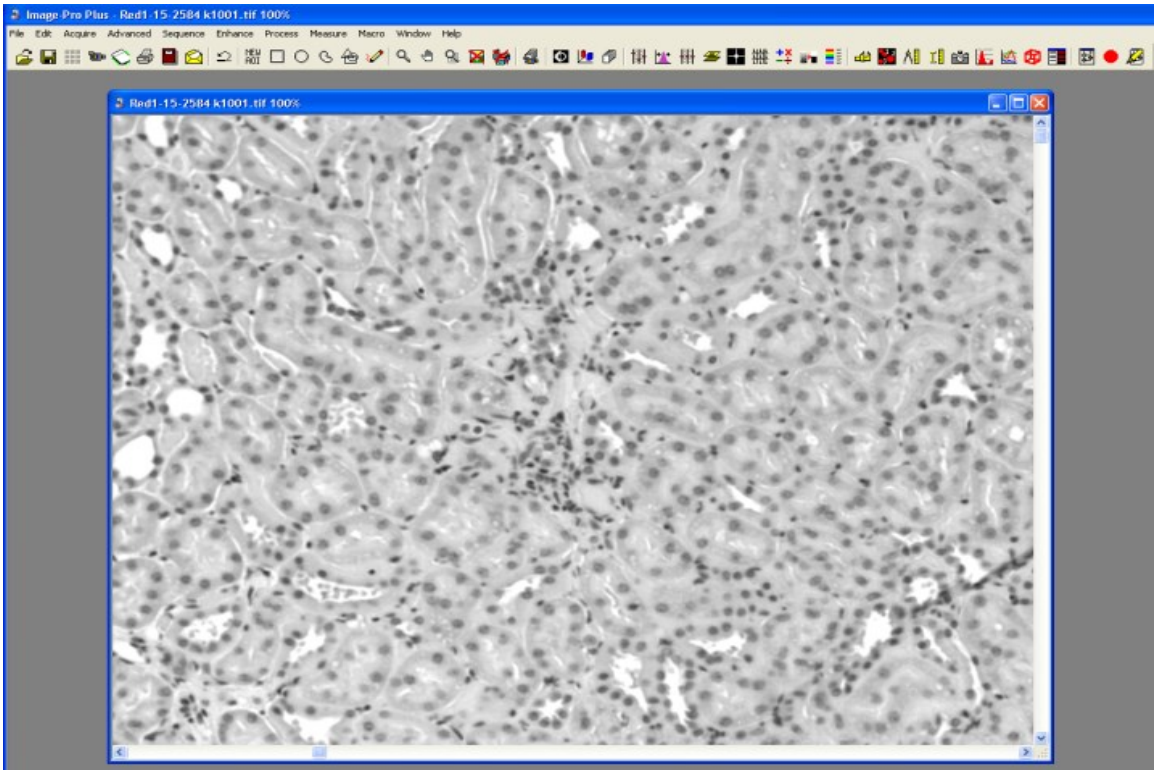

Figure A1.9 An image in the red channel, before using the Best-Fit tool.

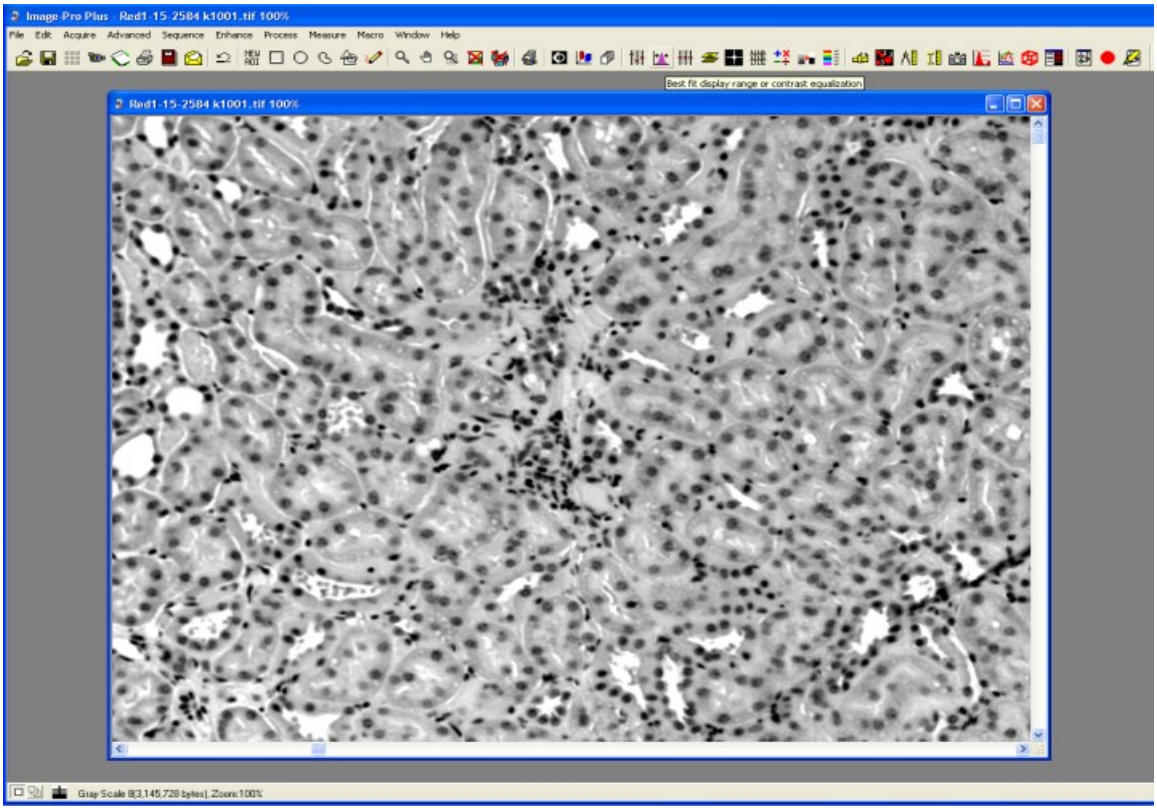

Figure A1.10 An image in the red channel, after using the Best-Fit tool, enhanced contrast of the nuclei of cells.

Appendix 2. IAT test results

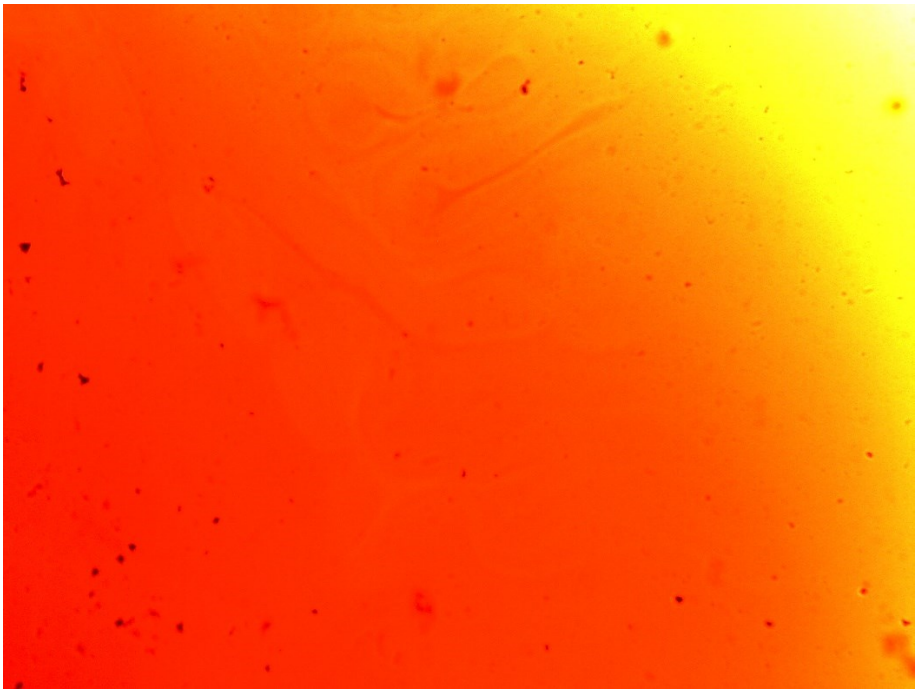

Figure A2.1 IAT score of (0), under a light microscope, X10 magnification.

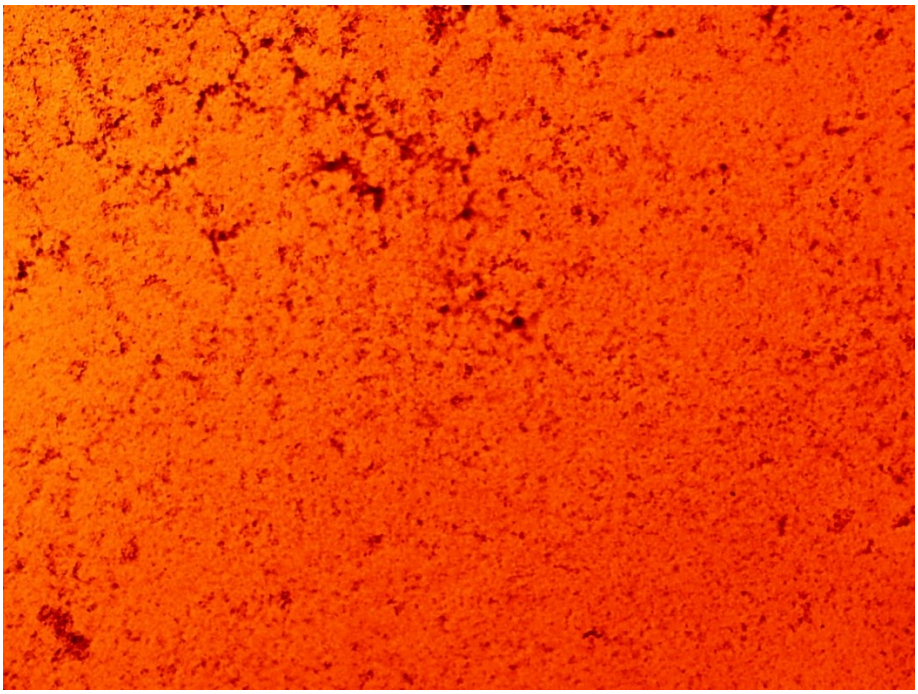

Figure A2.2 IAT score of (1), under a light microscope, X10 magnification.

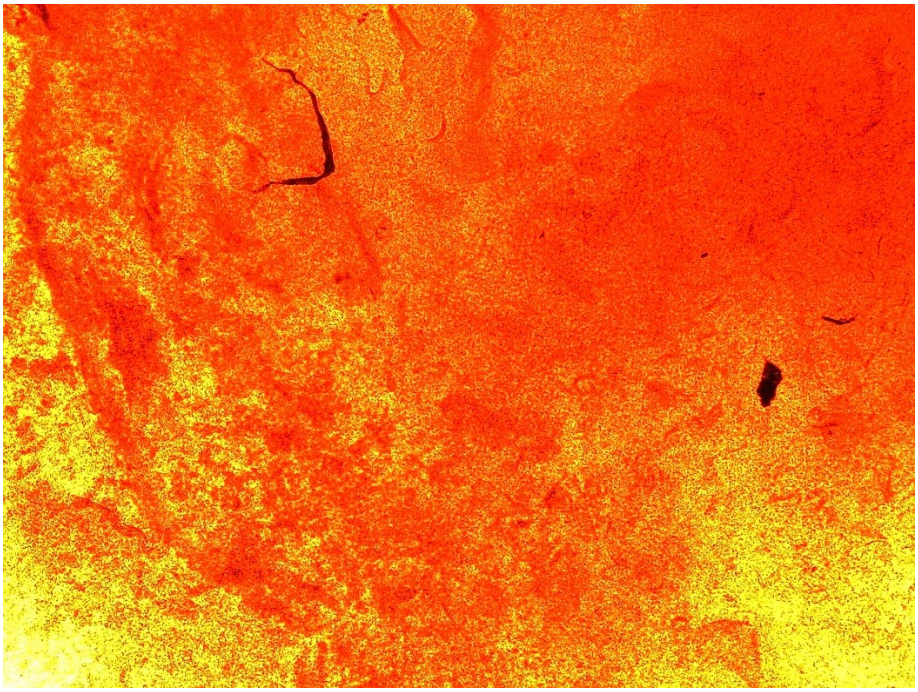

Figure A2.3 IAT score of (2), under a light microscope, X10 magnification.

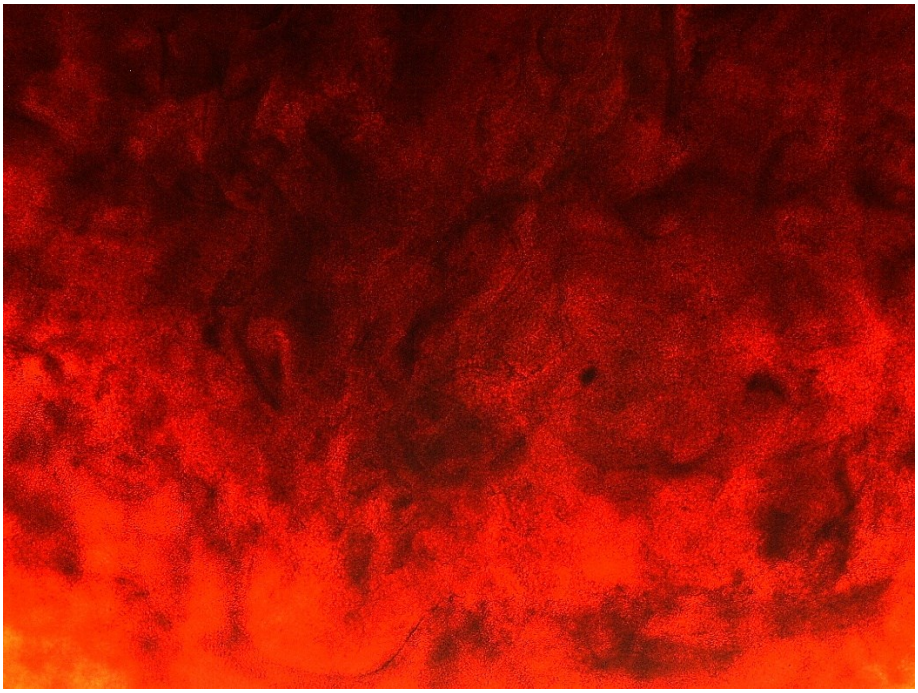

Figure A2.4 IAT score of (3), under a light microscope, X10 magnification.

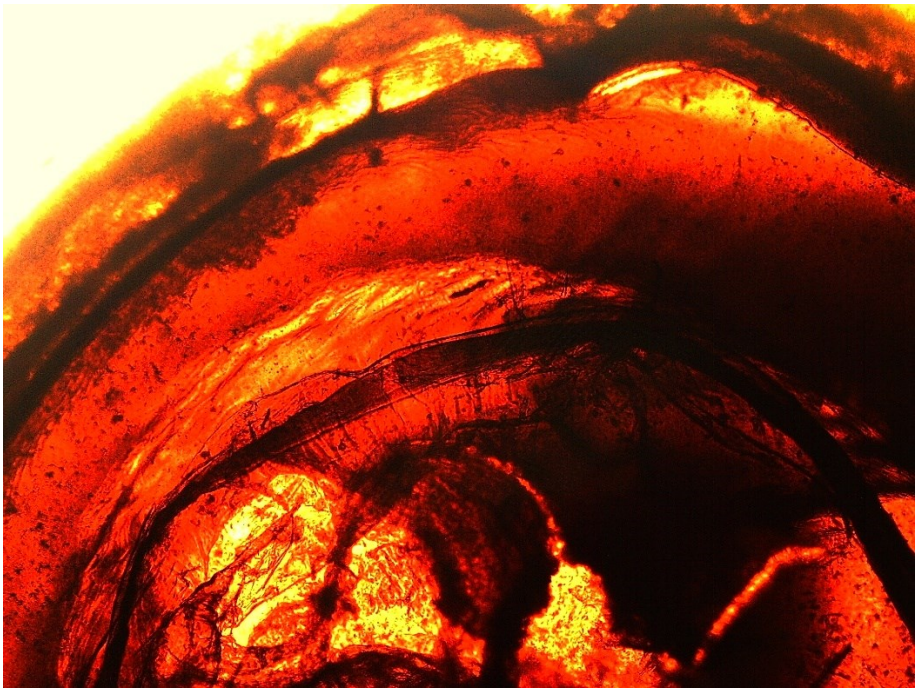

Figure A2.5 IAT score of (4) under a light microscope, X10 magnification.

Appendix 3. Histopathological images from organs of AMDV-infected mink

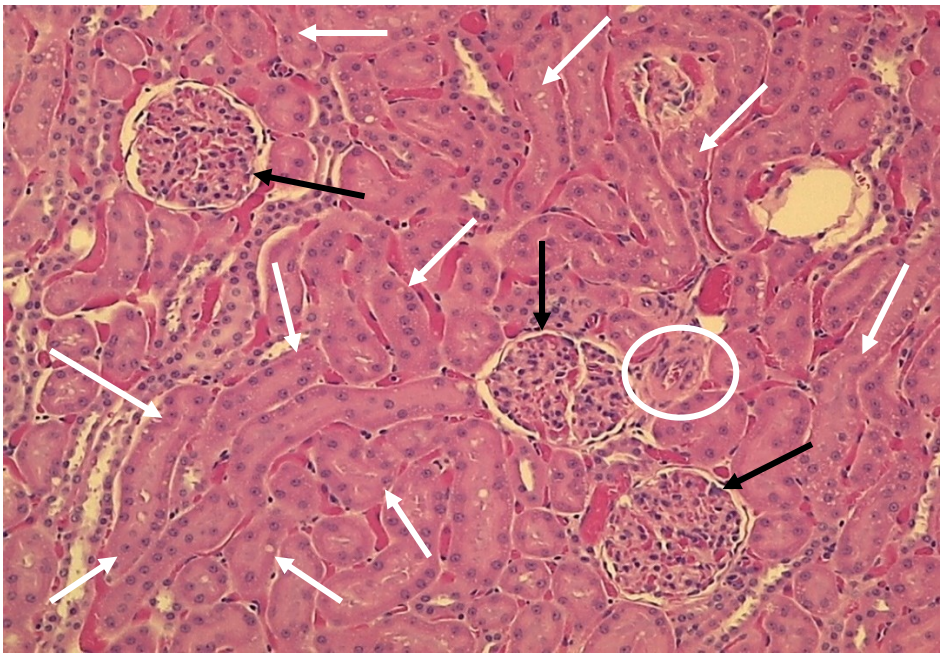

Figure A3.1 A typical image of a normal kidney slide, exhibiting proximal and distal convoluted tubules (white arrows), glomeruli (black arrows) and an artery (white circle).

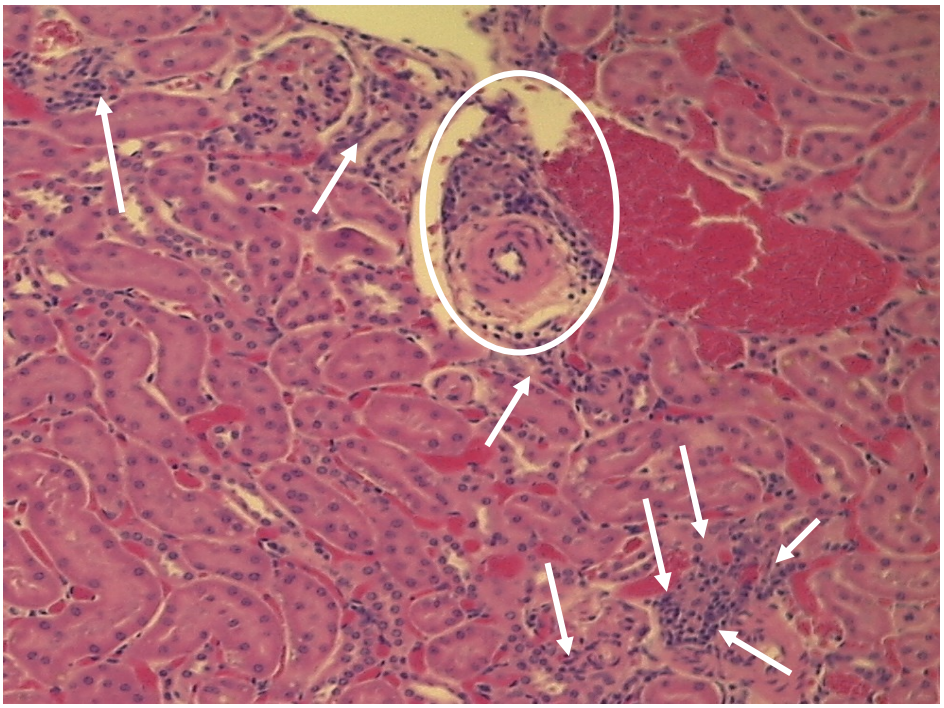

Figure A3.2 A typical image of a kidney slide, exhibiting infiltration of mononuclear cells within the renal tubules (white arrows) and around an artery (white circle).

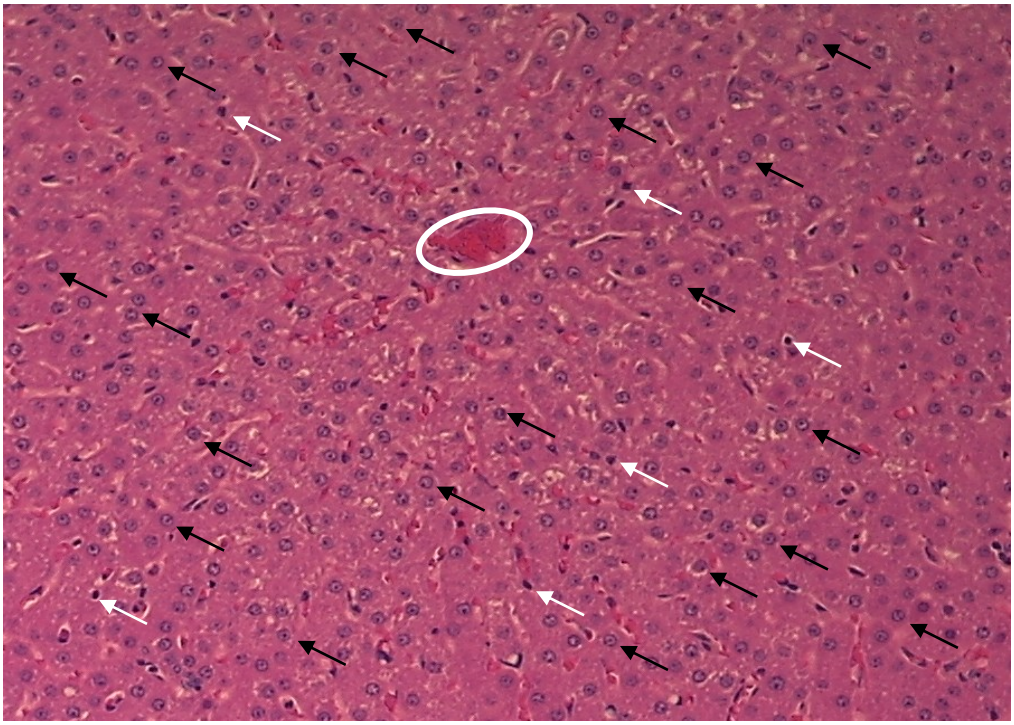

Figure A3.3 A typical image of a normal liver slide, exhibiting hepatocytes (black arrows), Kupffer cells (white arrows) arranged around a central vein (white circle).

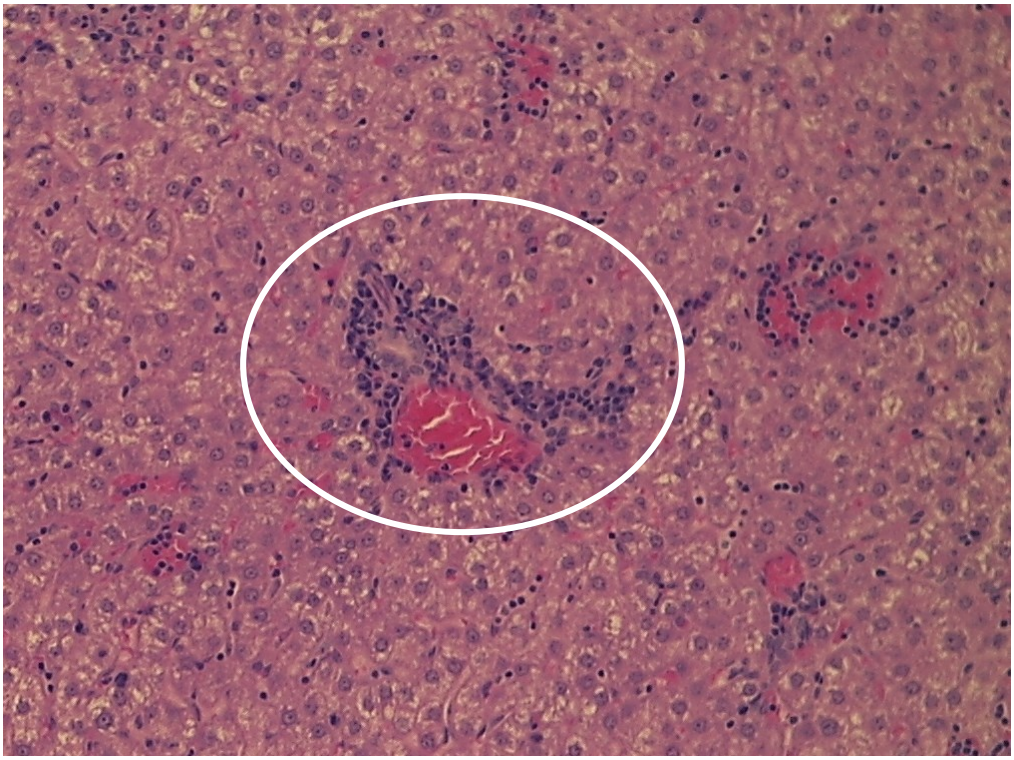

Figure A3.4 A typical image of a liver slide, exhibiting infiltration of mononuclear cells, mostly around a portal area (white circle).

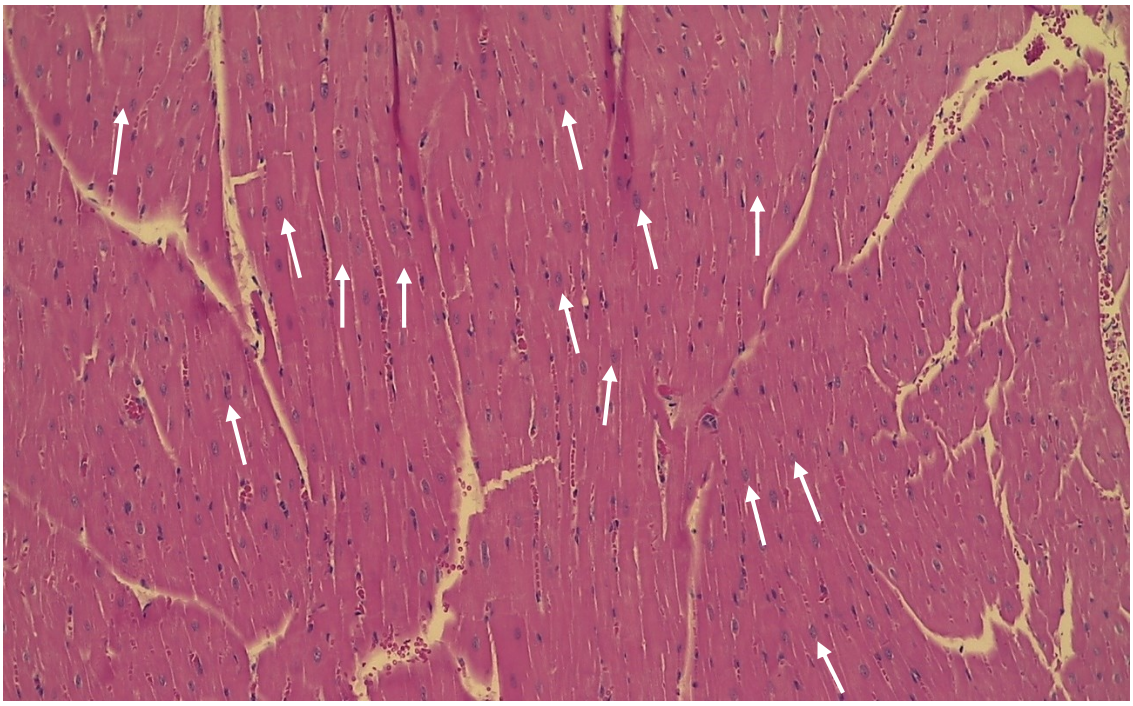

Figure A3.5 A typical image of a heart slide, exhibiting heart muscle cells, mostly arranged in a longitudinal orientation (white arrows).

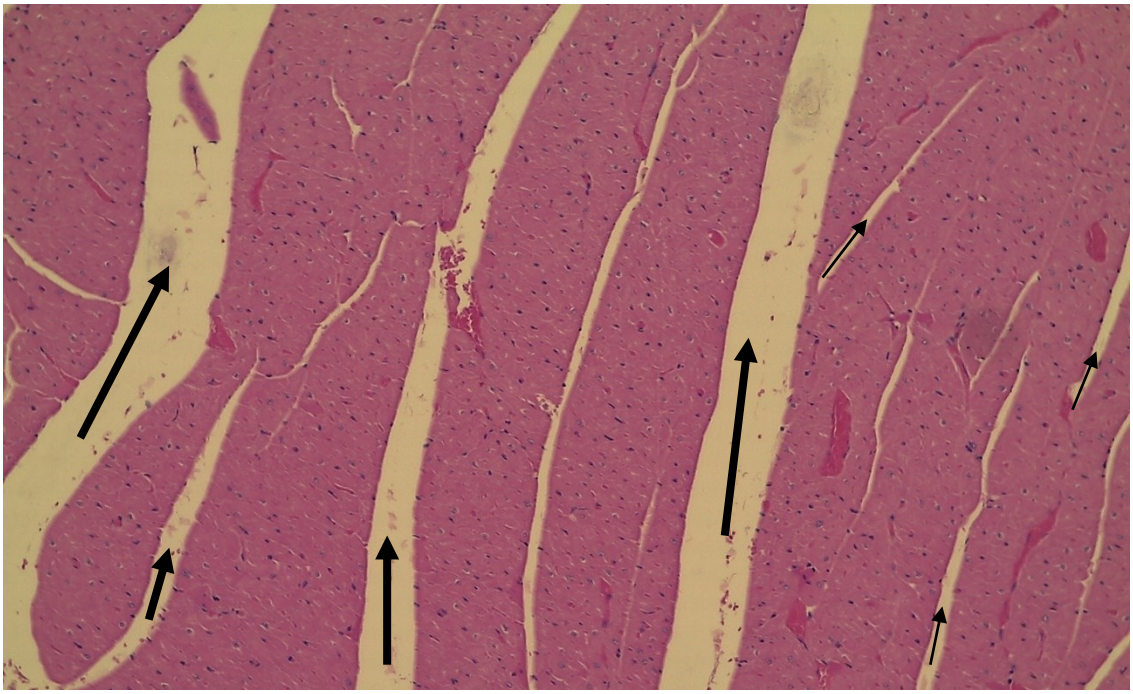

Figure A3.6 A typical image of a heart slide, exhibiting heart muscle cells, mostly arranged in a transvers orientation, and hallow areas related to anatomical chambers (black arrows).

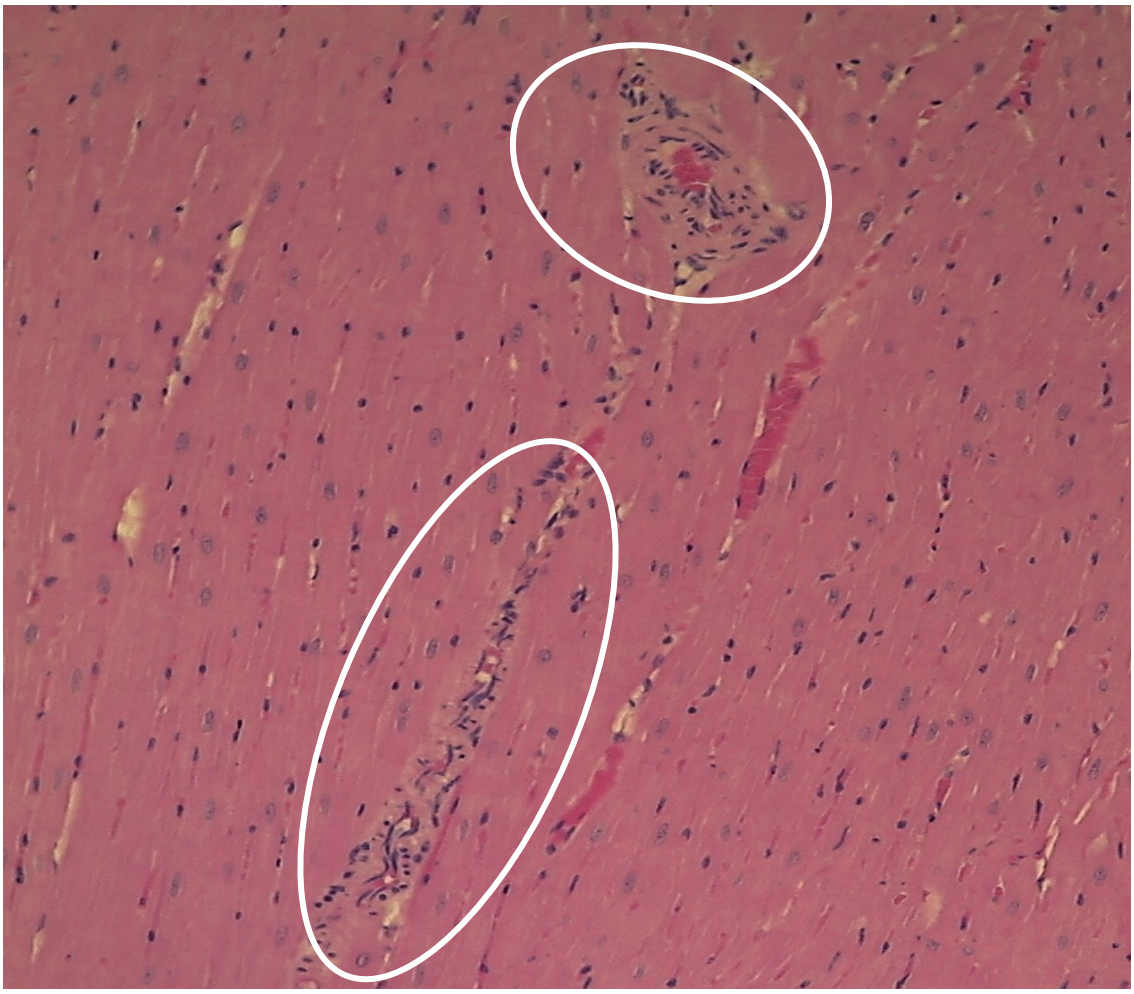

Figure A3.7 A typical image of a heart slide, exhibiting infiltration of mononuclear cells, mostly around and inside the walls of two blood vessels (white circles).